GEOGRID REINFORCEMENT OF RAILWAY BALLAST

Cho Ching Joe Kwan

Thesis submitted to the University of Nottingham
For the degree of Doctor of Philosophy

September 2006

TO MY MOTHER

DECLARATION

The work described in this thesis was conducted at the University of Nottingham, Department of Civil Engineering between November 2002 and February 2006. I declare that the work is my own and has not been submitted for a degree of another university.

ABSTRACT

The railway track system forms an integral part of the transportation infrastructure of this country as well as playing a significant role in sustaining a healthy economy. However, little radical improvement has taken place since Victorian times. Maintaining good track geometry under demanding operational conditions holds the key to an efficient railway system. With a good track geometry or alignment, track will have no need for frequent maintenance, which is costly and is the main cause of train delays.

This research centres on the investigation of geogrid reinforcement with the aim of minimising the rate of deterioration of track geometry. Research began with implementation of a series of element tests namely the Pull-out Test, Geogrid Stiffness Test and Particle Friction Test to assist in Discrete Element (DEM) modelling work performed by Dr Harrireche. DEM of a pull-out test performed in the laboratory provided important insight into the micro-mechanics of ballast-geogrid interlock.

The first of the two main strands of experimental work, the Composite Element Test (CET), is an approximate full-scale experimental simulation of the situation beneath a sleeper. The test compares an unreinforced setup to a geogrid reinforced composite. The test programme has covered variables such as the stiffness of foundation, physical attributes of geogrid (e.g. aperture size, geogrid junction strength etc), depth of geogrid installation, multiple geogrid installation as well as the influence of geotexile on geogrid performance. Test results indicated a significant reduction in the deformation of ballast over 30,000 cycles with the introduction of an appropriate geogrid.

The second strand of experimental work was based on a full scale simulation of rail track bed including 3 full sleepers is known as the Railway Test Facility (RTF). This realistic rail track simulation benefited from knowledge gathered from the CET. The test facility simulates the passage of a train at a speed of 28km/hr and the facility is

housed in a pit 1.8m deep, 4.1m long and 2.1m wide. Test duration was set at a million cycles at 92kN vertical load generated under a real axle load of about 250kN. The aim of this test was to validate the benefit of geogrid reinforcement in a realistic track environment. Four tests were performed in the RTF. Test 1 was an unreinforced test, Test 2 was a reinforced test with geogrid placed on a single layer of ballast and test 3, a reinforced test with geogrid directly placed on a geotexile while Test 4 was another unreinforced test. Tamping was introduced midway in Test 3 and Test 4. Results from the RTF supported the findings from the CET.

In addition to the laboratory work, a design guide was produced. It was based on the results obtained from the CET and RTF and structural analysis was performed using the Shell BISAR multilayer linear elastic program. The non-linear resilient characteristics of the ballast were modelled using repeated load triaxial test data. The model provides the basis for predicting extension to track life when grid reinforcement is used.

ACKNOWLEDGEMENTS

First and foremost, I would like to thank Professor Stephen Brown for his excellent guidance and tireless supervision throughout the course of this research project. His enthusiasm and passion has been my constant source of motivation.

I would like to thank Dr. Nicholas Thom, co-supervisor, for his invaluable advice, suggestions and encouragement that has contributed immeasurably to the completion of this dissertation.

Dr Glen McDowell, co-supervisor, for his invaluable inputs and recommendations.

My gratitude is also due to Dr Quahid Harireche for his help in the Discrete Modelling work in this project as well as the many interesting discussion on matters out of research. The same can be said for Dr Salah Zoorob for the many fascinating evening discussion in the research room. Also his proof reading of the dissertation is very much appreciated

I am also grateful to Barry Brodrick who has been an immense figure in my research with his technical support. He seemed to has unlimited energy around the laboratory. I am also thankful for his proof reading on the technical issue in this dissertation.

Dr James Grenfell for his friendship and for proof reading this dissertation.

My gratitude to the sponsoring organisation of this project – The Royal Society, Tensar International, Scott Wilson Pavement Engineering, Carillion Rail and Network Rail, without their kind contribution in finances or kind, it would not have been possible to complete the project.

I would also like to thank Phil Sharpe, independent rail consultant, for the coordination and provision of site trial results.

My appreciation are also due to the technical and secretarial staff of the Nottingham Centre for Pavement Engineering and the School of Civil Engineering, namely Angela Gilbert, Marzena Newton, Shelia Provost, Carol Yates and Chris Fox for their assistance.

All the colleagues and friends at the results office, particularly Mujib Rahman, Joel Oliveira, York Lee and Riccardo Isola for making this journey so much easier. Also to the one-dish parties brigade Hasan, Wahab, Sami, Young, Ted, Muslich, Pic, Nono, Phil, Jed, Junwei and Xiaoyi with whom I have had many enjoyable times.

Finally, I would like to thank my fiancée Winkie for her constant encouragement, sacrifices and support throughout the period of this project. I cannot forget also all members of my family who were with me right from the very start. They have always been my source of motivation.

LIST OF CONTENTS

LIST OF FIGURES

LIST OF TABLES

1 INTRODUCTION

1.1 Background and problem definition

The railway track system forms an integral part of the transportation infrastructure of a country, playing a significant role in sustaining a healthy economy. Many new railway projects are being planned and constructed around the world most notably the 1307km track linking Beijing to Shanghai. The annual investment to construct and maintain a viable track is enormous. In the U.K, the annual expenditure for maintaining a workable track can amount to almost 5 billion pounds per year with 3 billions pounds committed to track renewal work. (Network Rail Interim Review, 2003).

In the past, a lot of emphasis had been placed on the track superstructure which consists of the rails, the fasteners and the sleepers with little attention given to the substructure which consists of the ballast, subballast and subgrade. This is ironic as substructure components often form the major part of the cost of track maintenance. According to Selig and Waters (1994), the lack of attention to the substructure can be attributed to the difficulties in defining the many variables of the substructure compared to those of the superstructure.

An important requirement of any good railway track is that track geometry must be maintained during train operations. Many superstructure defects, such as rail breaks, are directly or indirectly caused by poor track geometry. Poor vertical alignment of conventional ballasted rail track can lead to poor passenger comfort, higher track maintenance and renewal cost, speed restrictions as well as potential derailment. Uneven track deterioration or settlement is the main cause of poor track geometry.

This irregular track deterioration is often caused by settlement of the substructure, which is often highly dependant on site conditions, e.g. type of subgrade, state of ballast etc.

Figure 1.1 shows a typical profile of the relative contributions of substructure components to track settlement based on a good subgrade foundation (Selig and Waters, 1994). It is clear from the figure that the ballast material accounts for most of the vertical deformation of a rail track, compared to the subgrade and subballast. Due to traffic loading, the ballast will be subjected to high stresses which are sufficient to induce significant strain in the ballast resulting in ballast breakage. This breakage is usually aggravated by track maintenance work to temporarily rectify track geometry, e.g. ballast tamping. Ultimately, this leads to track settlement and, depending on the site conditions, uneven deterioration will take place leading to poor track geometry.

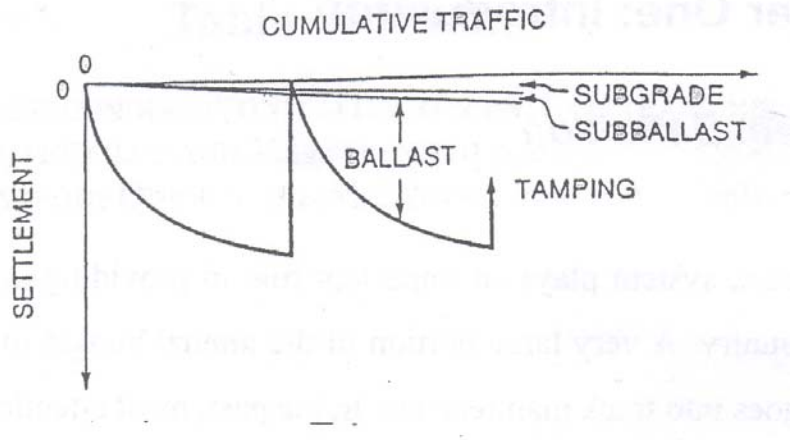

Figure 1.1 Substructure contributions to Settlement (Selig and Waters, 1994)

In order to reduce vertical track settlement, emphasis must be placed on the ballast material. Maintenance work to re-level the railway track, namely tamping, is often costly, destructive and disruptive. Lower train speed is expected after tamping (to allow track to settle) and this often creates disruption to the train schedules.

Since the introduction of the Tensar geogrid in the early 1980s, considerable research has been done on understanding the characteristics of grid/aggregate interaction.

However, the level of basic understanding of how reinforced aggregates can be efficiently designed into a rail track structure is still limited. The real potential of improving the rail track through the use of geogrid has not been properly investigated. Current practice involving geogrid track reinforcement is still limited to experience gathered on site based on *ad hoc* work.

The development and optimisation of geogrid reinforcement of railway ballast has the potential to reduce the rate at which ballast deforms. The correct use of geogrid reinforcement of railway ballast will allow longer maintenance cycles translating to cost savings, less disruption and, overall, a safer means of transportation (Tensar, 2001). Geogrid is also relatively easy to install and it can easily be assimilated into a routine track maintenance operations e.g. ballast cleaning etc.

This project will look into the details of grid/aggregate interaction to gain an understanding of the inter-relationship and identify the key elements involved. Figure 1.2 shows the interlock mechanism. Geogrid reinforcement of granular material relies on effective interlock between grid and aggregate. When reinforcing takes place, there will be a reduction in irrecoverable strain above the zone of influence of the grid, reducing vertical settlement of the ballast. To optimise the effect, the stiffness of grid, size of aperture, grid junction strength as well as the position of the grid within the ballast layer will be some of the elements that will be looked into in this project.

To achieve the project objectives, two main strands of experimental work, namely the Composite Element Test (CET) and the Railway Test Facility (RTF), have been developed and carried out. Several smaller element tests investigating geogrid pullout resistance, geogrid stiffness as well as particle friction were also performed to provide data and information to assist in numerical work. Discrete Element Modelling program PFC^{3D} developed by ITASCA has been used to model the grid and ballast interaction. Discrete Element Modelling (DEM) work in this project was performed by Research Fellow Dr Ouahid Harrireche. This numerical modelling approach models the movement and interaction of stressed assemblies of spherical balls. Ballast and geogrid can be modelled as described and Discrete Element simulation can then analyse their interaction within a defined system.

The CET was designed to provide comparative data that allowed the analysis of grid performance and the results have been fed into the RTF which allows full-scale testing of a track section.

It has long been recognised that the best method to validate laboratory results is to compare them with results obtained on-site. Hence, the results from a field trial, conducted on a heavily trafficked site along the West Coast Main Line, in Lancashire, near Wigan, provide a good comparison in terms of the validation of the findings obtained from the RTF and CET.

A design guide was produced utilising the results from the CET and RTF Structural analysis using the Shell BISAR multilayer linear elastic layered system program provided the background for the design method. The design guide is intended to provide guidance on the design of a ballasted rail track incorporating high tensile polymeric geogrid reinforcement.

A flowchart shown in Figure 1.3 describes the way in which the various strands of this project interact and contribute to meet the final aim.

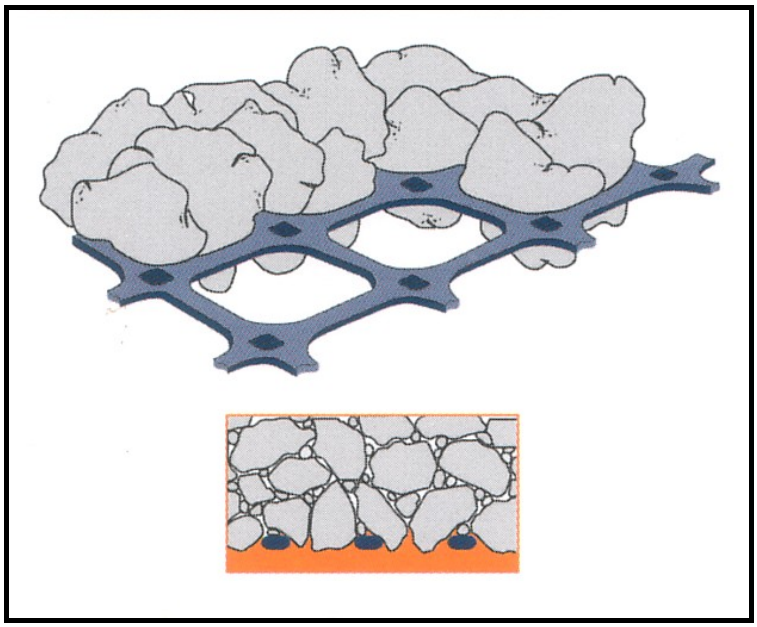

Figure 1.2 The Interlock Mechanism (Tensar International, 2001)

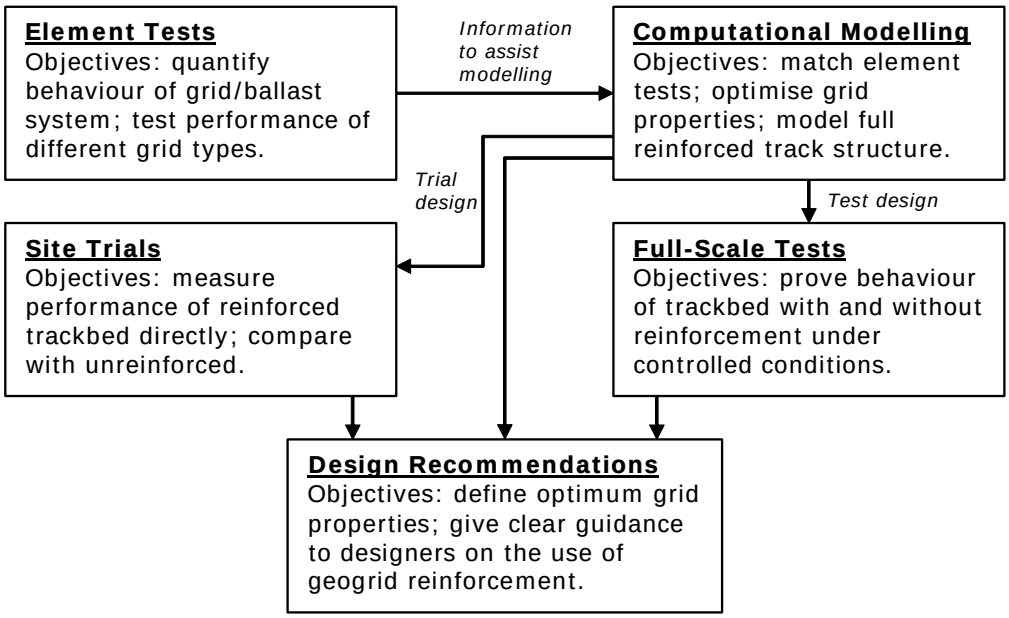

Figure 1.3 Project flowchart

1.2 Aims of the project

A summary of the aims of the project are:

- To investigate the benefits of using geogrid reinforcement in minimising the rate of deterioration of ballasted rail track geometry.

- To identify the mechanisms that will improve ballast/grid interlock.

- To optimise the grid properties, such as grid stiffness and aperture size, in order to maximise performance.

- To produce a design guide, based on simplified elastic analysis, to predict the rate of settlement in a ballasted rail track incorporating high tensile polymeric geogrid reinforcement.

1.3 Thesis outline

This thesis is divided into eight chapters. A brief outline of this thesis is given below.

Following this introductory chapter, Chapter 2 contains a literature review consisting of five main sections: track components and functions, ballast, track geometry and track quality, polymer grid as well as the behaviour of a grid reinforced granular material layer. The review begins with a general appreciation of various track components and its function. This is followed by an examination of ballast stone, which includes its specifications and the cause of ballast fouling. An overview of the resilient and permanent behaviour of granular material will also be presented in the same section. Several settlement models are also described in this section. Review of track geometry and track quality covers the various causes of differential settlement on a rail track. The following section will touch on the reinforcing principle of polymer geogrid. An introduction to the various types of Tensar grids used in this project is also included in the same section. This chapter concludes with a review of the behaviour of a grid reinforced granular layer.

Chapter 3 describes the various element tests performed in this project as well as a brief introduction to Discrete Element Modelling (DEM) using PFC^{3D}. The apparatus and test procedure of the Pull-Out Test and Particle Friction Test as well as the rib test are presented. Discussion of the assumptions made and analysis of the experimental results are also included. A comparison of the DEM data and the experimental results conclude this chapter.

The Composite Element Test (CET) test apparatus and the adopted test procedures are described in Chapter 4. This chapter includes an analysis of the test results with a discussion of the findings and their influence on the test arrangement of the Railway Test Facility (RTF).

Chapter 5 will begin with a detailed introduction to the RTF test set-up and adopted test procedure. This chapter will also include an analysis of the test results and a discussion of the findings.

A Network Rail commissioned field trial will be presented in Chapter 6. This will include a brief site introduction together with an analysis of the site results obtained. A discussion of the comparison of the field trial results with the experimental results from this project will complete the chapter.

Chapter 7 will present the development of a design method for reinforced rail track. The simplified elastic theory, as well as a full presentation of the evolution of the design guide will complete the chapter.

Last but not the least, this thesis will conclude with a presentation of the conclusions derived from the research performed in this project. This chapter will conclude with recommendations for future work.

2 LITERATURE REVIEW

1.1 Introduction

This literature review is divided into 5 main sections and begins with Section 2.2 exploring track components and their various functions, providing a basic understanding and appreciation of how a conventional rail track functions. Section 2.3 explores the material properties of ballast as well as highlighting the effects of external influences such as loading and fouling. This section will conclude with ballast deformation and its contribution to the overall track deterioration. Section 2.4 presents track geometry and track quality and it covers the various renewal techniques, track geometry measurement methods as well as quantification of track quality. Section 2.5 will be based on a review on the polymer geogrid. This literature review will conclude with a presentation of the behaviour of grid reinforced granular material layers with Section 2.6.

1.2 Track Components and Functions

The purpose of a modern railway is to provide economical and relatively rapid transportation. To achieve this, the railway track structure has to provide a safe and stable platform under stringent vertical and horizontal alignment constraints. It is therefore important to identify the specific roles that each different component plays and how they combine and perform as an entity.

A ballasted rail track is categorised by 2 main divisions of components: the superstructure and the substructure. The superstructure comprises the rails, fastening

system and the sleepers. The substructure covers the ballast, the sub-ballast and the subgrade. Figures 2.1 and 2.2 present the components of a conventional track.

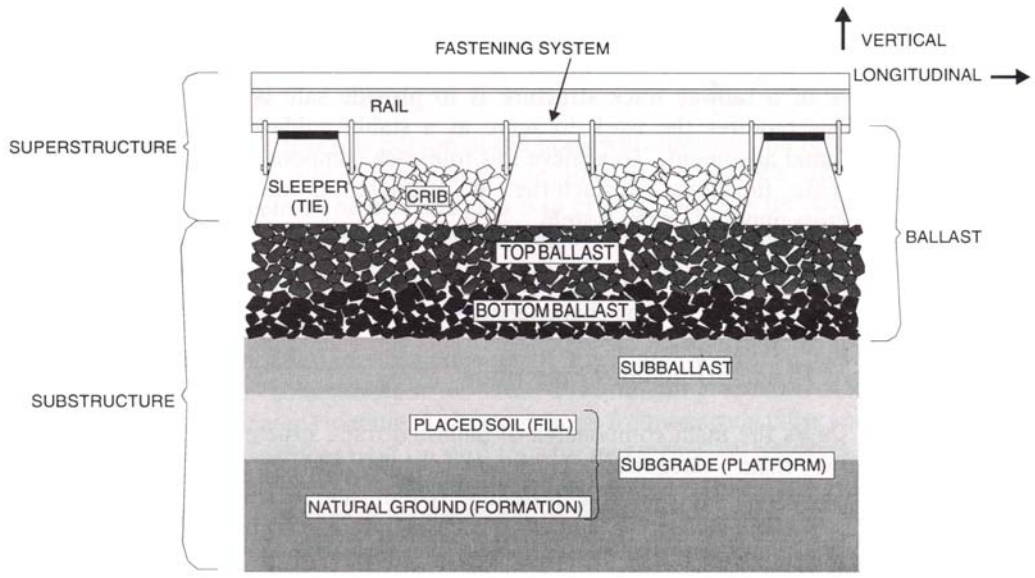

Figure 2.1 Components in a typical rail track (Selig and Waters, 1994)

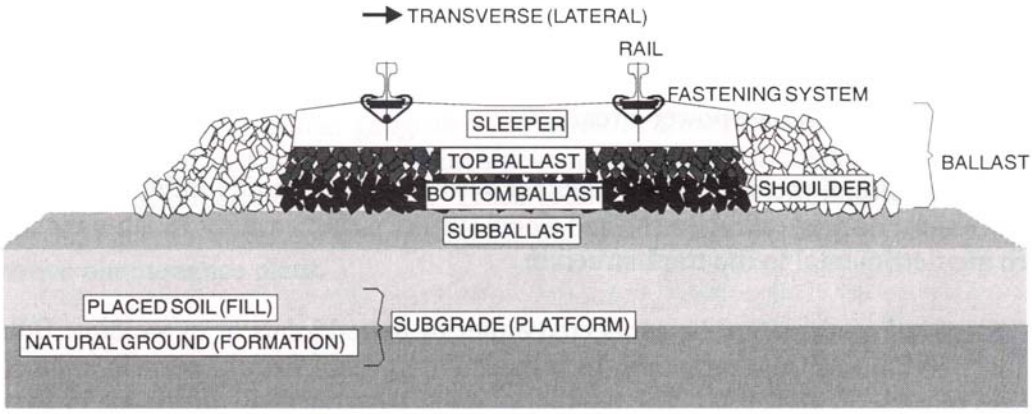

Figure 2.2 Cross sectional view of a typical rail track (Selig and Waters, 1994)

As an integral member of the superstructure, the main purpose of the rails is to guide train wheels. The rails are also the only part of the track component that comes into direct contact with the train. These longitudinal steel members must have sufficient stiffness to transfer the concentrated wheel loads onto the sleepers with minimum deflection between sleeper supports. In Europe, the axle load can often reach 22.5t and speeds up to 300km/hr. Hence the rails must be of certain dimensions and profile. The profile of the rail coupled with the profile of the wheel has a significant bearing on the ride quality. Defects in the profile of either entity can cause large dynamic loads which can compromise the track structure. One of the known problems is the uneven settlement of track which will be further discussed in this chapter.

The fastening system acts as a means of retaining the rails against the sleepers. The general functions and requirements of the fastenings are to absorb rail loads elastically and transfer them to the sleeper. The fastenings must be able to help the rails resist any vertical, lateral, longitudinal and overturning movements. The fastenings are also an aid to damp traffic vibrations, prevent or reduce rail/sleeper attrition as well as providing electrical insulation for track signals.

The general functions and requirements of the sleepers are to receive the rail loads and distribute them over the ballast. The sleepers also act as a restraint against any lateral, longitudinal and vertical rail movement through anchorage of the superstructure into the ballast. The sleeper must also be resistant to mechanical wear and weathering. The two most common types of sleepers are wood and concrete sleepers.

Ballast is the crushed granular material which is placed in the top layer of the substructure. These coarse grained materials are used to support and confine the sleepers, and to minimise any vertical and lateral movement transferred to the sleepers, and hence retain track position. The ballast material also reduces sleeper pressures and distributes it to the underlying materials, e.g. sub-ballast and subgrade.

Ballast also provides a certain amount of resilience as well as energy absorption for the rail track. The provision of large voids in the ballast layer facilitates the storage

of fouling materials (discussed in 2.3.5) as well as immediate draining of water from the track. More discussion on the ballast materials follows in Section 2.3.

Sub-ballast sits between the ballast and the subgrade material and is often referred to as the blanket layer. The role of these broadly-graded crushed natural aggregates or processed sand-gravel mixtures is very similar to that of the ballast. This is to reduce the traffic induced stress and distribute it to the subgrade. Sub-ballast also allows good drainage of water. One of the key functions of the sub-ballast layer is to prevent mixing of the subgrade and ballast. Some of the functions of the sub-ballast may be achieved through the use of sand, or geosynthetic materials such as membranes and filter fabrics (geotextiles).

The subgrade provides the platform on which the track is constructed. This formation must have sufficient bearing strength and stability as well as reasonable settlement behaviour. The lack of such quality is often the cause of many track defects. This will be discussed in depth under section 2.3.6.

1.3 Ballast

Traditionally, ballast has been used in rail track as it is relatively cheap and effective. As introduced in Section 2.2, ballast has many desirable qualities that make it an ideal material. Typically, crushed gravel, limestone, basalt and granite have been used for their various characteristics that include hardness, abrasion resistance, resistance to weathering action etc. However, there has not been universal agreement on the specification of the index characteristics such as size, abrasion resistance, hardness, angularity etc. The lack of such guidelines has hence resulted in a wide variety of materials used. In this section, the many aspects of how ballast functions on a rail track will be explored, and its resilient behaviour in the wider context of a granular material will be discussed. External forces on ballast and the effect on the material and on the rail track system as a whole will also be covered in this section.

2.3.1 Ballast Specifications

Ideally, ballast particles used for rail track should be hard, durable, have good angularity, chemical resistance and be free from dust. Typical ballast ranges from 20 to 50mm in diameter and its performance is governed by the physical characteristics as well as the packing assembly. No single characteristic controls ballast behaviour and many relevant characteristics are listed in Table 2.1. The United Kingdom follows the European railway ballast specification BS EN 13450 (2002). This specification requires the ballast to conform to the particle size distributions shown in Table 2.2. This standard comprises 5 properties which define the specification of track ballast: ballast grading, Los Angeles Abrasion (LAA), micro-Deval attrition, flakiness index, and particle length.

The LAA test measures a material toughness or tendency to break. The test measures the particle resistance to fragmentation with the provision of a Los Angeles Abrasion (LAA) coefficient. The LAA coefficient is the percentage of material passing through the 1.6mm sieve upon completion of the test. The LAA test involves rotating 10kg of dry ballast with 12 steel balls weighing a total of 5kg in a large steel drum. The dry ballast is subjected to 1000 revolutions with a rotational speed of 31-33 rotations per minute. The shelves inside the steel drums will pick up and drop the ballast at a distance almost equivalent to the drum diameter making the LAA a smashing test. The ballast is then sieved to achieve the LAA coefficient. A high LAA value signifies a brittle material. BS EN 13450 (2002) limits the LAA value to 20 (Lim, 2004).

In accordance with BS EN 13450 (2002), the Deval attrition test measures the particle resistance to wear with the provision of a Micro-Deval Attrition (MDA) coefficient. The Deval attrition test is very similar to the LAA test; however, the Deval attrition is a wet test in contrast to the dry LAA test. In the micro-Deval test, 2 specimens of dry ballast material, 5kg each, are segregated in two separate steel drums. Steel balls (9.5mm diameter) weighing a total of 5kg, smaller than those used in the LAA are also added into the steel drums together with 2 litres of water. 14,000 revolutions are then applied to the steel drums. The rotational speed is approximately 100 rotations per minute. The MDA coefficient is the percentage of material passing

through the 1.6mm sieve upon completion of the test. A high MDA coefficient indicates the ballast specimen is more susceptible to wear. BS EN 13450 (2002) requires the mean value of MDA to be less than or equal to 7 (Lim, 2004).

The flakiness index test measures the 'flatness' of a particle. The British Standard (British Standard 812, 1983) defines a flaky particle as one where the thickness to width ratio is less than 0.6. The flakiness index test involves 2 sieving operations. The first operation involves sieving the particles into various particle size fractions. The second operation involves sieving each fraction with bar sieves which have parallel slots of width 0.5 times that of the standard sieve. The flakiness index is defined as the percent by weight of flaky particles passing the bar sieve. BS EN 13450 (2002) indicates that the flakiness index shall be less than or equal to 35.

Particle length index is defined as the percent of particles with length equal or more than 100mm for a sample size exceeding 40kg. The test involves manual measurement of each particle. BS EN 13450 (2002) states that the particle length index shall be less than or equal to 4.

Table 2.1 Typical Ballast Characteristics

KEY CHARACTERISTICS	**BS EN STANDARDS/ SPECIFICATIONS**
DURABILITY	
Los Angeles Abrasion	BS EN 1097-2: 1998 / LAA index ≤ 20
Deval Abrasion (wet and dry)	BS EN 1097-1: 1996/ M_{DE} index ≤ 7
Crushing value	BS 812-111: 1990/ ACV ≤22%
SHAPE CHARACTERISTICS	
Flakiness/ Elongation/ Angularity or Particle Length (shape index)	BS EN 933-2/3: 1997/ Flakiness index ≤ 35 and Elongation index ≤ 50. Particle Length ≤ 4
GRADATION	
Size distribution	BS EN 933-2: 1996/ Size to be between 31.5mm to 50mm.
UNIT WEIGHT	
Particle density/ Water adsorption	BS EN 1097-6: 2000/ Specifications of categories in BS EN still not considered appropriate for rail track use
Bulk density and voids	BS EN 1097-3: 1998/ Not available
ENVIRONMENTAL	
Freeze-thaw breakdown	BS EN 1367-1: 2000/ Refer to BS EN 13450: 2002, Annex F
Sulfate soundness	BS EN 1367-2:1998/ Refer to BS EN 13550: 2002, Annex G
COMPOSITION	
Chemical analysis	BS EN 1744-1: 1998/ Not available

Table 2.2 Particle Size Distribution Specification
(RT/CE/S/006 Issue 3, 2000)

Square Mesh Sieve (mm)	Cumulative % by mass passing BS sieve
63	100
50	70-100
40	30-65
31.5	0-25
22.4	0-3
32-50	≥ 50

2.3.2 Track Forces on Ballast

To understand how ballast works in rail track, it is vital to understand the various types and magnitudes of forces that exist in a rail track. In general, the types of forces exerted on the track structure are classified as mechanical and thermal. In this section, the emphasis will be on the mechanical force on ballast.

There are two main mechanical/external forces acting on the ballast namely the vertical force exerted by passing trains onto the sleeper**,** as well as the plunging**,** squeezing and vertical action of tamping during maintenance work. The vertical force encompasses static and dynamic components. The static load consists of the dead weight of the superstructure and train whereas the dynamic load is a function of the speed of the train (Selig and Waters, 1994).

When the vertical force is applied, there will be a reaction at the rail-wheel contact point leading to the rail tending to lift up either side of the contact, as shown in Figure 2.3. With the advancing wheel, the uplifted sleeper will be forced down sometimes creating a high impact load onto the ballast particles and the track structure as a whole. The degree of impact is very much dependent on the train speed, load and padding support of the track. Selig and Waters (1994) stated that additional factors such as track condition, rail defects as well as track irregularity also affect the dynamic increment**.**

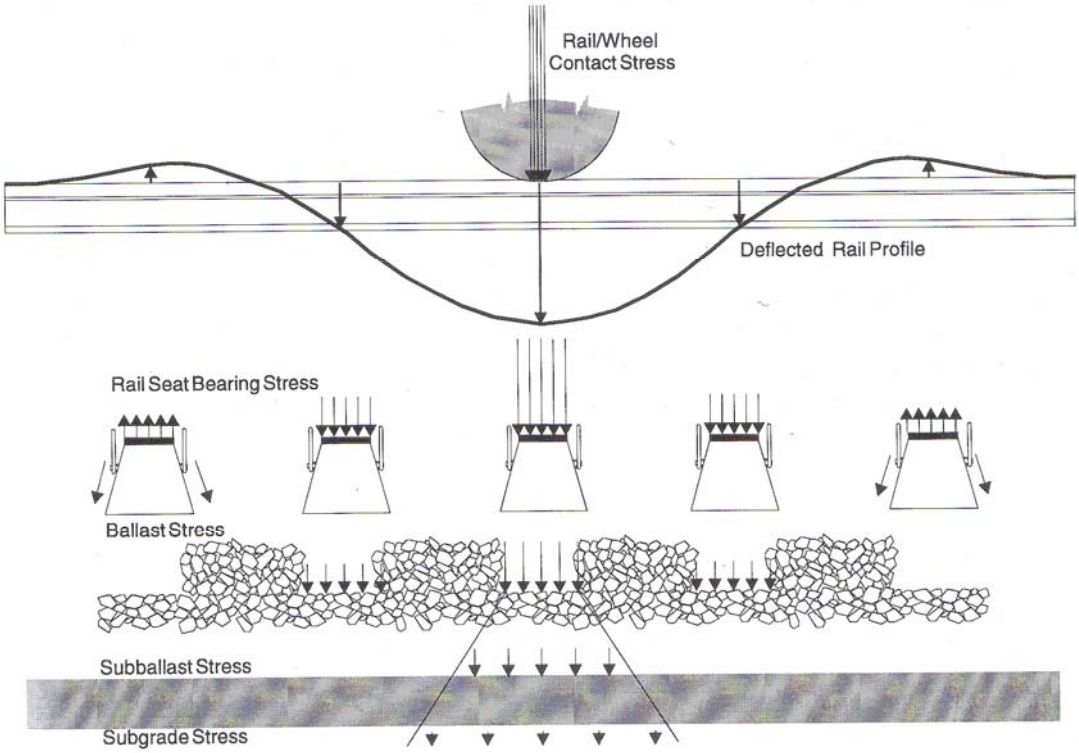

Figure 2.3 Uplift of rails (Selig and Waters. 1994)

Esveld (2001) concluded that the total vertical wheel load on the rail is made up of 4 main components

$$Q_{tot} = (Q_{stat} + Q_{centr} + Q_{wind}) + Q_{dyn} \qquad (2.1)$$

In which:

Q_{stat} : static wheel load = half the static axle load, measured on straight horizontal track;

Q_{centr} : increase in wheel load on the outer rail in curves in connection with non-compensated centrifugal force;

Q_{wind} : cross winds;

Q_{dyn} : dynamic wheel load components.

Selig and Waters (1994) stated that the vertical wheel force consists of a static component equal to the weight of the train divided by the number of wheels plus a

dynamic variance. This is similar to Esveld's definition. Selig and Waters further added vertical dynamic variation such as track geometry induced vehicle-rail interaction causing 'bounce' as well as the wheel impact forces caused by wheel flats or wheel/rail defects which can cause huge impacts and vibrations. The vibrations can contribute to powdering and shoulder flow of ballast.

Selig and Waters (1994) provided a good illustration that shows the effect of dynamic components on vertical loading. Vertical wheel load measurements from concrete sleeper sites in the United States, namely a Colorado test track and the main line between New York and Washington, were recorded with the help of strain gauges attached to the rail to measure the vertical force. Results are shown plotted in the form of cumulative frequency distribution curves in Figure 2.4. The statistical vertical axis represents the percent of the total number of wheel loads that exceed the corresponding wheel load given on the horizontal axis.

In the first example (a), the dynamic wheel load distribution is similar to the static wheel load distribution whereas in (b); the dynamic wheel load deviates significantly from the static load at the high end of the range. Passenger trains that travel at high speed caused large dynamic loads in 2% of the cases. As such, it can be concluded that a high dynamic load is caused by a high train speed, which in turn exerts a high stress onto the ballast material causing possible breakage of material.

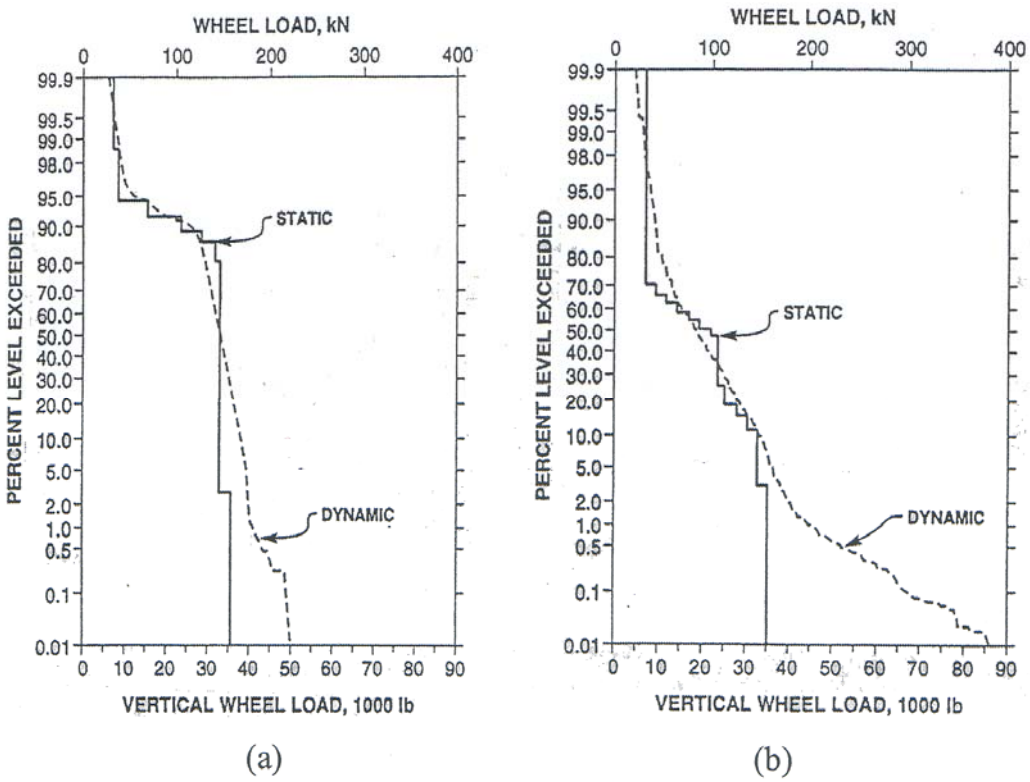

Figure 2.4 Static and dynamic wheel loads plotted in the form of cumulative frequency distribution for (a) Colorado Test Track and (b) Main line Track between New York and Washington (Selig and Waters, 1994)

The other very significant track force on the ballast is achieved through 'squeezing' the ballast. This can be credited almost solely to the tamping procedure. Ballast tamping has been recognised as the most effective method to correct and restore track geometry. Not surprisingly, it is also the most common railway maintenance technique used today. The tamping procedure includes lifting the rail and inserting tines which will vibrate and move towards each other, 'squeezing' the ballast underneath the sleeper into position. The high squeezing and plunging force often causes material breakage and this is known to be the most destructive element in railway operation in terms of ballast deterioration, even more than that due to a high speed train (Wright, 1983). Figure 2.5 illustrates the tamping procedure.

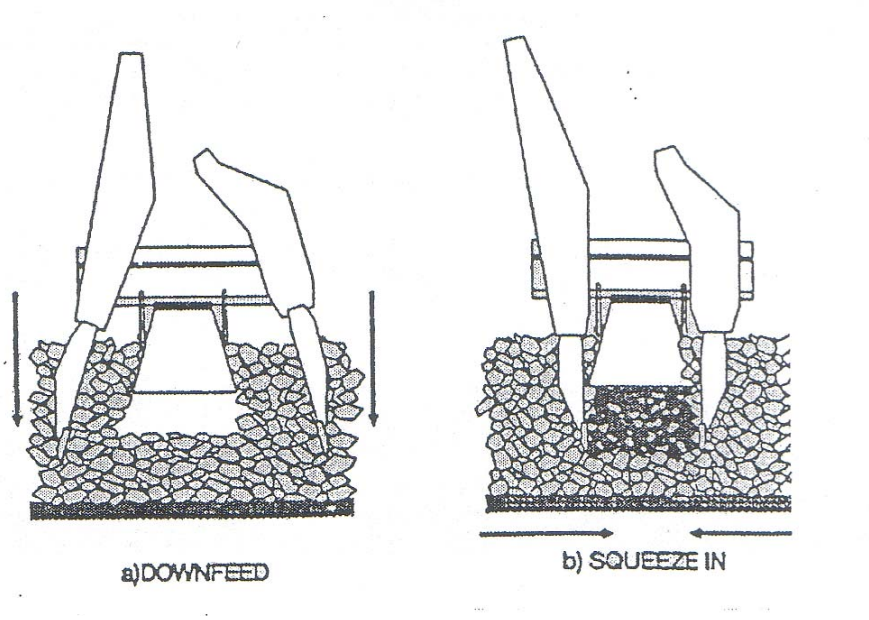

Figure 2.5 Tamping procedures (Selig and Waters, 1994)

2.3.3 Resilient Behaviour of Granular Material

The understanding of the behaviour of granular material plays a very important role in the modern railway system. The deformation response of granular material under repeated loading is commonly characterised by a residual (permanent) deformation as well as a recoverable (resilient) deformation which will be discussed in this section of the literature review. The behaviour of a granular material under repeated loading is non-linear and is stress dependent. The magnitude of plastic strain per cycle generally decreases with the number of load cycles and the difference between the maximum strain under peak load and the permanent strain after unloading for each cycle is known as the resilient strain. It is important to understand the non-linearity behaviour of granular material as it affects the stress condition and ultimately settlement behaviour. Since 1960, there have been numerous research projects committed to characterizing the resilient behaviour of granular materials. The resilient modulus as defined by Seed et al (1962) is the repeated deviator stress divided by the recoverable (resilient) axial strain during unloading in a triaxial test. It is vital to have a good understanding of the resilient behaviour of the trackbed material as this is known to have an effect on the degradation and rate of settlement of the rail track. From the literature, it is widely agreed that the behaviour of granular material may be affected, with varying degrees of importance, by various conditions

and factors that will be discussed later in this section. Figure 2.6 illustrates the typical strain in a granular material.

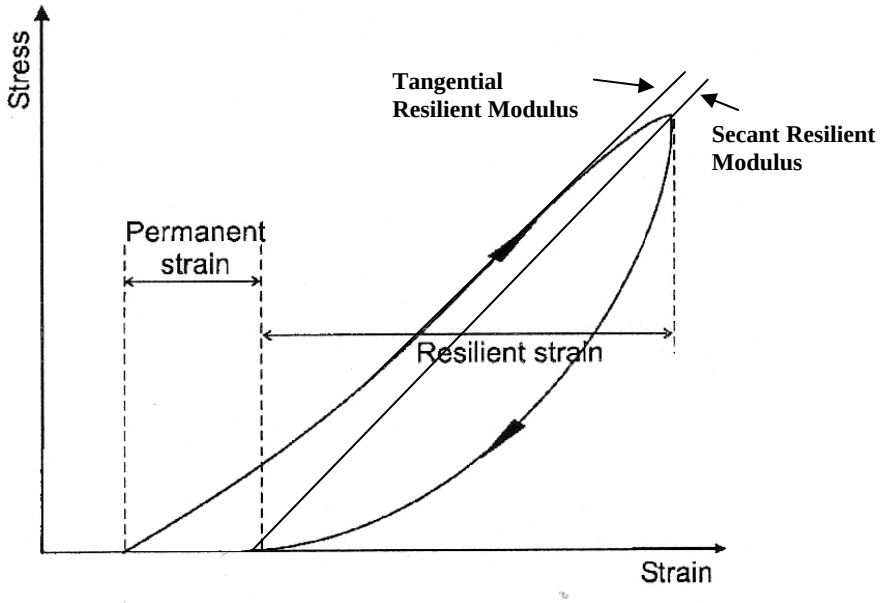

Figure 2.6 Strains in granular material during one cycle of load application (Wright, 1983)

Effect of Stress

From the early investigations by Williams (1963) until the more recent studies by Kolisoja (1997) all researchers, have, without fail, emphasised the importance and the magnitude of influence that stress level has on the resilient behaviour of granular material. It is worth noting that numerous works [e.g. Miltry (1964), Monismith et al. (1967), Hicks (1970), Smith and Nair (1973), Uzan (1985) and Sweere (1990)] show the sizable influence of confining pressure and the sum of principal stresses on the resilient behaviour of granular material. Monismith et al (1967) stated that a change from 20 to 200kPa in the confining pressure would result in an increase of 500% in the resilient modulus. In a separate test, Smith and Nair (1973) reported an increase of 50% in the resilient modulus when the sum of the principal stresses increased from 70 to 140kPa (See Lekarp et al. 2000). Shenton's (1974) results from a series of

tests on ballast using an Instron test machine also showed that there is a tendency for the resilient modulus to increase with increasing confining stress. It is also worth noting that in a study conducted by Morgan (1966), the resilient modulus was shown to decrease with increasing deviator stress under constant confinement. Clearly, compared to confining pressure, deviator stress has less influence on the resilient behaviour of granular material.

Effect of Aggregate Type and Particle Shape

Heydinger et al. (1996) has claimed that gravel, when compared to crushed limestone exhibits a higher resilient modulus. This is in direct contradiction to the majority of other researchers, [e.g. Hicks (1970), Hicks and Monismith (1971), Allen (1973), Allen and Thompson (1974), Thom (1988), Barksdale and Itani (1989), Thom and Brown (1989)] who reported that crushed aggregate, with its increased angularity, demonstrates better load spreading capability and a higher resilient modulus than uncrushed gravel with its rather characteristically rounded aggregate. Barksdale and Itani (1989) in particular, tested various types of granular material with the same grading and found a 50% increase in resilient modulus of angular material at low mean normal stress condition compared to that of rounded gravel (see M. Karasahin 1993). In addition, Thom (1988) and Thom and Brown (1989) performed repeated load triaxial tests on different granular materials and found that at low strain, the resilient modulus of granular material may be influenced by particle texture and that a correlation exists between elastic stiffness and surface friction of a material.

Effect of Moisture Content

It is generally agreed in the literature that the moisture content of granular material will have an effect on the resilient behaviour of the material. Smith and Nair (1973) and Vuong (1992) established that the resilient response of dry and most partially saturated granular material is similar; however, the resilient response will be affected significantly as the material approaches saturation. Researchers down the years [e.g. Haynes and Yoder (1963), Hicks and Monismith (1971), Barksdale and Itani (1989),

Dawson et al. (1996) and Heydinger et al. (1996)] have all commented on the considerable dependence of resilient modulus on moisture content at high levels of saturation. Haynes and Yoder (1963) in particular, reported a 50% reduction in resilient modulus with an increment in the degree of saturation from 70% to 97%. This is especially relevant to the working condition of ballast material in the rail track system where an excessive amount of water is often found within the granular layer. Under repeated loading, saturated granular materials will develop excess pore water pressure that will reduce the effective stress in the material and consequently give a reduction in both its strength and stiffness. It may be argued that it is essentially the pore water pressure that ultimately affects the resilient deformation of the material rather than the water moisture content. Thom and Brown (1987) suggested that the presence of moisture, even in the absence of any pore water pressure, is still capable of increasing the deformation in the aggregates, giving a reduced resilient modulus. They assigned this to the lubricating effect of moisture on the particles. This is confirmed by a series of repeated load triaxial tests on a crushed rock with variable moisture content. Using drained tests and loading frequencies between 0.1 to 3 Hz, in the apparent absence of pore water pressure up to 85% saturation, there was a reduction in the resilient modulus with increasing moisture content. For the benefit of this thesis however, it must be noted that ballast material, especially on a rail track, never gets saturated.

Effect of Stress History and Number of Load Cycles

It is widely reported in literature that stress or loading history exerts a certain degree of influence over the resilient behaviour of granular material. For example, Boyce (1976) reported a series of repeated load triaxial tests on samples of well-graded crushed limestone of the same compaction and density characteristics in a dry state, which reinforced that belief. In Boyce's account, the results indicated that the material was subjected to effects of stress history that could be reduced by a preloading regime. Hicks (1970) concluded that the effect of stress history could be nearly eliminated and a constant resilient response could be achieved after a 100-cycle application of the same stress amplitude. However, Hicks' (1970) observations were challenged by Boyce (1976) who claimed that it will take approximately 2000

cycles before the resilient strain reaches a steady value. Shenton (1976) put this number closer to 1,000 cycles.

Effect of Aggregate Type and Particle Shape

The general view regarding the effect of aggregate type is that crushed aggregate with its angular shape compared to rounded aggregate has a higher resilient modulus with a better load spreading capability. According to Barksdale and Itani (1989), the resilient modulus of rough, angular crushed material compared to that of rounded gravel, with the same grading, was found to be higher by a factor of 50% at low mean normal stress and about 25% at high mean normal stress. However, it is important to note that the effect of aggregate type is only apparent when other parameters such as grading, density and applied stresses are kept constant (M. Karasahin, 1993).

Effect of Load Duration and Load Sequence

There is widespread agreement among researchers that load duration and frequency has little or no impact on the resilient behaviour of granular material. [e.g. Seed et al. (1965), Morgan (1966), Hicks (1970), Boyce et al. (1976) and Thom and Brown (1987)]. Seed et al. (1965) reported in his account that the resilient modulus of sand showed a modest increase from 160 to 190 MPa when the loading duration was decreased dramatically from 20 minutes to 0.3 seconds. Hicks (1970) complemented these observations by conducting tests at stress durations of 0.1, 0.15 and 0.25 seconds, which again showed no change in the resilient modulus or Poisson's ratio. Hicks (1970) and Allen (1973) reported that the test sequence has relatively little impact on the resilient properties of granular material when they subjected their specimens to various test sequences and orders in which stress was applied.

Computational Modelling of Resilient Response

One of the most simplified methods in dealing with the effect of stress on material stiffness is the expression of resilient modulus as a function of the sum of the principal stresses commonly known as the *K*-θ model:

$$M_r = k_1\theta^{k2} \qquad (2.2)$$

Where M_r = resilient modulus;

Seed et al. (1967), Brown and Pell (1967), and Hicks (1970) suggest the above hyperbolic relationship due to its simplicity. This model has been extremely useful and is widely accepted for analysis of the stress dependence of material stiffness. However, a major set back for this model is that it assumes a constant Poisson's ratio, which is used to calculate radial strain. Studies by Hicks (1970), Hicks and Monismith (1971), Brown and Hyde (1975), Boyce (1980) as well as Kolisoja (1997) have shown that Poisson's Ratio varies with applied stress. However, this model has undergone many modifications that can be found in the literature.

2.3.4 Permanent Strain Behaviour of Granular Material

The irrecoverable strain of granular material as shown in Figure 2.6 is often a trigger for maintenance activities on a rail track. On a rail track, the accumulation of such permanent strain is due to the rearrangement of particles as well as particle breakage.

Effect of Stress

From the literature available, it is evident that stress level is one of the most important factors governing the development of permanent deformation in granular materials. Morgan (1966) reported that the accumulation of axial permanent deformation is related to deviator stress and inversely linked to confining pressure.

(Knutson (1976) reported that the permanent strain accumulated over a certain number of load cycles is directly related to the stress ratio, defined as the ratio of deviatoric stress q to confining stress σ_3. According to his report, increasing the stress ratio q / σ_3 will result in the increase in permanent strain as shown in Figure 2.7. The figure also shows that for the same stress ratio, (i.e. 20/5 and 60/15) increasing the stress path length will increase the amount of permanent strain. Lashine et al. (1971) investigated this through repeated load tests on crushed stones and found comparable relationship between the measured axial deformation and the ratio of deviator stress to confining pressure. Brown and Hyde (1975) also reported similar findings.

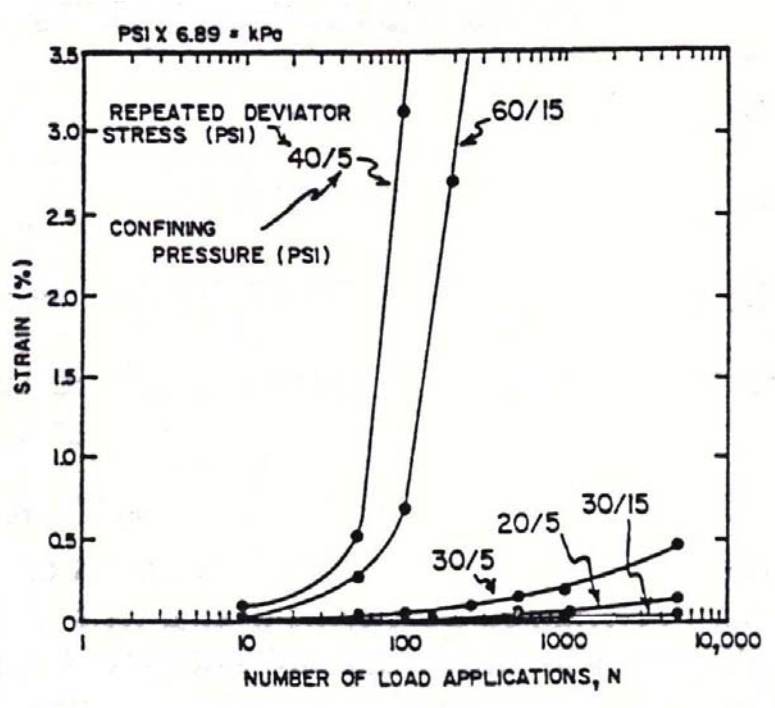

Figure 2.7 Effect of stress ratio on permanent strain (Knutson, 1976)

Effect of Number of Load Applications

The increase in the permanent deformation in granular material is a gradual process with each load application contributing to an increment of strain. In the context of a railway line, each passing axle of the train acts as a load that will in turn induce strain causing permanent deformation. With reference to the literature, the significance of the number of load cycles is well documented by many prominent

researchers, with many varying observations. Several researchers [e.g. Morgan (1966), Barksdale (1972), Sweere (1990)] have indicated continuously increasing permanent strain under repeated loading. In Morgan (1966)'s account, he noted increasing permanent strain even after 2,000,000 load cycles. This was challenged by Brown and Hyde (1975), who noted an equilibrium state after only 1,000 load applications. In Shenton's (1974) account, he claimed that the first load cycle produced a very large permanent settlement with subsequent settlement proportional to the logarithm of the number of load cycles (see Figure 2.8). Shenton's (1974) work was based on triaxial testing on ballast particles. Paute et al. (1996) stated that there will be a decrease in the rate of permanent deformation in granular material under repeated loading and that it is possible to derive a limit value for the accumulation of permanent strain.

Lekarp (1997) and Lekarp and Dawson (1998) extended the statement by Paute et al. (1996) suggesting that this will be achieved only when the applied stress is low. In Kolisoja's (1998) work which involved testing at a large number of cycles, he revealed that a material which may appear to be stable will have the tendency to further deform through the application of further loading. In it, he added that the permanent strain response of granular material must be treated as a complex problem but did not expound on it.

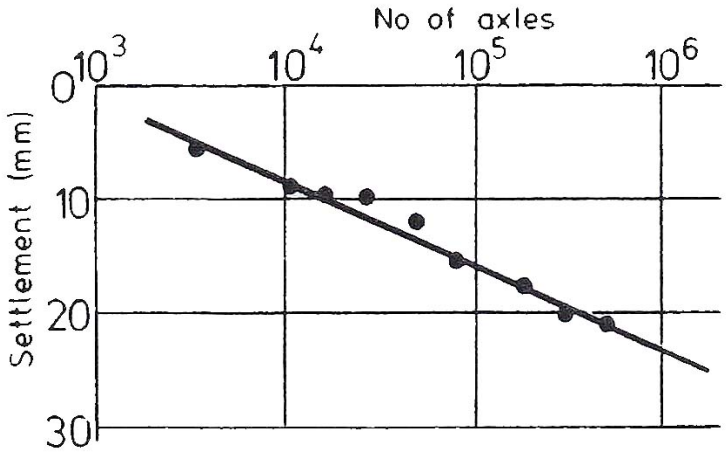

Figure 2.8 Effect of repeated load applications

on settlement (Shenton, 1974)

Effect of Moisture Content

The presence of moisture in granular material has both merit and disadvantage. On the one hand, an adequate amount of water may produce negative pore water pressure that in turn increases the stiffness and strength of unbound granular material. On the other hand, as saturation approaches, excessive pore water pressure reduces the effective stress and results in a poorer permanent deformation resistance.

Haynes and Yoder (1963), Barksdale (1972), Maree et al. (1982), Thom and Brown (1987), Dawson et al. (1996) all agree that a combination of high saturation and poor permeability, due to poor drainage, can lead to a reduced stiffness and poor permanent deformation resistance (Lekarp et al. 2000). In fact, this is the reason why many railway lines require more maintenance work, due to the resulting permanent deformation, than initially expected. Haynes and Yoder (1963) reported an increase of more than 100% in deformation with a 20% increase in saturation from 60% to 80%. Barksdale (1972) also observed an increase of up to 68% permanent axial strain in a soaked sample compared to a semi-drained one. According to Thom and Brown (1987), a relatively small amount of water can trigger a huge increase in the permanent strain even in the absence of excess pore water pressure. This, they put down to the lubricating effect of water in the granular assembly. Figure 2.9 illustrates the effect of drainage on permanent strain development in granular materials. It must be noted that the results should in Figure 2.9 is true for the material tested but not for ballast.

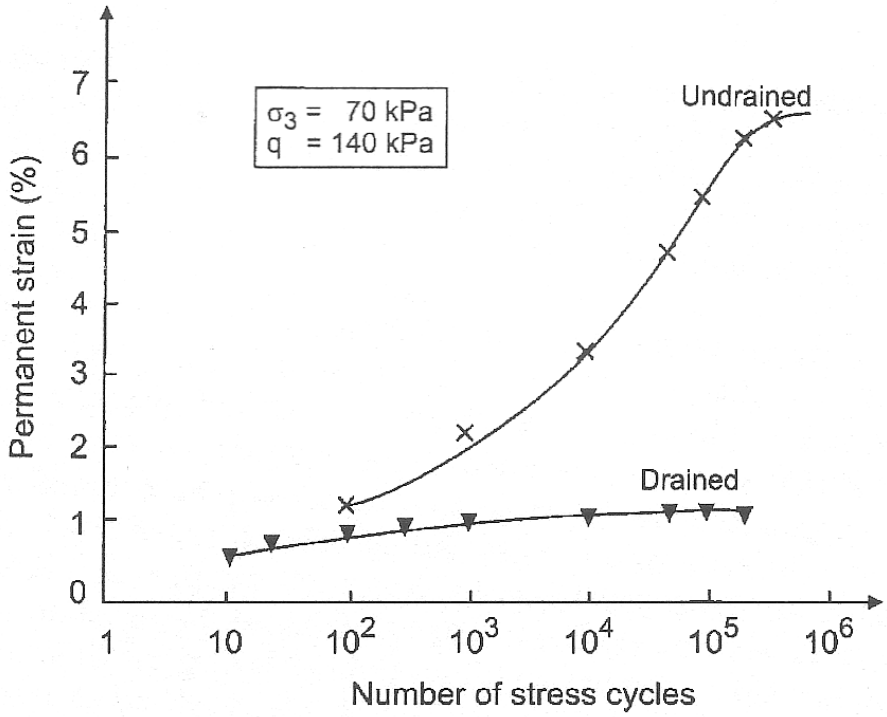

Figure 2.9 Influence of Drainage on Permanent Deformation Development (Thom and Brown, 1987)

Effect of Stress History

Brown and Hyde (1975) showed in their research that the permanent deformation behaviour of granular material is related to its stress history (order of the application of loads). In it, they showed that permanent deformation in a granular material is much higher when full load is applied immediately rather than when it is increased in successions. Lekarp et al. (2000) state that when repetitive loads are applied, the effect of stress history appears as a result of gradual material stiffening by each load application, causing a reduction in the proportion of permanent to resilient strains during subsequent loading cycles. The effect of stress history has not been well explored even though it is well documented in the literature. More work has to be done to quantify this effect.

Effect of Density

The effect of density, often described in conjunction with the degree of compaction in a material, is reported by many sources as a very important factor for the long-term behaviour of granular material. Resistance to permanent deformation under repeated loading is improved with increased density. Allen (1973) reported an 80% and 22% reduction in permanent strain, in crushed limestone and gravel respectively, when the material density was increased from Proctor to modified Proctor density (90% – 92% of modified Procter density is equivalent to the specified 95% standard Procter density except for fine sand where the difference is bigger). Holubec (1969) added that this effect of density on permanent strain is particularly apparent in angular material if there is no accompanying transient pore pressure during loading. In the case of rounded particles, e.g. gravel, the effect is deemed to be less significant due to the fact of its initially higher relative density for the same compactive effort.

2.3.5 Ballast Fouling

The life and performance of the railway track is very much dependant on the ballast layer. The ballast layer is subjected to deformation and degradation during traffic loading. Various sources of ballast fouling have been identified and in Selig and Water's (1994) account, they have listed the 5 main sources of ballast fouling.

I) Ballast Breakdown
II) Infiltration from ballast surface
III) Sleeper wear
IV) Infiltration from underlying granular layers
V) Subgrade infiltration

In most literature, it has been widely agreed that ballast breakdown is the major source of ballast fouling. This is quantified in Figure 2.10 based on a study by the

University of Massachusetts. The report from the University of Massachusetts is based on a variety of mainline track conditions across North America.

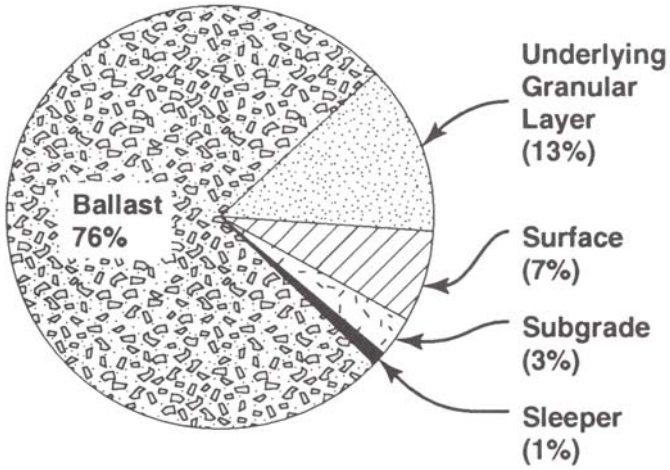

Figure 2.10 Major source of ballast fouling (Selig and Waters, 1994)

Selig (1985) and Meeker (1990) reported that the initial stage of ballast breakage occurred during transportation and construction work. Selig and Waters (1994) expected 1 to 2% of the weight of fouling material to accumulate when new ballast is placed. Fouling materials are deemed as particles of less than 6mm diameter. Selig and Waters (1994) summarised the sources of fouling in Table 2.3.

Ionescu (2004) investigated the mechanical degradation of a rail track. He reported that the volume of voids in a newly constructed track was around 45%. When the rail track settles under cyclic train loading, the ballast grains rearrange into a denser packing reducing the volume of voids. At this stage, ballast crushing takes place at contact points of the coarser grains resulting in loss of corners and sharp edges which will be collected as fines in the voids. This grain rearrangement will carry on with additional ballast crushing with further traffic loads.

Table 2.3 Sources of ballast fouling
I. Ballast breakage a) Handling (related to IIA) 1) At quarry 2) During transporting 3) From dumping b) Thermal stress from heating (desert) c) Chemical weathering (inc. acid rain) d) Tamping damage e) Traffic damage 1) Repeated load 2) Vibration 3) Hydraulic action of slurry
II. Infiltration from ballast surface Delivered with ballast Dropped from trains Wind blown Water borne Splashing from adjacent wet spots
III. Sleeper wear
IV. Infiltration from underlying granular layers Old track bed breakdown Subballast particle migration from inadequate gradation
V. Subgrade infiltration

In Ionescu (2004)'s account, he did not investigate the contribution of rail track maintenance work, e.g. tamping. Wright (1983) conducted several studies on the effect of tamping on ballast degradation. In his research conducted at British Rail Research, he found that approximately 2 to 4 kg of fines less than 14mm was generated with a single tamp on a single sleeper. This is a substantial output from a

single activity and Table 2.4 shows the British Railway Research representative estimate of tamping on overall track fouling. The British classified any material less than 14mm in size to be fouled material. This is likely to be one of the reasons that caused the discrepancy in source of ballast fouling compared to the report from the University of Massachusetts (see Figure 2.10).

Table 2.4 British Railways source of fouling

No.	Source	Degradation	
		kg/sleeper	% of total
1.	Delivered with ballast (2%)	29	7
2.	Tamping: 7 insertions during renewal and 1 tamp/yr for 15 years	88	20
3.	Attrition from various causes including traffic and concrete sleeper wear (Traffic loading: 0.2kg/sleeper/million tons of traffic, MGT)	90	21
4.	External input at 15kg/yr (Wagon spillage : 4.0kg/ sq m/yr) (Airborne dirt: 0.8kg/ sq m/yr)	225	52
	Total	432	100

2.3.6 Ballast deformation and track settlement

According to Dahlberg (2001), most descriptions of track settlement found in the literature are empirical. He added that track settlement is mostly considered to be a function of the magnitude of loading or a function of loading cycles. Properties of ballast and subgrade materials should be added into the model.

Railway track will settle due to the permanent deformation of ballast and the subgrade. Traffic loading is the main cause for settlement and the intensity is often governed by the quality and behaviour of ballast, sub-ballast and the subgrade.

According to Dahlberg (2001), track settlement occurs in two phases:

1 Immediately after tamping where rate of settlement is fast until consolidation.

2 Settlement with time in an approximate linear relationship.

The second phase of settlement is governed by several basic ballast and subgrade behaviour mechanisms:

1. Continuation of volumetric densification caused by repeated train loading.

2. Ballast material penetrates/sinks into the sub-ballast and subgrade.

3. Ballast breakage from train loads and environmental factors (see Table 2.3) causing volumetric reduction i.e. particle divided into two or more smaller pieces resulting in better compaction.

4. Volume reduction due to abrasive wear. Particles diminish in volume upon abrasive contact with other particles.

5. Inelastic recovery due to micro-slip between ballast particles at loading. Deformation will not be fully recoverable upon unloading.

6. Lateral movement of ballast or subgrade particles will result in the sleeper sinking deeper into ballast layer.

7. Lateral and longitudinal (in the direction of rail), movement of sleeper creating the ‘pushing’ effect of ballast. Sleeper will sink deeper into the ballast layer.

Cause of Vertical Track Deterioration

Deterioration of the vertical geometry on a railway track is commonly understood to be mainly caused by the differential settlement of the ballast layer as well as the subgrade. According to Shenton (1985), there are several mechanisms of deterioration which can all take place simultaneously creating differential settlement:

(a) Dynamic Forces/ Wheel Irregularities

Due to irregularities over the running surface or irregularities in the vertical geometry, the vertical wheel load will vary continuously over a length of track. This will lead to irregular impact loads and cause sleepers at different locations to deform at a different pace even when the ballast bed is uniform and the subgrade condition is comparable over the length of track.

(b) Rail Shape

Defects in the longitudinal shape of the rails (lack of straightness) can arise during manufacture or during the installation of the rail. Even with a constant axle load and a uniform trackbed the lack of straightness of the rail can cause sleepers to carry different loads leading to differential settlement of the ballast or track.

(c) Sleeper Spacing

This mechanism is deemed as the least likely to influence differential settlement on track. This is due to the tight guidelines and limits placed on sleeper spacing criteria. However, where sleeper spacing is not consistent throughout the track, individual sleepers will transmit varying loads onto the ballast layer which will in turn create differential settlement over the length of track.

(d) Sleeper Support

A sleeper with a stiffer support will carry more loads than the adjacent sleeper on a softer support. The sleeper with the softer support will have a tendency to settle more.

(e) Ballast Settlement

Ballast is a random arrangement of stones and the lack of homogeneity will cause an irregular distribution of load, creating uneven settlement. Various factors can contribute to the differential movement such as the variability of subgrade and maintenance activities i.e. tamping, which will be dealt with later in this section.

(f) Substructure

The final contribution to differential settlement according to Shenton (1985) comes from the deeper ballast, sub-structure layers and from the subgrade. This is deemed to have very little short term effect as most tracks have an adequately designed foundation.

Settlement Models

Sato (1995)'s expression of track settlement y under repeated loading x is expressed in the form:

$$y = \gamma (1 - e^{-\alpha x}) + \beta x \qquad (2.3)$$

Where x = loading of the track either expressed as a number of load cycles or as tonnage carried by the track (see Figure 2.11). The constants γ, β and α are parameters describing the short-term and long term settlement behaviour.

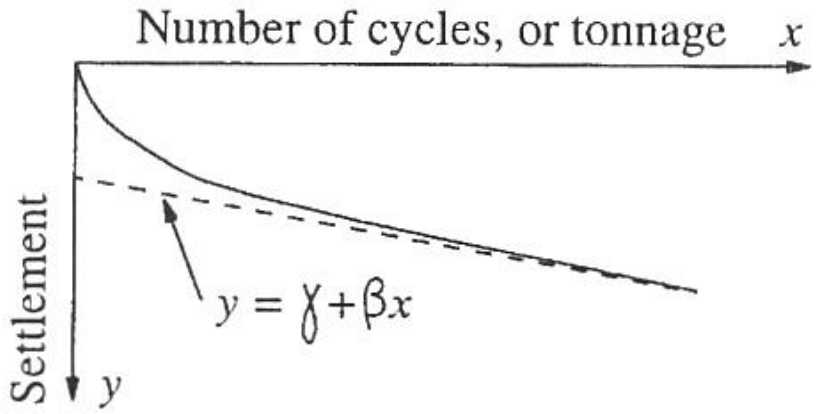

Figure 2.11 Track settlements as a function of x (Sato, 1995)

Sato (1995)'s model is divided into two phases. The first part of the equation represents the initial settlement phase while the second part represents the long term settlement. This is in agreement with Dahlberg (2001)'s observation.

Using this formulation, no distinction between the loading cycles of different magnitudes can be made. Only the mean value of the magnitude of loading is being deployed. This is in contradiction with other findings e.g. Brown and Hyde (1975) that the permanent deformation behaviour of granular material is related to its stress history.

In Sato (1995)'s expression, $\gamma (1 - e^{-\alpha x})$ describes the short-term settlement effect immediately after tamping and γ indicates its severity. The factor α indicates the rate at which the initial settlement attenuates. Long term settlement is denoted by βx. The factor β indicates the severity of settlement, which is proportional to the loading x.

In the same paper, Sato (1995) presented a model which considers the growth of track irregularities. Interestingly, a subgrade factor is included. Sato's (1995) model includes five parameters which account for major sources of track irregularities:

traffic tonnage T (million tonnes per year), the average running speed v (km/h), the structure (via a structure factor M), the rail (via a factor L) and the subgrade (via a factor P). S denotes the irregularity growth equation (S in mm per 100 days).

$$S = \text{constant} \times T^{0.31} M^{1.1} L^{0.21} P^{0.26} v^{0.98} \qquad (2.4)$$

As can be seen, irregularity in this model is almost proportional to the mean speed of the train and proportional to the third root of the applied tonnage. The structure factor M is dependent on the quasistatic ballast pressure, train acceleration and impact factor, dependent on rail properties. Rail properties are covered by L.

He concluded from his measurements that a poor subgrade (adhesive soil) settles twice as fast as good subgrade (sandy soil). He did not however, provide more explanation in what he constitutes to be a poor and good subgrade. Sato added that the growth of track irregularities with a 60kg/m rail is 70% of that with a 50kg/m rail. The higher bending stiffness of the rail will allow a better distribution of load over the sleepers, resulting in a lower sleeper pressure on the ballast, thus less settlement. This is in accordance with most of the literature.

Alva-Hurtado and Selig (1981) developed a methodology based on the assumption that ballast deformation starts from an uncompressed state. The model, gives total permanent strain ε after N cycles:

$$\varepsilon = \varepsilon_1 [1 + C \log (N)] \qquad (2.5)$$

The model is based on identical loading cycles. ε_1 denotes the permanent strain after the first cycle and C is a dimensionless constant denoting the rate of growth of settlement. Selig and Waters (1994) reported typical value of C to be 0.2 and 0.4. This simplified model is based on the assumption of identical loading cycles (i.e.

same amplitude). This can be converted to settlement, y, taking an average value multiplying it by the thickness of the ballast layer (see Figure 2.13).

The authors claimed that the increase in plastic strain is directly proportional to the ratio of maximum applied deviator stress to failure deviator stress. Figure 2.12 shows representative results of a constant-amplitude load test with full unloading.

Based on a comparison done by Dahlberg for equation 2.3 from Sato (1995) and equation 2.5 from Alva-Hurtado and Selig, there are major differences in the modelling of long term settlement. The discrepancy is shown in Figure 2.13.

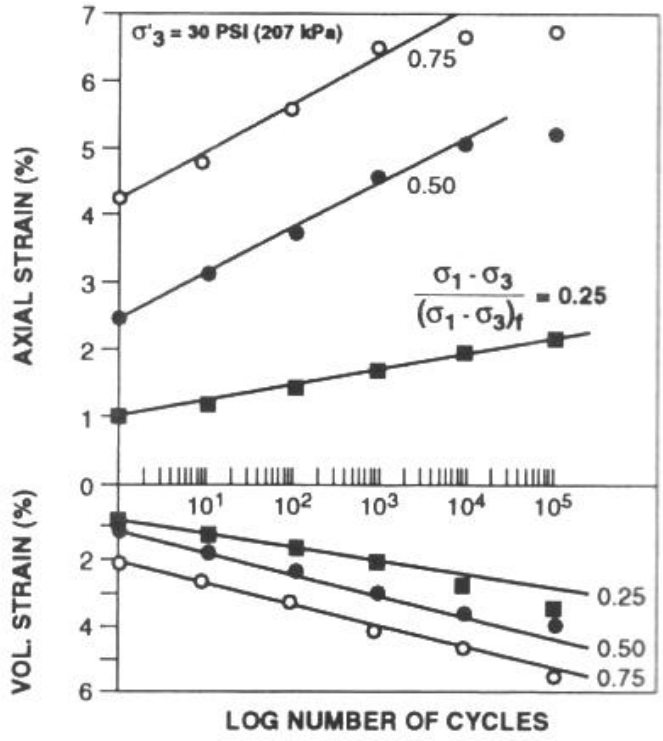

Figure 2.12 Strain response of dolomite ballast (Selig and Waters, 1994)

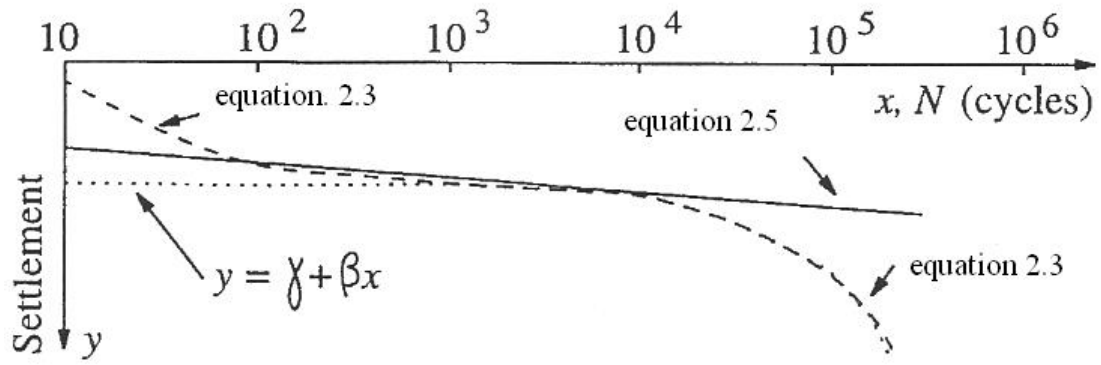

Figure 2.13 Comparison of track settlement (Dahlberg, 2001)

As seen in Figure 2.13, the discrepancy between the two models can be large especially after a large number of loading cycles. As observed by Dalhberg (2001), the difference can be as large as 100% at 200 000 cycles when the parameters are chosen to give good agreement at N= 500, 5000 and 10,000 cycles.

ORE (Office for Research and Experiments) of the International Union of Railways (UIC) presented their model as shown in equation 2.6, to estimate track settlement. Like Sato (1995), their model is based on two phases. The first phase represents the settlement immediately after tamping (denoted by e_0). The second part includes deterioration dependent parameters of traffic volume T, dynamic axle load $2Q$ and speed v.

$$e = e_0 + h\mathrm{T}^{\alpha}(2Q)^{\beta}\mathrm{v}^{\gamma} \qquad (2.7)$$

Again h is a constant while parameters α, β and γ are evaluated from experimental data. The lack of experimental data provided calls into question the validity of this model. It is also noticed that no track parameters are involved in this settlement model.

Shenton (1985) argued that logarithmic settlement laws, (i.e. Alva-Hurtado and Selig's (1981) proposal shown in equation 2.5) tend to underestimate settlement in the event of large numbers of loading cycles. Based on laboratory and field results

shown in Figure 2.14, he claimed that the best approximation can be obtained when the settlement is considered to be proportional to the fifth root of the number of load application. The best fit comes in the form

$$S = K_1 N^{0.2} + K_2 N \qquad (2.8)$$

where $K_1 N^{0.2}$ predominates for values of N up to 10^6 and $K_2 N$ will be relevant only above this value.

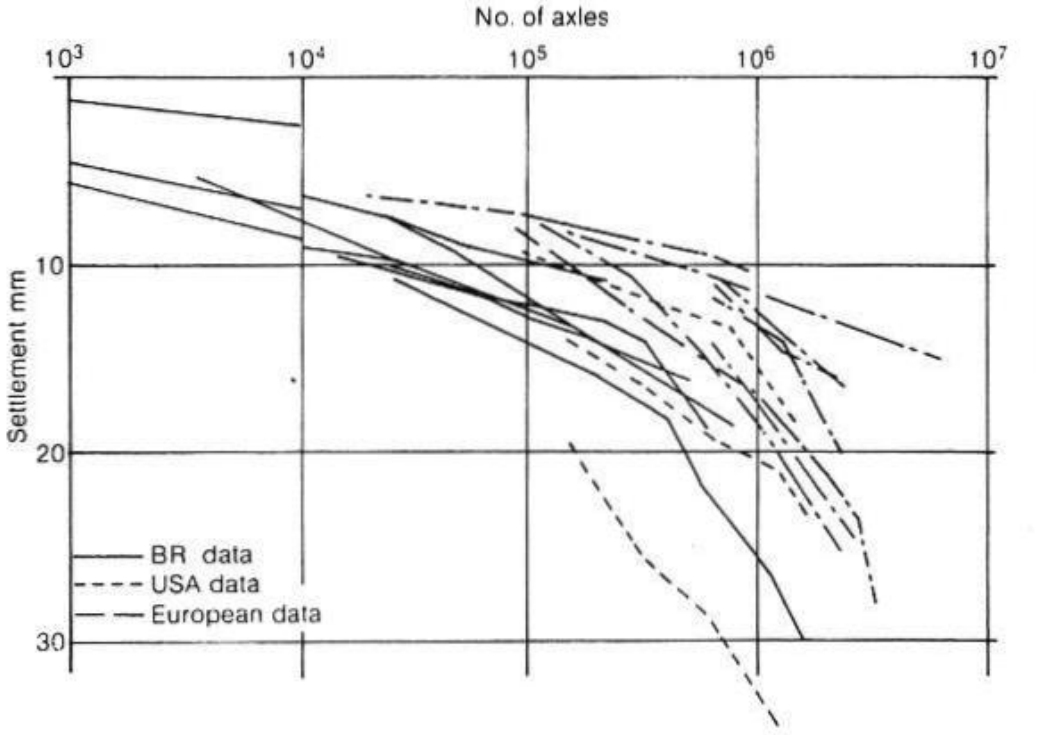

Figure 2.14 Settlement of test sites (Shenton, 1984)

Shenton (1985) stated that the factors K1 and K2 are dependent on axle load, rail section, sleeper spacing and foundation stiffness. He added that axle load is likely to be a key factor in track settlement.

2.4 Track geometry and track quality

According to Selig and Waters (1994), there is considerable evidence that ballast is the primary cause of differential settlement between maintenance operations. They termed it short term settlement as opposed to long term settlement which is subgrade related. Tamping is the surfacing operation known to have the most effect on rail track short term settlement.

Routine maintenance done on railway lines is mainly executed by tamping. For the mechanism of tamping see Section 2.3.2. Upon rectification of track geometry via tamping, deterioration is known to happen very rapidly with initial traffic loading and then subsequently at a slower rate. Figure 2.15 shows the standard deviation or roughness of a rail track surface profile measured over 35m length describing the quality of track after tamping.

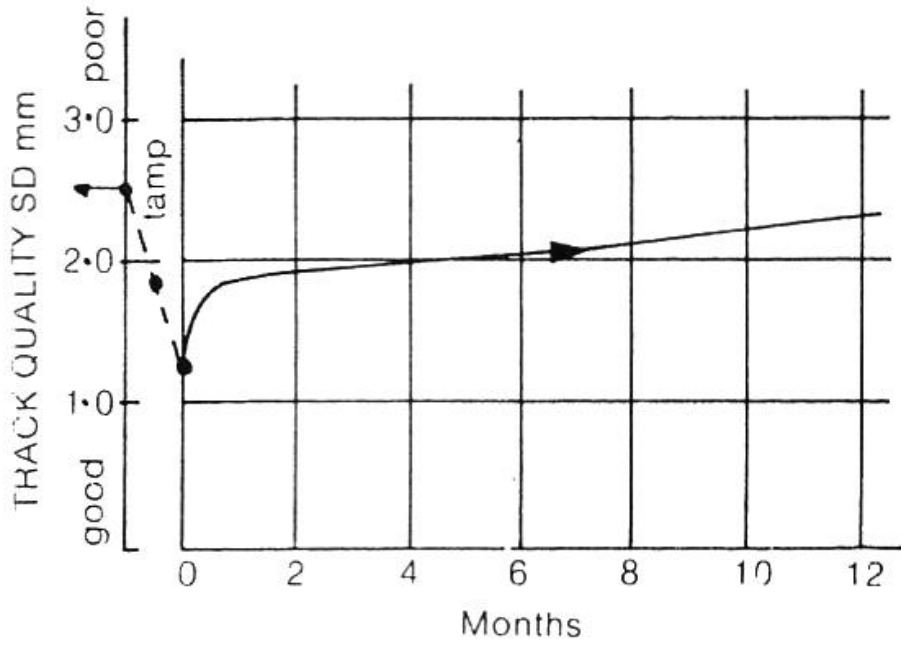

Figure 2.15 Change in vertical track geometry after tamping (Shenton, 1984)
(SD = Standard Deviation)

Sparrow (1981) noted the relation between track quality before maintenance and deterioration following tamping. He noticed greater initial loss of track quality and higher rate of deterioration for poorer pre-maintenance track. This is shown in Figures 2.16 and 2.17.

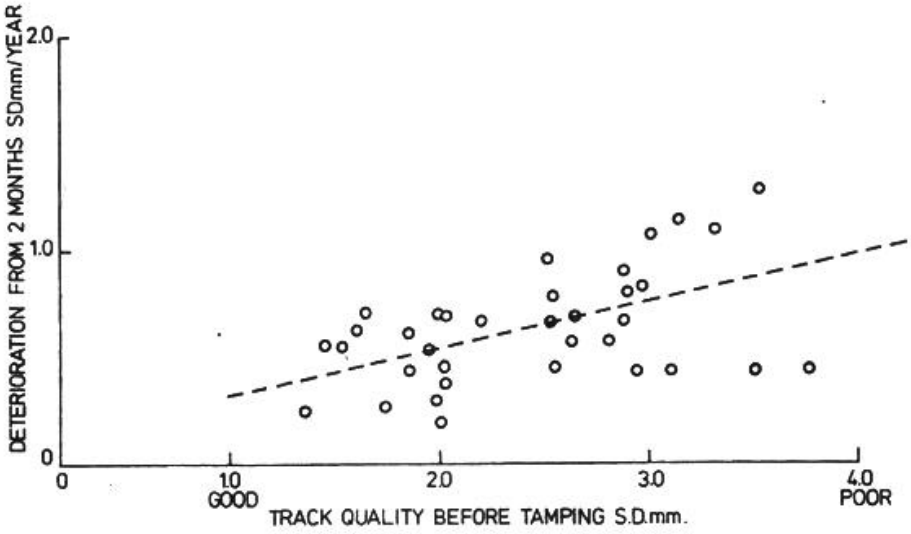

Figure 2.16 Comparison of Standard Deviation (S.D) of good and poor track after tamping (Sparrow, 1981)

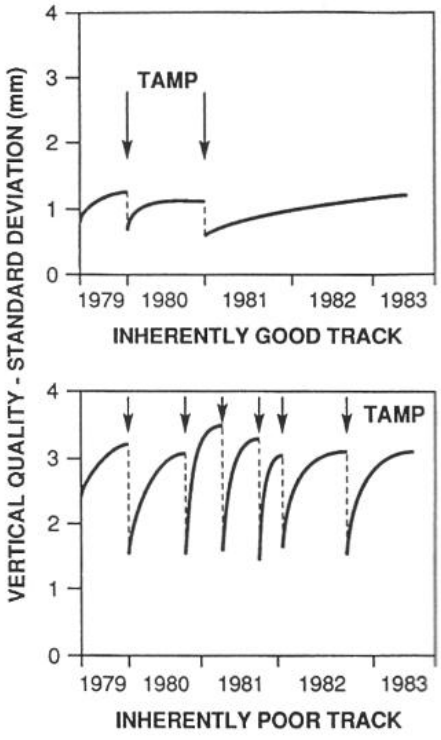

Figure 2.17 Quality of track (Selig and Waters, 1994)

Shenton (1985) noted that the track appears to have an inherent shape throughout its service life. This is confirmed in the literature. Selig and Waters (1994) reported that this inherent shape is likely to be influenced by its construction. Figure 2.18 shows an example of inherent track shape persisting over several tamping cycles.

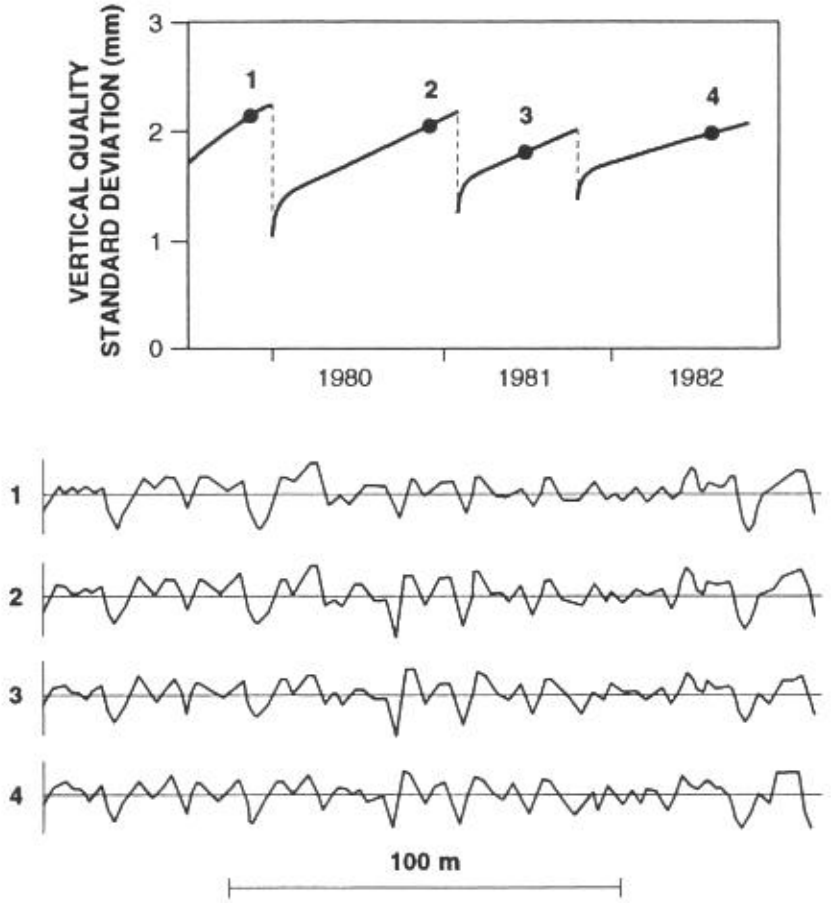

Figure 2.18 Persistence of inherent track shape over tamping cycles (Selig and Waters, 1994)

It is well recorded in the literature that for a nominal load on a sleeper, the amount of lift given by the tamping machine will determine the settlement under subsequent traffic. Shenton (1985) reported that the greater the lift to the sleeper, the larger the settlement. Figure 2.19 reiterates this point. Selig and Waters (1994) added that for a relatively low lift, the lift is approximately equal to the settlement over the following 66 weeks of traffic.

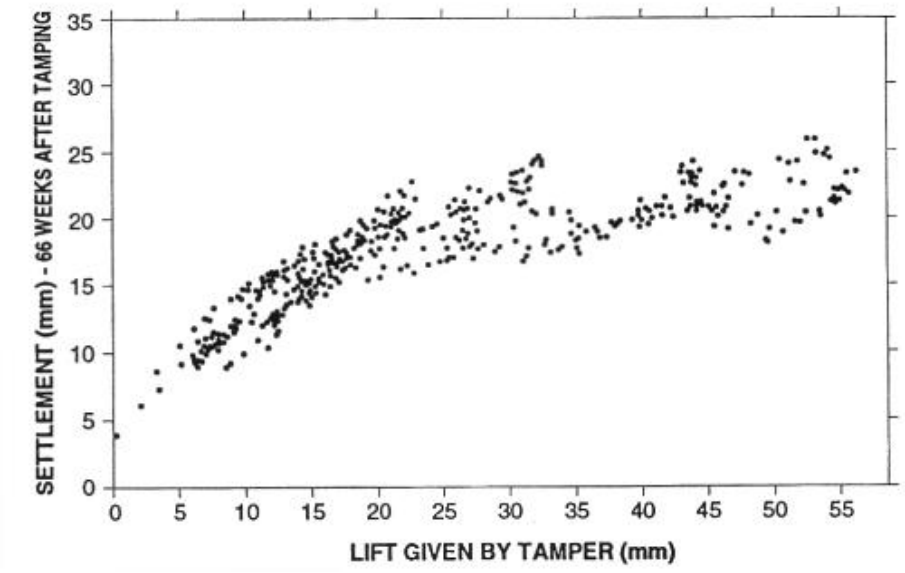

Figure 2.19 Sleeper Settlement as a function of tamping lift (Selig and Waters, 1994)

Track geometry is also dependent on the vertical deterioration characteristic of the track, as discussed in Section 2.3.6.

A good inherent quality track will result in good ride quality as well as an increased maintenance cycle. Shenton (1985) insisted on the presence of straight rails and ballast with uniform settlement properties to achieve it. This is independent of the speed or type of traffic. Figure 2.20 depicts this.

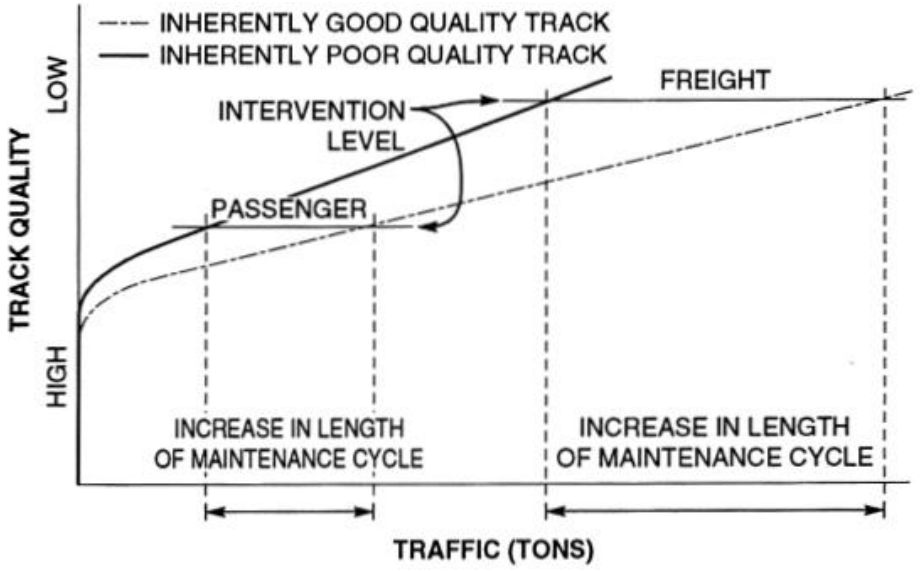

Figure 2.20 Influence of track quality on length of maintenance cycle (Selig and Waters, 1994)

2.5 Polymer Geogrid

Polymer geogrid has been proposed and tried as a reinforcement material, especially in the base course layer of flexible pavements, for many years. Polymer geogrid is also used as a reinforcing material on rail track.

Extensive research has been done to better understand the basic mechanisms in the separation, filtration, and reinforcement effects of polymer geogrids. The emphasis of such research usually concentrates on the reinforcing function, where the greatest improvements to performance and largest economic savings can be achieved.

2.5.1 Reinforcing Principle

A geosynthetic placed strategically in a construction at the position of maximum tensile plastic strain is able to reduce such strain by carrying tensile stress in itself. This requires good transfer of stress from the soil to the geosynthetic. In the case of a geogrid, this requires good interlock. Applying this to ballasted railway track, Figure 2.21 shows reinforcement in a railway trackbed where the geosynthetic resists granular extension strains with confinement provided by the tensile strength of the polymer geogrid.

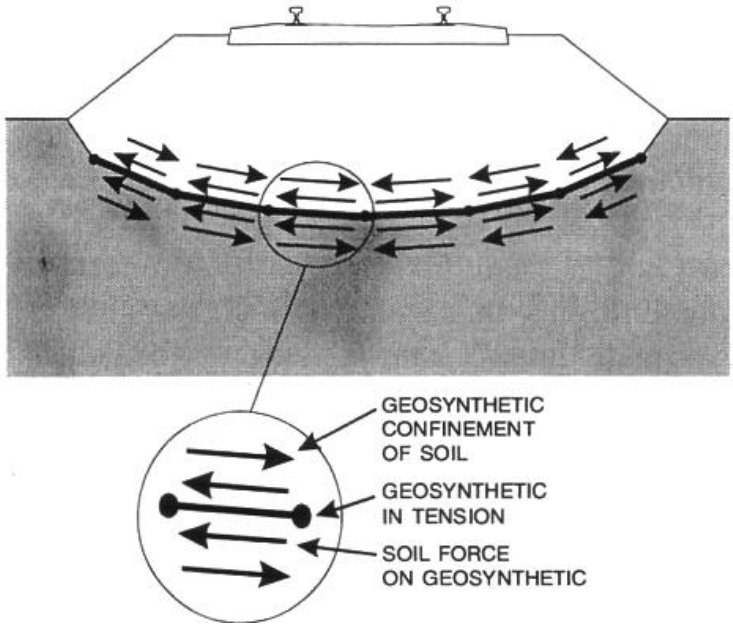

Figure 2.21 Reinforcing effect of polymer geogrid (Selig and Waters, 1994)

It is widely agreed that to achieve the reinforcing potential of a polymer geogrid, an appropriate stiffness and an ability to interlock effectively with the host material is vital (Brown, 1996).

Geogrid uses the interlocking effect of soil particles, which penetrate the apertures and are locked into position between the strands of the geogrid. This immobilisation of the particles leads to a strong horizontal shear resistance, which will increase the bearing capacity of the soil. Figure 2.22 shows the interlocking mechanism of a typical Tensar polymer geogrid.

Selig and Waters (1994) described polymer geogrids as plastic sheets in the form of a grid with aligned long-chain polymer molecules stretched to achieve high stiffness and strength.

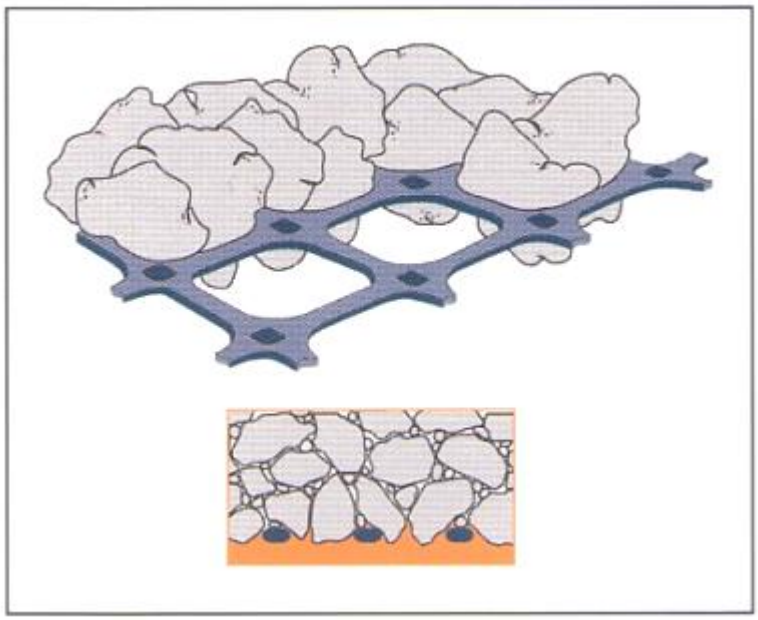

Figure 2.22 Interlock mechanism of polymer geogrid
(Tensar International, 2001)

2.5.2 Soil Grid Interaction

Potyondy (1961) carried out a series of skin friction tests to measure shear resistance between soils and construction materials. A direct shear box was used and he defined the resistance to sliding by the angle of skin friction δ. This method is now widely adopted as the standard test for friction measurement between soil and plane reinforcement surfaces (Scholosser et al., 1979).

Jewell et al (1985) showed three mechanisms of interaction that may resist direct sliding, in Figure 2.23.

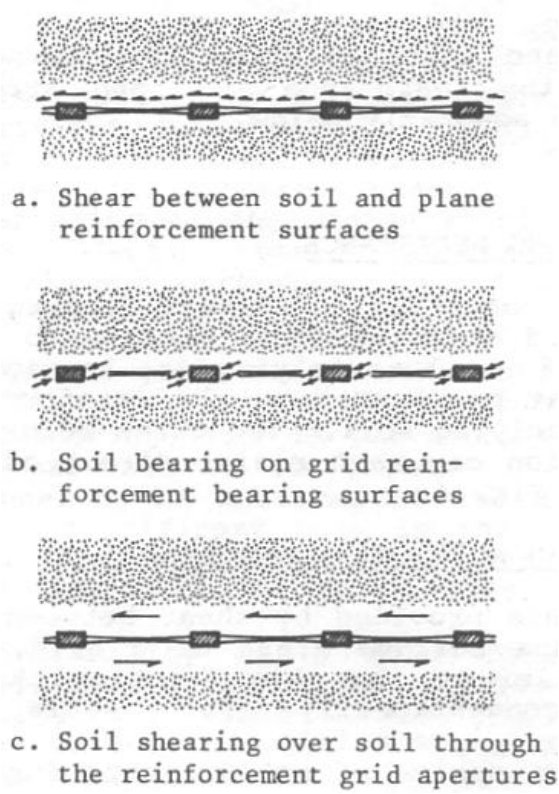

Figure 2.23 Three mechanism of direct sliding (Jewell et al., 1985)

Jewell et al (1985) noted that the relative size of soil particles to grid aperture size has direct influence on the sliding resistance. Figures 2.24 and 2.25 show the qualitative effect of increased particle size on direct sliding. The reinforcement

medium is a Tensar polymer grid. In Figure 2.25, direct sliding resistance is expressed as a factored reduction in soil direct shear resistance.

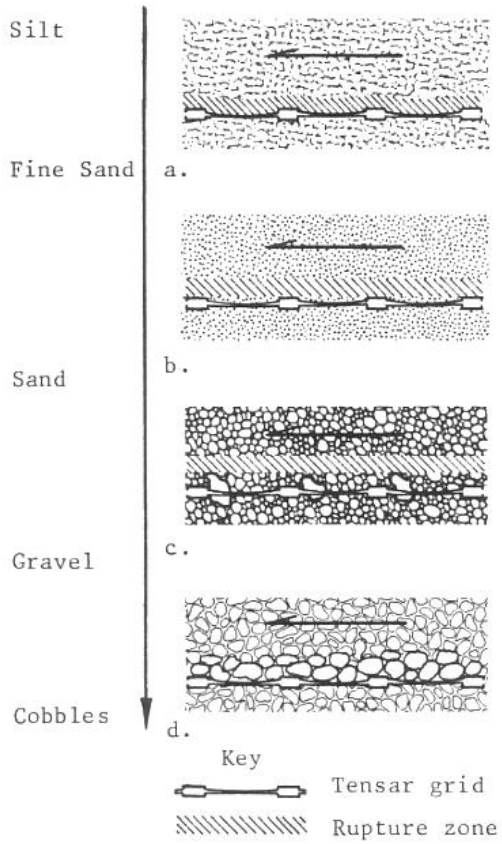

Figure 2.24 Cross sectional view of the qualitative effect of increased particle size on direct sliding resistance (Jewell et al., 1985)

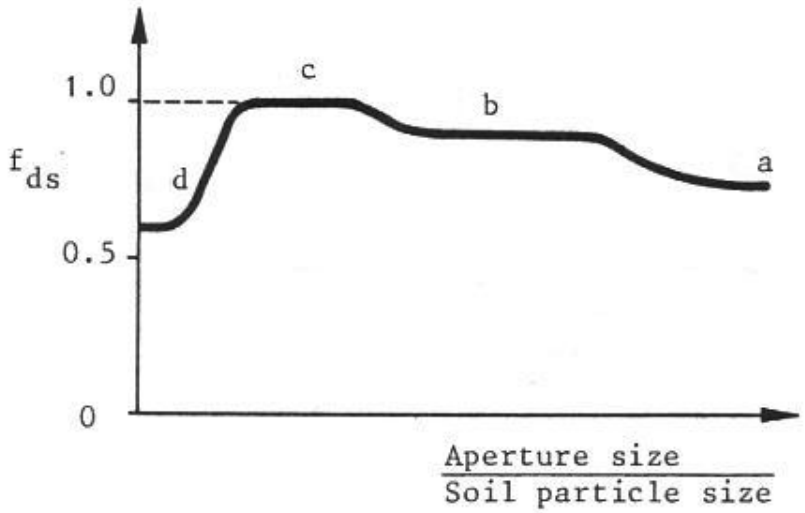

Figure 2.25 Schematic illustration of the influence of particle size on direct sliding $f_{ds}\tan\theta_{ds}$ (Jewell et al., 1985)

Jewell et al (1985) explained that silt and fine sand (denoted by 'a' in Figure 2.27) tends to slide across the relatively smooth surface of the Tensar grid hence registering a relatively small coefficient of resistance. The authors pointed out that if the soil contains particles (gravel as shown in Figure 2.24 and denoted by 'c' in Figure 2.25) that are similar in size to the grid aperture, particles will not be able to take advantage of the smooth grid surface and that the rupture zone will be forced away from the grid fully into the soil. In this case, the shear resistance to direct sliding will be equal to the soil shear resistance. For a particle that is bigger than the size of the grid aperture, they noted that the resistance to direct sliding can be as little as the contact shear resistance between the soil and the plane grid surface.

Jewell et al's theoretical expression for direct sliding is

$$f_{ds} \tan\theta_{ds} = \alpha_{ds}\tan\delta + f_{ds} \tan\theta_{ds} \qquad (2.9)$$

Where f_{ds} = coefficient of resistance to direct sliding

θ_{ds} = angle of friction for soil in direct shear

δ = angle of skin friction for soil on plane reinforcement surface

α_{ds}= fraction of grid surface area that resists direct shear with soil

The authors introduced the parameter α_{ds} to cover the four variations of direct sliding resistance as shown in Figure 2.27.

2.5.3 Tensar Polymer Grid

Tensar polymer grid depends on an efficient interlock with granular materials to make a structural contribution to construction layers. Tensar biaxial geogrids were developed in the 1980s to reinforce unbound and bound materials.

Tensar biaxial grids are manufactured through precise extrusion of sheets of polypropylene. Accurate patterns of punched holes are stretched under controlled

temperature conditions. It is termed a biaxial grid as it is stretched in two orthogonal directions.

The interlock mobilises maximum bearing capacity of a fill as the grid resists horizontal shear from the granular materials. The restraint on the granular material will reduce lateral spread, e.g. on a railway line.

A typical Tensar geogrid, as shown in Figure 2.26, exhibits high tensile stiffness in both the longitudinal and transverse direction with rigid square apertures. From the literature, very little work has been done to classify and optimise the physical dimensions of polymer grids.

According to Tensar (2001), the high strength of the junctions and the shape and stiffness of the ribs allows load to be taken at very low strains as well as allowing effective interlock. On a railway track, the interlock between grid and ballast limits lateral movement of particles reducing the rate of ballast settlement. This is illustrated in Figure 2.27.

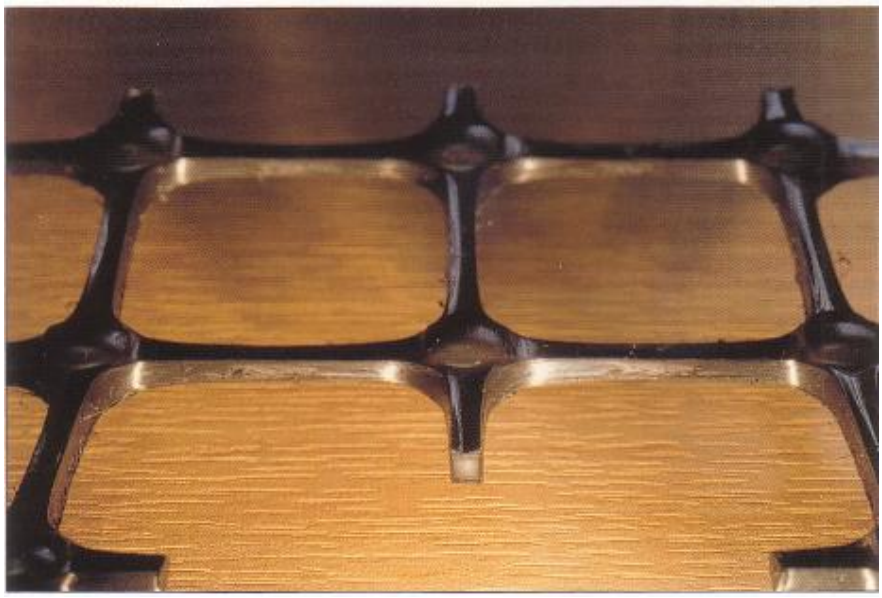

Figure 2.26 Physical attributes of a Tensar biaxial grid (Tensar International, 2001)

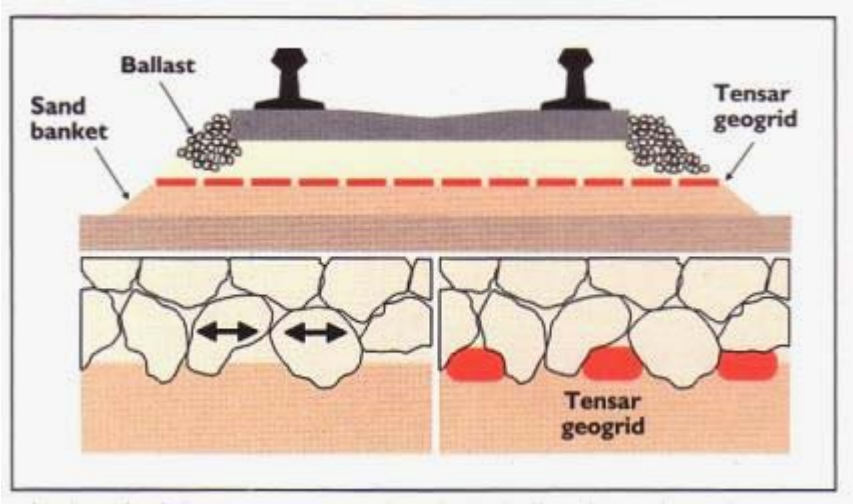

Figure 2.27 Effective interlock minimise lateral movement of particles (Tensar International, 2001)

Tensar SS geogrids, shown in Figure 2.28, are mainly used for the reinforcement of soil and aggregates, often in road pavements and foundation reinforcement projects. The SS geogrids are stiff grids with integral junctions and are oriented in two directions with the resulting ribs having a high degree of molecular orientation and hence high strength. As seen, the SS geogrids have an approximately rectangular cross section with sharp corners. Tensar produce a range of SS grids with different strengths and aperture sizes. The Specifications are shown in Table 2.5

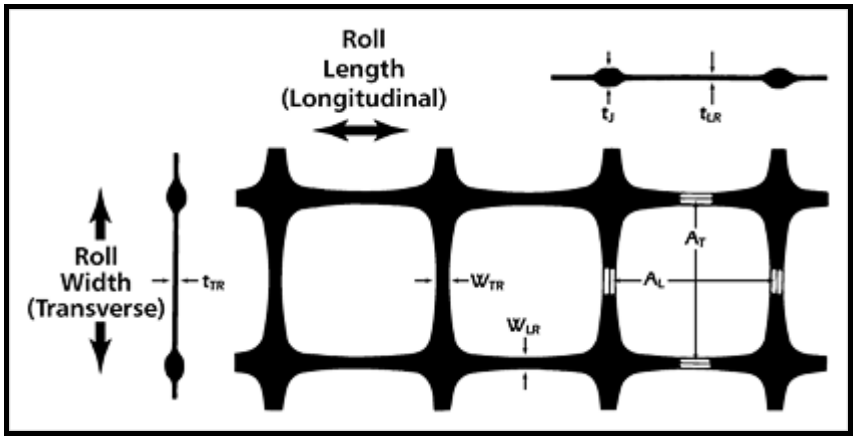

Figure 2.28 Tensar SS geogrid (Tensar International, 2001)

Table 2.5 Tensar SS geogrid typical dimension (Tensar International, 2001)

	A_L (mm)	A_T (mm)	W_{LR}/B_{WT} (mm)	W_{TR}/F_{WL} (mm)	t_J/t_B (mm)	t_{LR}/t_F (mm)	t_{TR} (mm)
SS20	39	39	2.2	2.4	4.1	1.1	0.8
SS30	39	39	2.3	2.8	5	2.2	1.3
SS40	33	33	2.2	2.5	5.8	2.2	1.4
SSLA 20	65	65	4.0	4.0	4.4	0.8	0.8
SSLA 30	65	65	4.0	4.0	7.0	1.7	1.5

2.6 Behaviour of Grid Reinforced Granular Layer

Oxford University carried out model footing experiments to investigate the benefit of reinforcing a granular layer over soft clay. The test consistently demonstrated a 40% improvement in bearing capacity. It was concluded that the interlocking mechanism of the polymer grid resisted tensile strains preventing lateral movement of particles in the loaded area (Milligan and Love, 1985).

Data from the test indicated that the mean angle of load spread increased from 38 degrees in the unreinforced case to more than 50 degrees with a polymer grid. It was concluded that a reinforced granular layer can reduce construction thickness by approximately 50% to achieve a similar stress on the subgrade.

Research carried out at the University of Waterloo, Canada, showed a 300% increase in the number of load applications in a reinforced pavement. In their tests, asphalt pavement sections were laid over a granular base layer. A test load of 40kN applied via a 300mm diameter circular plate was used representing a standard 80kN design axle. Figure 2.29 shows the test sections (Hass et al., 1988).

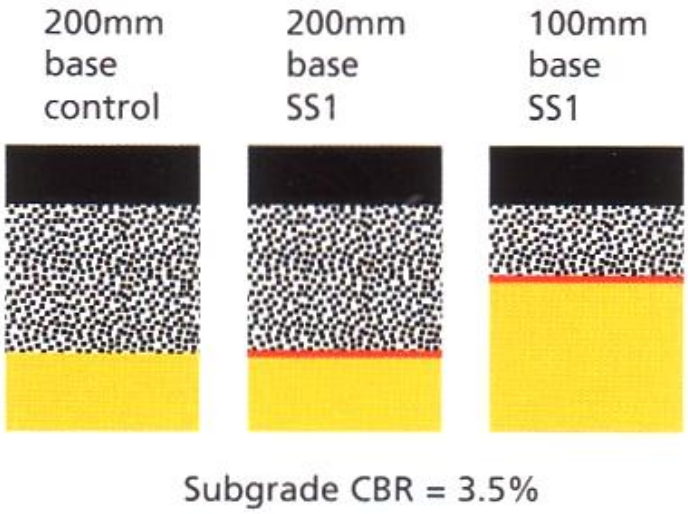

Figure 2.29 Test section (Tensar International, 2001)

It was observed that a 200mm reinforced section sees a threefold increase in load applications to reach a given settlement. Interestingly, the 100mm reinforced section performed as well as the 200mm control.

The test was performed with CBRs ranging from 0.5 to 8%. This validates the results over a range of subgrade conditions.

In the mid 1980s, the United Kingdom's Transport and Road Research Laboratory (TRRL - now known as TRL) investigated the effect of polymer grid reinforcement on rut depth. Comparable findings to those of the University of Waterloo were obtained. Geogrid reinforcement for a given sub-base thickness carried 3.5 times more traffic.

TRL (Chaddock et al., 1998) concluded that effective interlock is achieved with minimal geogrid deformation and that tensile strains within the subgrade are reduced. They added that there is reduced lateral particle movement and that rut depth is reduced for a similar pavement life.

Chan (1990) did a series of full-scale experiments to investigate the influence of geosynthetics on the permanent deformation characteristics of granular bases in a pavement. In his experiments, he considered different types and stiffnesses of geosynthetics as well as varying placement level in the granular base. He concluded that:

1) the permanent deformation resistance of most geosynthetic-reinforced granular bases was improved,

2) the improvement level depends largely on the quality and thickness of the granular base as well as the location of the geosynthetic within the base.

For weak granular bases, e.g. low elastic stiffness, such as those constructed of sand and gravel, a significant improvement in permanent deformation resistance was achieved with the introduction of a polymer grid. The effect is most obvious with the grid installed either in the middle or at the bottom of the layer. A stiffer grid also produced better results with the large vertical deformations and high stress which Chan applied to his granular base.

In Chan's (1990) account, there is minimal benefit if the geosynthetic is placed too far down in the layer. In his opinion, placing geosynthetics at the middle of a base layer not exceeding 200mm depth, gives an optimum improvement.

Chan also noted that geogrid performs better than geotexile in terms of reducing permanent deformation, even where it has a lower stiffness. He attributed this to the interlocking effect of the geogrid.

Chan (1990) concluded in his thesis that geosynthetics have proven to be effective in reducing the permanent deformation of granular bases. He added that their use in heavily loaded pavements should be particularly beneficial and will greatly reduce the maintenance frequency compared to an unreinforced pavement.

Hughes (1986) performed a series of full-scale experiments to investigate the effect of polymer grid reinforcement on asphalt pavements. Two pilot scaled pavements

were constructed and a large shear box test was developed to examine the effect of grid reinforcement at the asphalt interface.

From his results, he concluded that there was an approximate 3-fold decrease in permanent deformation rate when a grid is present. He added that to inhibit permanent deformation, the grid should be ideally located at the region of maximum shear strain in the bituminous layer or in the lower layers of the structures which were susceptible to deformation e.g. at the base of the asphalt layer.

In the mid 1990s, German Rail Authorities investigated the effect of polymer grid reinforcement on a railway track between Hochstadt and Probstzella. Geogrid reinforcement was carried out on a poor subgrade. Plate test results showed that a reinforced 400mm ballast layer performed as well as a 600mm unreinforced layer. It was added that the stiffness of both 400mm and 600mm reinforced layers increased by a factor of two compared to corresponding unreinforced layers (Tensar, 2001b)

Figures 2.30 and 2.31 show the installation of the polymer grid as well as the increase in modulus of deformation from the German investigations.

Figure 2.30 Installation of polymer grid (Tensar International, 2001b)

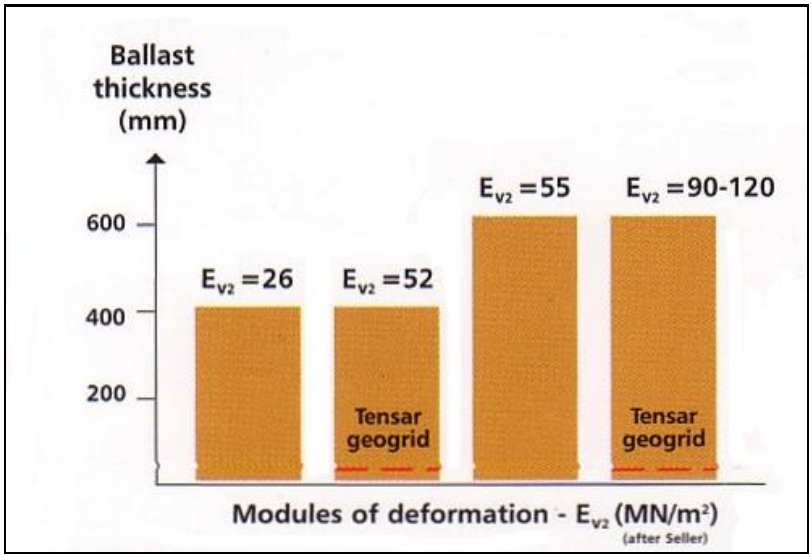

Figure 2.31 Improved track performance (Tensar International, 2001b)

Tensar (2001b) published in their report a case study of European Corridor No. 4, the Prague to Vienna line. In their report, Tensar SS40 geogrid increased the bearing capacity from 8-10MPa to 50-60MPa. A 40% reduction in sub-base thickness was also recorded.

Raymond (2001) studied the behaviour of reinforced ballast subjected to repeated loading. He studied the performance of a thin layer of granular material, reinforced and unreinforced, when acting as a foundation material under repeated loading. A schematic layout of his test is shown in Figure 2.32. Compressibility of the subgrade was varied through the use of rubber layers.

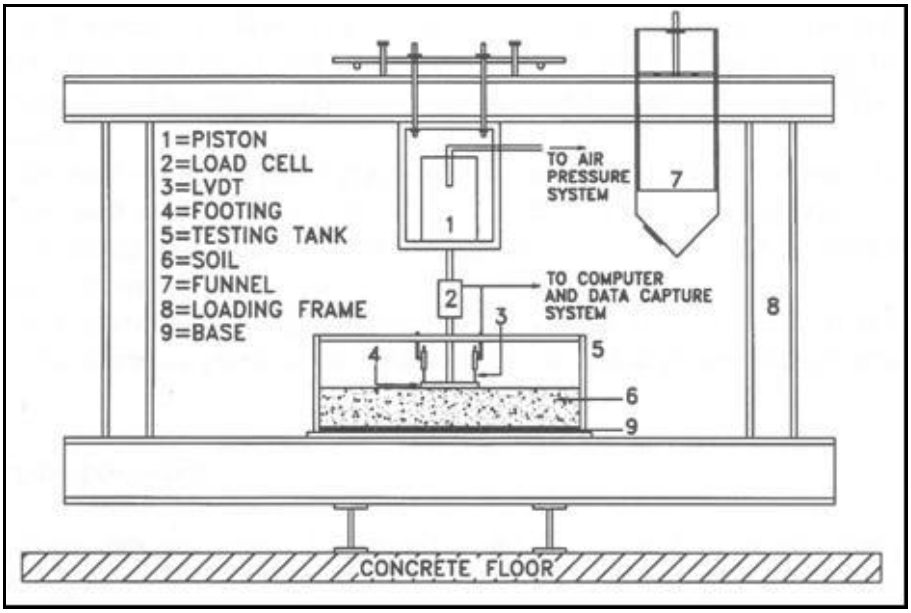

Figure 2.32 Schematic of test equipment (Raymond, 2001)

Raymond (2001) concluded that grid reinforcement reduces plastic settlement by 13-30%. He noted that a bigger improvement was observed when the foundation was weak. He later deduced that the inclusion of a geogrid on railway trackbed can extend the existing 3 months maintenance cycle to a cycle of over 3 years.

It must be remembered that Raymond's (2001) experiment was a scaled down version of an actual track and included small aggregate sizes. The geogrid used is thought to have been relatively larger than it should relative to the size of particle used. Hence, the results may not be realistic though the findings are consistent compared with the rest of the literature.

British Rail Research (BRR) conducted a full-scale test (Figure 2.33) showing the behaviour of reinforced granular material in rail track. The configuration of SS35 Tensar Geogrid, used in the tests, is as shown in Figure 2.34.

Figure 2.33 BRR's rolling load rig (Matharu, 1994)

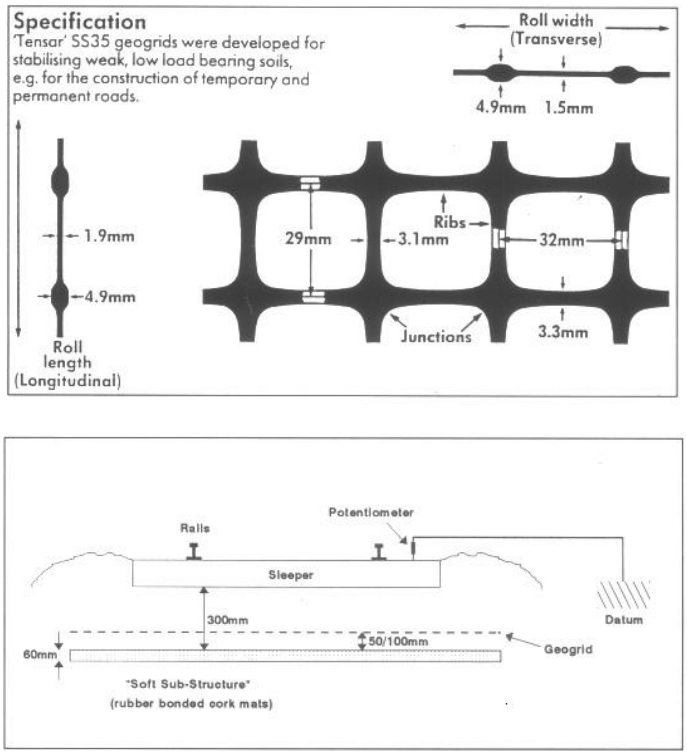

Figure 2.34 Detail of grid and placement (Matharu, 1994)

The test track was divided into reinforced and unreinforced zones. Tamping was done before the test. A simulated 2 million gross tonnes provided traffic loading. Figure 2.35 shows the elastic deflection of a sample sleeper. BRR report results of an approximate reduction of 40% in elastic deflection in the geogrid-reinforced track. Figure 2.36 shows the settlements by comparing initial lift (lift at the position of the

sleeper due to the tamping procedure) during tamping to the residual (or remaining) lift after trafficking.

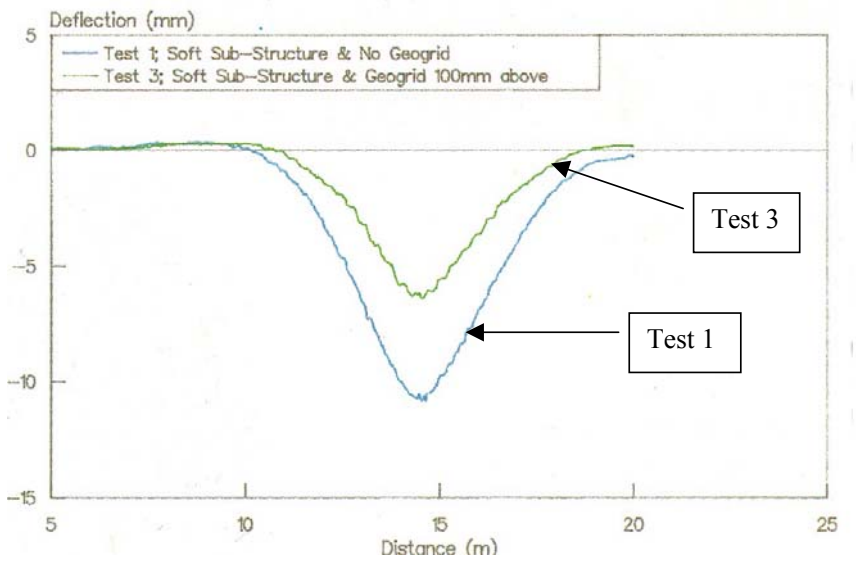

Figure 2.35 Deflection Influence Lines (Matharu, 1994)

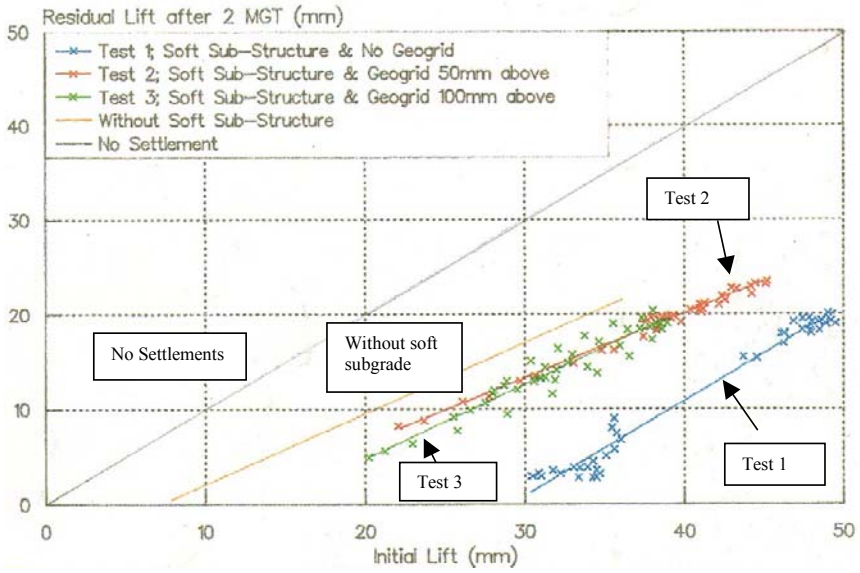

Figure 2.36 Initial Vs Residual Lift (Matharu, 1994)

BRR reported that for a typical lift of 35mm, a track laid on soft subgrade will have a residual lift of only 5mm after 2MGT of traffic compared to 21mm on a stiff subgrade. BRR reported a residual lift of 16mm for a reinforced granular layer on soft subgrade.

BRR concluded that a soft subgrade has a detrimental effect on track durability and geogrid reinforcement provides improvements.

2.7 Summary

The literature review presented in this chapter provided understanding and appreciation of how a conventional rail track functions with added focus on the ballast material. The ballast specifications and its typical characteristics were discussed and with the track forces on the material expounded upon.

The review also indicated good understanding on the subject regarding the resilient and permanent behaviour of granular material. Effect of stress, moisture content, stress history and number of load cycles were among others reported to affect the behaviour of granular material.

A number of track settlement models were quoted though no developed model at present is capable of describing comprehensively the settlement behaviour of the rail track.

The reinforcing principle of polymer grids was discussed and experimental results of the grid reinforced granular layer suggested improved permanent deformation resistance. However, the fundamental characteristics of grid/aggregate interaction have not been researched at a detailed level since the early work associated with Tensar geogrids started in the early 1980's. The understanding of the basic mechanism governing the reinforcing action of the geogrid or how geogrid reinforcement can be designed into rail track structures for different situation is still limited.

The remainder of this thesis examines the use of element tests, the full scale Railway Test Facility (RTF), field trials as well as a theoretical analysis to gain insight into the optimisation of grid reinforcement and to produce a design guide for reinforced track designers.

3 GRID/BALLAST INTERACTION

3.1 Discrete Element Modelling using PFC^{3D}

The discrete element method developed by Cundall and Strack (1979) was used in the modelling of grid/ballast interaction using the computer code PFC3D developed by ITASCA. The objective of this computational work was to gain an understanding of the micro-mechanics of ballast-geogrid interaction which complemented experimental work. Discrete Element Modelling (DEM) work in this project was performed by Research Fellow Dr Ouahid Harrireche.

Due to the strongly discontinuous nature of railway ballast, the DEM approach is ideally suited. In this method, contact laws, in terms of stiffness, strength and friction coefficient etc, can be defined to an individual sphere or agglomerate (combination of spheres, overlapped if necessary).

Figure 3.1 shows a PFC model of a simulated triaxial cell set up by Harrireche to develop and calibrate a suitable model for railway ballast particles. The triaxial cell had dimensions of 300mm diameter x 600mm height. An octagonal prism was chosen to approximate the cylindrical shape of the cell.

The key steps in his triaxial modelling were:

- An assembly of virtual spheres (or clusters of spheres), with a slightly larger than targeted porosity under confinement, was generated within the simulated triaxial cell. Virtual spheres (or clusters) were generated at random without overlapping. For this process to be completed in a reasonable number of

trials, the virtual spheres (or clusters) were generated at half their final diameter (20mm rather than 40mm)

- The virtual spheres (or clusters) were then expanded to their true size and the system cycled to equilibrium. To minimise computational time, walls and particles were frictionless at this stage. Walls remain frictionless during the whole triaxial simulation.

- Simulated lateral walls were then moved away at a low rate along their normal axes to achieve an initial state free of internal forces.

- The required confining pressure was applied using a simulated numerical servo-control of the wall motion. Friction between particles was maintained artificially low in order to match the packing achieved in practice.

- The modelled test, with an appropriate level of inter-particle friction, was simulated by the steady lowering of the top platen while the motion of the simulated frictionless walls maintained the confining stress.

A series of theoretical test simulations were made to develop the most suitable ballast model. Harrireche experimented with various starting densities due to the difference in the shape of the idealised particles from those in reality. The best match to the laboratory experimental data reported by Indraratna et al (1998) was achieved with a relatively loose packing and a porosity of 0.44.

Harrireche then tried to vary the value of the inter-particle friction, μ, from 0.6 1.5. The 0.6 value is an approximate value determined by laboratory measurements (see Section 3.3) and derived based on $F = \mu R$ where F is the peak shear force and μ is the coefficient of inter-particle friction while R is the normal reaction force. This was done in an attempt to match measured triaxial data from Indraratna et al (1998) without having to use clusters. However, as shown in Figure 3.2, the axial stress-strain results indicated that the predicted peak stress, even at a coefficient of 1.5, was well short of that measured (just over 1.2MPa in

this test). The volumetric behaviour was becoming unrealistic as well; hence, he decided to progress with the use of clusters as shown in Figure 3.3. He found the most effective cluster to be an eight sphere cubic packing with partial overlap.

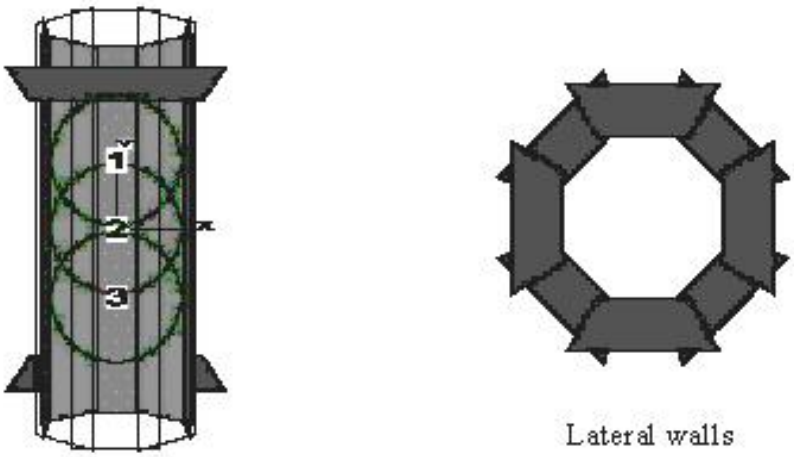

Figure 3.1 PFC model of triaxial cell

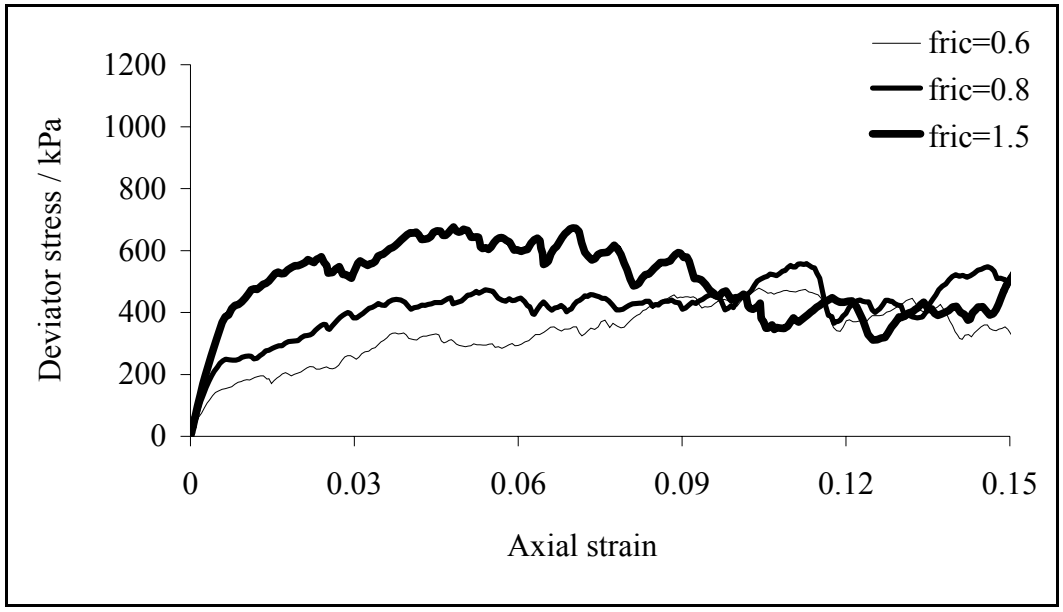

Figure 3.2 Effect of Inter-Particle friction on Ballast Modelling

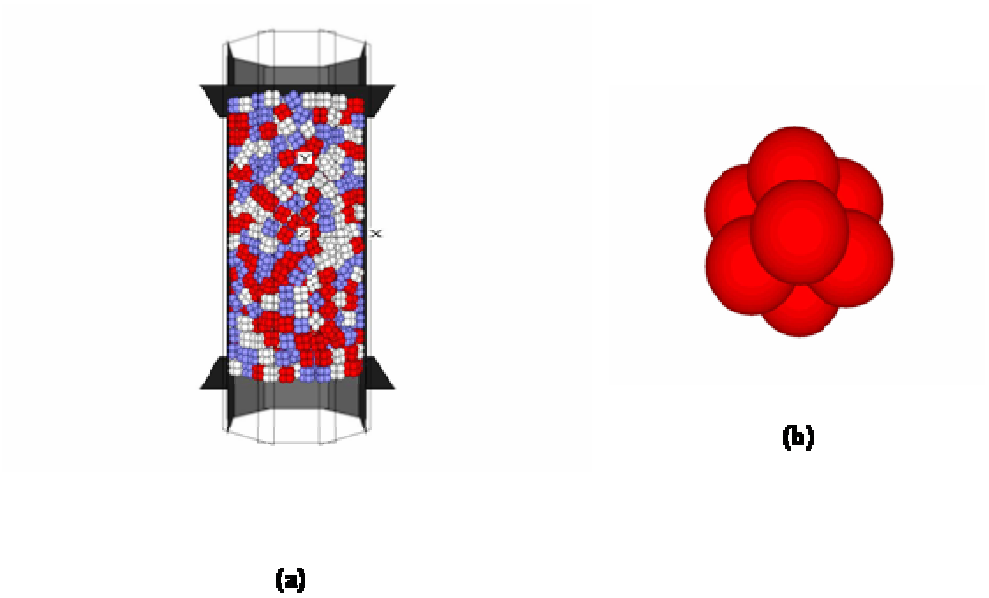

Figure 3.3 PFC model for triaxial test (a) assembly of cubic clusters in triaxial cell (b) cubic cluster used in model

The geogrid was modelled using spherical paricles bonded by contact and parallel bonds. Figure 3.4 shows a model of the Tensar SSLA 20 grid (refer to Table 2.5 for grid size). A single simulated rib test in simple tension provided a calibration for the micro-properties of the contact and parallel bonds. For the SSLA 20 geogrid, the micro-mechanical parameters were calibrated to provide a single rib failure force of 1.1kN at a failure strain of 11%.

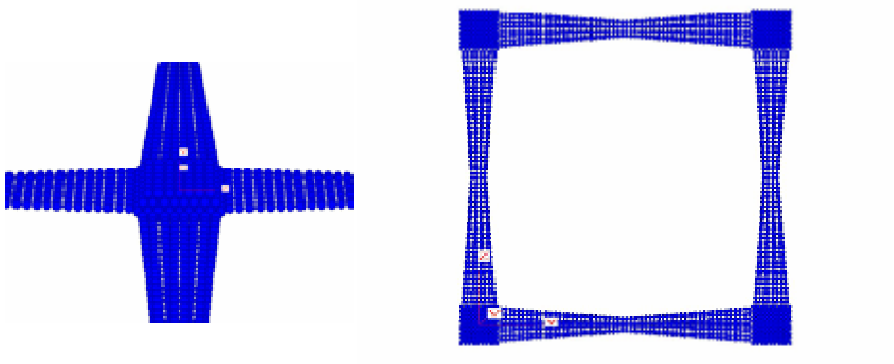

Figure 3.4 Geogrid model

3.2 Pull Out Test

Polymer geogrid utilises the interlocking effects of soil particles with the ribs forming its aperture to achieve the reinforcing effect. Traditionally, the interaction between reinforcement and fill is investigated experimentally through the use of a modified direct shear box test or a pull-out test. For this project, due to the particle size, a pull-out test was chosen. Another reason is because of the limit on computing time for a larger test configuration (DEM model). The pull-out test performed provided comparative data for the computational modelling element of the project as well as a basic understanding of grid/ballast interaction. The pull-out test however, is not designed to be a representation of the field condition.

3.2.1 Test Procedures

Tests were carried out in a wooden box measuring 300mm long x 200mm wide x 400mm deep. The box was filled with ballast with the geogrid placed at mid-depth protruding out of the box through a slot in one end of the box. The ballast used was from Glensanda quarry, measuring approximately 31.5 to 50mm. The granite stone comprises mainly plagioclase (35%), quartz (30%) and alkali feldspar (20%). Physical properties relating to particle shape are quoted in Lim (2004) with his results presented in Table 3.1. The particle shape shown in Table 3.1 is presented according to RT/CE/S006, Issue 3 (2000) and BS EN 123450 (2003). The same type of ballast was used throughout the tests performed in this project. The Glensanda ballast can be generally described as uniformly graded crushed hard stone which is durable, angular, equidimensional in shape and is relatively non flaky. The grading curve of the ballast is shown in Figure 3.5.

Table 3.1 Particle shape according to RT/CE/S/006, Issue 3:2000 and BS EN 13450: 2002 (Modified from Lim, 2004)

Ballast	RT/CE/S006		BS EN 13450	
	Flakiness Index	Elongation Index	Flakiness Index	Length Index
Glensanda	5	20	7	1

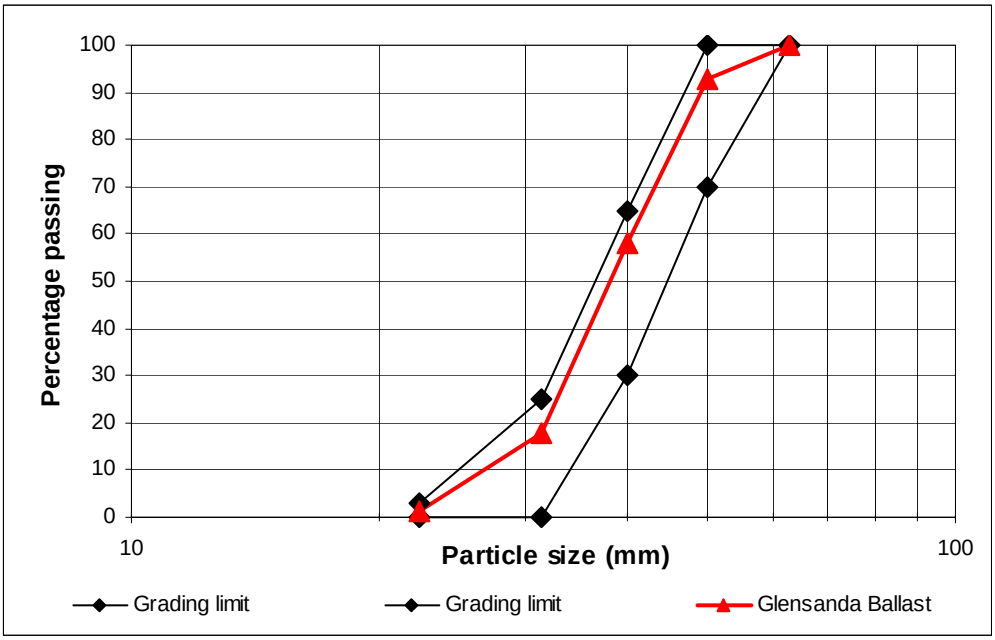

Figure 3.5 Grading curve of ballast used in the project
(Grading limit from TR/CE/S006, Issue 3:2000)

The width of the box was chosen to allow at least 2 geogrid apertures to fit across (in the case of Tensar SSLA 20 geogrid) to mimic the effective interlock between apertures and ballast particles. Figure 3.6 shows the principle of the pull-out test.

The test was performed with the grid being pulled horizontally at an approximately constant rate and the resulting force measured. The geogrid was secured by a clamp connected to a hand jack actuator which was mounted to a loading frame to provide the pulling force. A dial gauge was set up against the clamp to measure regular displacement intervals of 1mm over a stretch of 40mm. A vertical actuator, as seen in Figure 3.7, provided vertical stress to the ballast particles. The vertical actuator transmitted loading over a steel plate on the top of the ballast particles. Following early trials, the effective grid area was set at 130mm x 140mm commencing 170mm from the opened slot of the box.

A plastic membrane was used to cover the aperture through the opening of the slot to prevent trapping of the ballast particles between the ribs and the wall of the box.

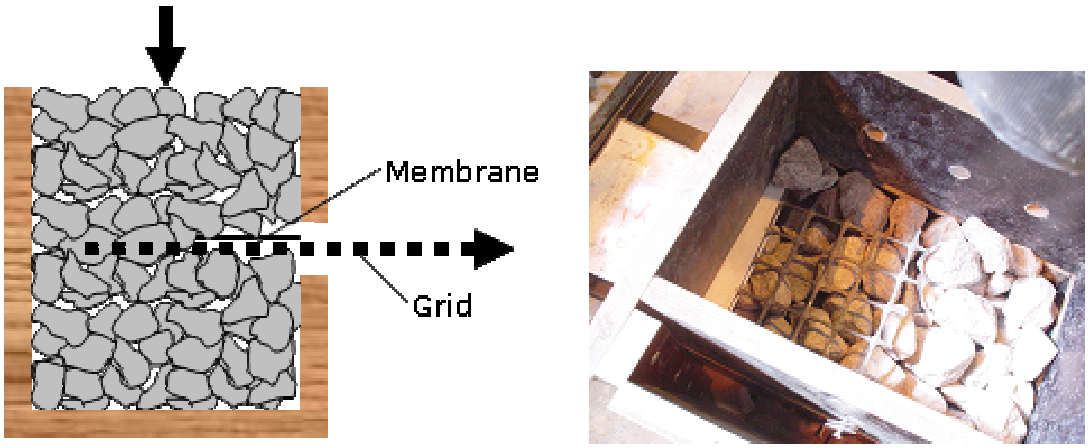

Figure 3.6 Pull-out Test arrangements

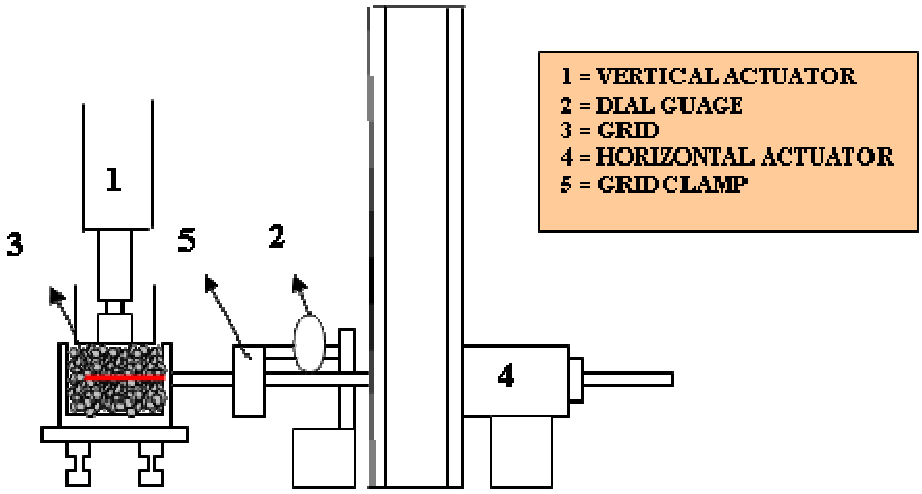

Figure 3.7 Schematic diagram of Pull-out Test

The applied vertical stress ranged from 0kPa to a maximum of 25kPa. It must be noted vertical load does not include the self weight of the ballast material measured at 20kg, contributing 3.3kPa in vertical stress. The force required to pull the geogrid was measured at every 1mm displacement interval. Tests were continued to displacements of 40mm. Tensar 20-65 (SSLA20), 30-65 (SSLA 30) and 40-32 (SS40) geogrids were tested. The grid is referenced in terms of its nominal tensile strength (kN/m) and aperture size (mm), e.g. 20-65 indicates a tensile strength of 20kN/m and aperture size of 65mm (refer to Table 4.1).

3.2.2 Results

The initial plan was to have 3 repeat tests at 0kN, 0.5kN, 1kN, 1.5kN vertical loads for the three grid types. However, it was observed that at higher vertical loads of 1kN upwards, there was permanent deformation at the ribs of the test grids. As the test was designed to investigate the interlocking effect between ballast and grid but not the tensile strength of the ribs, it was decided that the test should proceed at the lower vertical stress of 11.6kPa (0.5kN load + overburden). The overburdened stress in the railway track bed of 300mm thick ballast equates to approximately 7kPa. The stress achieved in the Pull-out Test equates to the overburdened stress at 500mm depth in the railway track bed.

Figures 3.8 to 3.13 compare the replicate test results of the pull-out tests conducted with 20-65, 30-65 and 40-32 Tensar grids with vertical loads of 0kN and 0.5kN. The detail of the Aperture to Grid Ratio (A/B) was also included. Size of ballast was taken to be at 40mm. Good agreement was observed in all the replicate tests. The jagged natures of the plots illustrate intermittent slippages in the interlock within the geogrid during straining of the system. Figures 3.9 and 3.10 compare the results of the pull-out test with two geogrids with tensile strength of 20 and 30kN/m respectively. Both the grids have an aperture size of 65mm and were subjected to no vertical stress. The results indicate an increase in the maximum pull-out force due to the difference in rib profile (30-65 grid has a thicker rib compared to the 20-65 grid) and to a smaller extent, higher stiffness resulting from the increased thickness of the geogrid.

However, comparing Figures 3.8 and 3.9, it is evident that the 20-65 grid induced a higher average interlock with the ballast particles than the 40-32 grid and a significantly higher peak force. This indicated the importance of aperture size over tensile strength or thicker rib profile of grid. Figures 3.11 to 3.13 show the same trend and reinforce the observations from the previous set of figures.

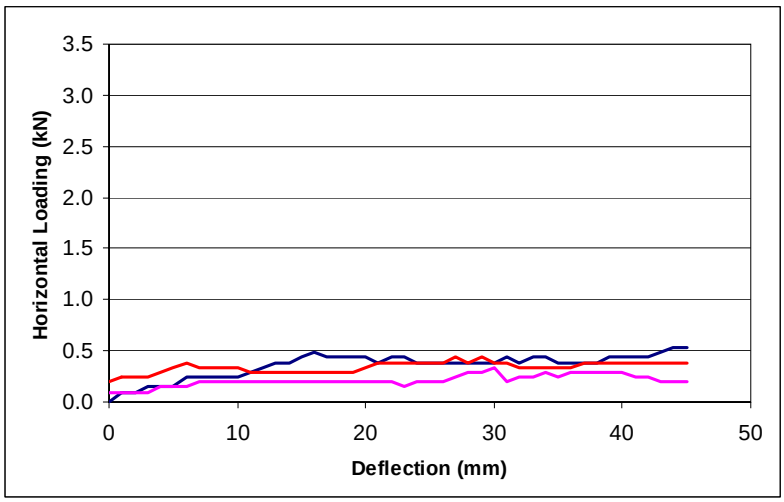

Figure 3.8 Pull-out Test results for 40-32 grid under 0kN vertical load (A/B: 0.8)

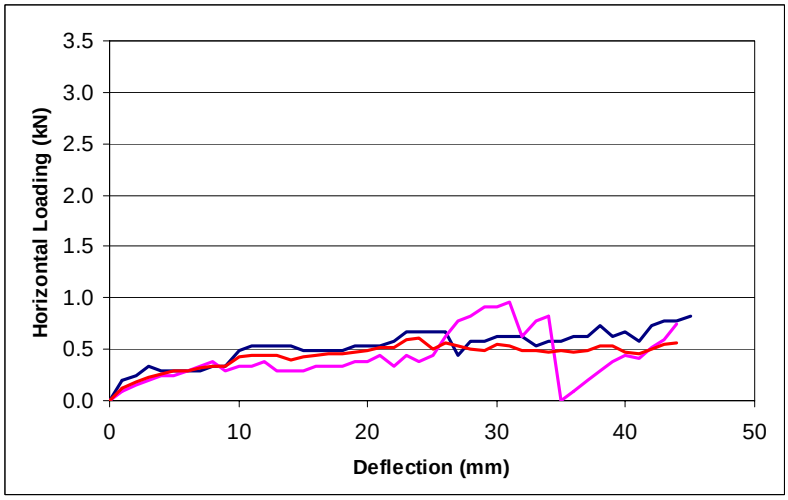

Figure 3.9 Pull-out Test results for 20-65 grid under 0kN vertical load (A/B: 1.6)

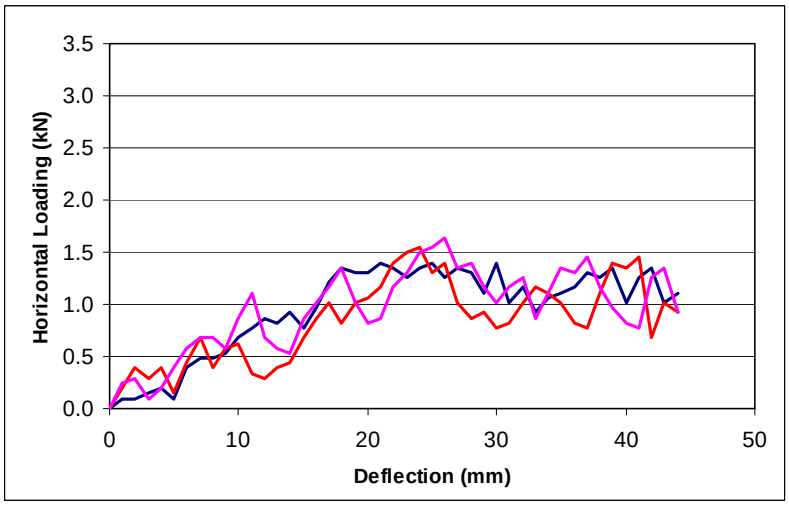

Figure 3.10 Pull-out Test results for 30-65 grid under 0kN vertical load (A/B: 1.6)

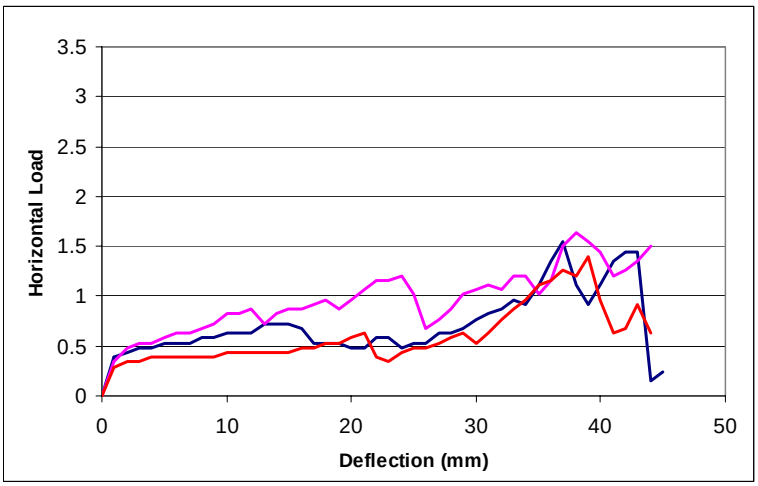

Figure 3.11 Pull-out Test results for 40-32 grid under 0.5kN vertical load (A/B: 0.8)

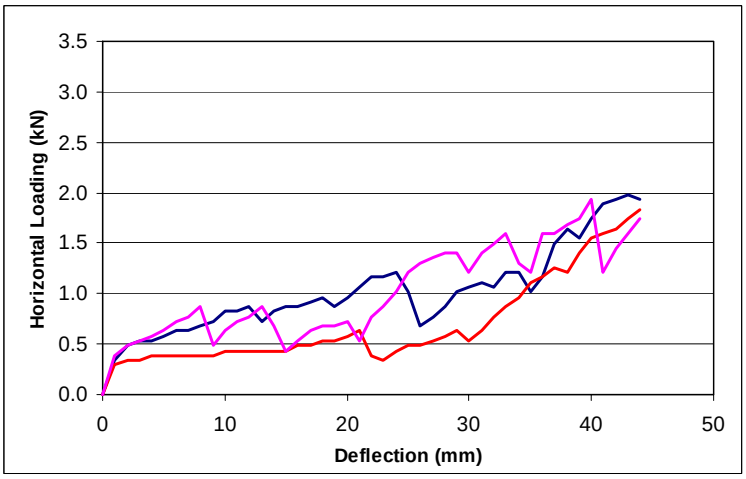

Figure 3.12 Pull-out Test results for 20-65 grid under 0.5kN vertical load (A/B: 1.6)

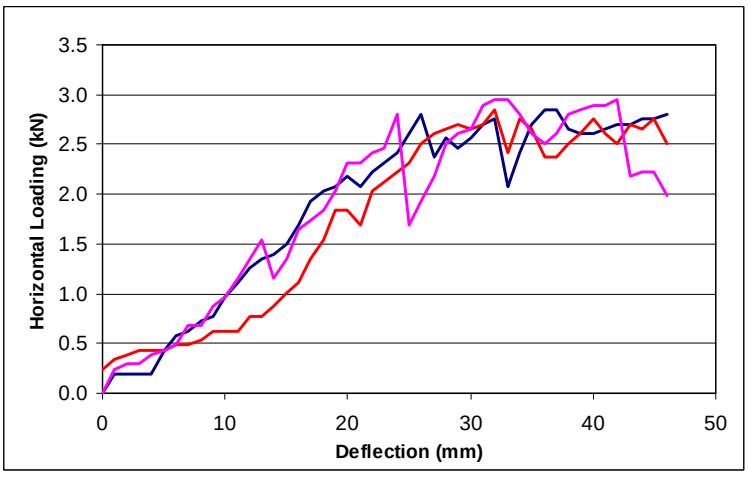

Figure 3.13 Pull-out Test results for 30-65 grid under 0.5kN vertical load (A/B: 1.6)

3.2.3 Discussion

The primary purpose of the pull-out test was to provide comparative data for the computational model performed using PFC^{3D}. The strength of the pull-out test is the relatively quick turnover of tests and the figures illustrate a good repeatability of results. The jagged nature of the plots illustrates the stick/slip nature of ballast particle movement.

The inclusion of a plastic membrane covering the grid close to the opening slot of the box was observed to have greatly improved the reliability and repeatability of the test.

The tests have provided valuable data for the verification and validation of the computational model discussed in Section 3.1.

Valuable information regarding grid/ballast interaction has been obtained. From Figures 3.9 and 3.10, it is evident that thicker ribs giving better ballast confinement, results in better grid/ballast interlock. Comparing Figure 3.8 and 3.10, it can be seen that 65mm aperture outperforms the 32mm aperture. This is consistent with Jewell et al's (1985) observation where they claimed that the relative size of soil particles to grid aperture size has a direct influence on the sliding resistance or interlock. In fact, the importance of the ratio of geogrid aperture size to particle diameter outweighs that of tensile strength or thickness of grid as illustrated by the comparison of Figures 3.8 and 3.9 as well as Figures 3.11 and 3.12. When there is good interaction between the aggregate and the grid where the aperture size is considerably larger than the particle size, then the greater stiffness geogrid leads to a peak strength at a lower deflection. On the other hand, based on stiffness alone, isn't of so much benefit if there isn't a good interaction between aggregate and grid (compare Figures 3.8 to 3.10 and Figures 3.11 to 3.13).

Boundary conditions remain a problem in this set-up. The test should ideally be conducted in a bigger box. This would eliminate or reduce the friction caused by the boundary. It would also further improve the reliability of results with more apertures being tested.

The usefulness of the test could be extended by the introduction of a controlled test. The control test would investigate the effect of a dead weight on a geotexile or a material with a similar surface friction to that of the Tensar grids. The geotexile would be pulled horizontally at an approximate constant rate and the required force measured. This would provide good comparative data and will isolate the interlocking effect of grid/ballast.

3.3 Particle Friction Test

The aim of this test is to obtain the frictional properties of ballast particles to quantify one of the input parameters for computational modelling. In this test, two relatively flat-faced ballast particles from Glensanda quarry were set in epoxy mortar in the upper and lower halves of a shear box test apparatus. Various normal loads were applied and the horizontal force measured as shear was applied. Hence the frictional coefficient was obtained. Figure 3.14 shows a schematic test arrangement. The choice of test is due to its simplicity and that the test has the advantage of a quick turn around with relatively low technology requirements.

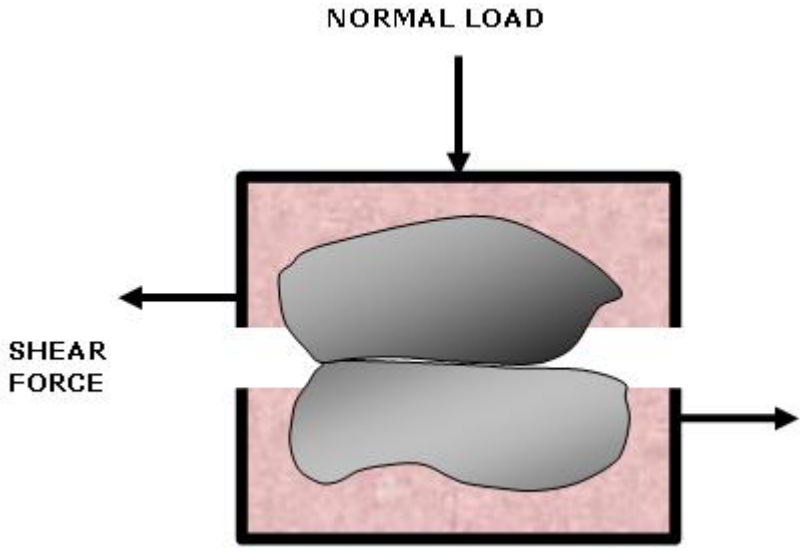

Figure 3.14 Particle Friction Test schematic diagram

1.4 3.3.1 Test Procedures

The test was performed with a shear box test apparatus. During shear, the sample is horizontally displaced manually by turning a screw. Regular 1mm interval horizontal displacements were determined with a dial gauge. The shearing force is measured using a proving ring. The normal load is applied with the use of free weights and applied through a weight hanger. The epoxy mortar is allowed to set overnight in an oven. The test is typically run to a horizontal displacement of 2.3mm.

3.3.2 Test Results

The laboratory results are presented in Figures 3.15 and 3.16. Clean virgin ballast particles were used for each test to best represents the frictional characteristics. The shear force required to induce slip between the two particles exhibits a fluctuation due to the unevenness of the surface of the ballast. The scatter in the experimental data is also a function of the small numbers of particles involved.

Figure 3.17 presents the frictional measurement data plotted in the form of peak shear force. The maximum shear force is abstracted at each level of the normal load in the figure. Tests 1 and 2 shows good agreement and the frictional coefficient and angle of friction are found to be approximately 0.6 and 30^{o} respectively.

1.5 3.3.3 Discussion

A high level of consistency is obtained with the data. The initial key challenge of modifying the shear box aperture to securely accommodate the ballast particles was effectively resolved with the use of an epoxy mortar. The data will be fed into the Discrete Element Modelling.

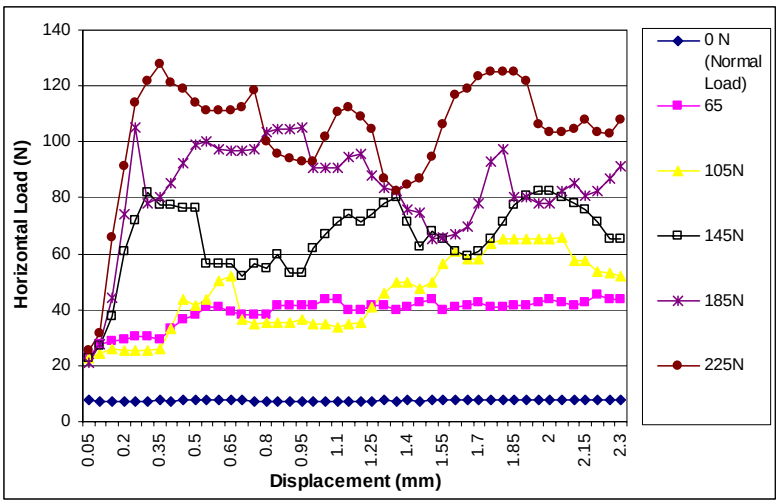

Figure 3.15 Inter-particle friction measurements (Test 1)

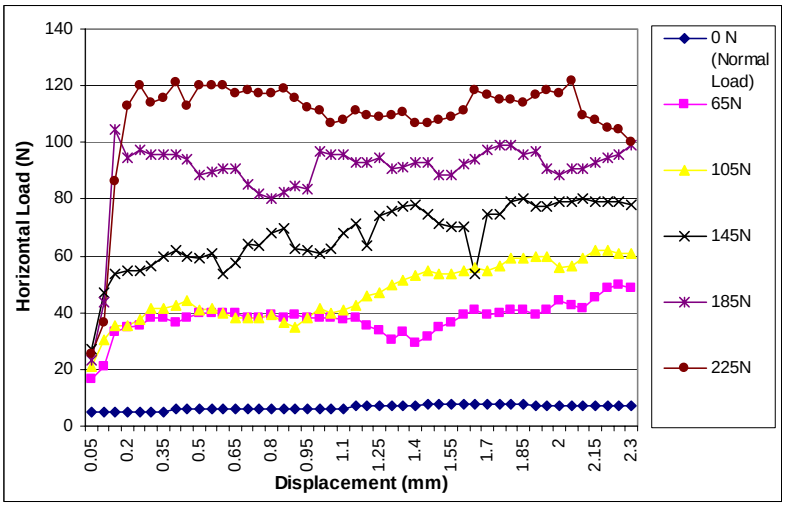

Figure 3.16 Inter-particle friction measurements (Test 2)

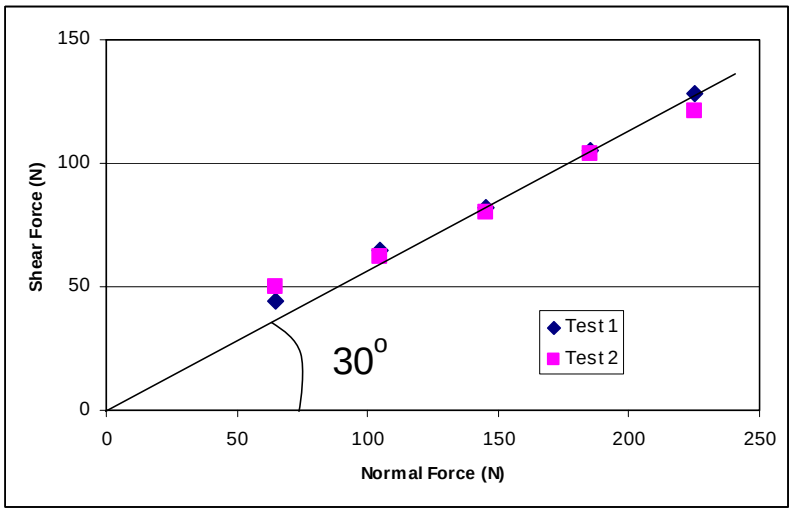

Figure 3.17 Friction measurement data plotted in the form of peak shear force

1.6 3.4 Geogrid Stiffness Test

A grid stiffness test was developed to determine the stiffness value of the Tensar 65mm aperture grid range. The geogrid stiffness test results will help explain and better understand some of the Composite Element Test (CET) results discussed in Chapter 4 of this thesis.

1.7 3.4.1 Test Procedures

Tensile stiffness tests were performed in an Instron servo-controlled hydraulic test machine. The test arrangement is shown in Figure 3.18. Special clamps, as shown in Figure 3.19, had been designed and supplied by Tensar International. The clamps, shown in Figure 3.20, are adapted to fit the hydraulic jaws of the Instron and at the same time securing the geogrid at the nodes.

Four Tensar 65mm aperture grid range samples were tested, each approximately 325mm long (5 apertures) by 195mm wide (3 apertures). Each grid was subjected to cyclic loading and deformation was measured using the displacement transducer attached to the main Instron actuator. After several trials, the peak tensile load was selected as 1kN, as any load above it will cause the polymer grid to deform elastically. This represents less than 10% of the strength of all grids tested. The frequency of the test was set at 3Hz. The reason for the chosen frequency was that it was similar to the frequency performed in the Railway Test Facility (RTF) (see Chapter 5). In the experiment, a static load of approximately 0.2kN was applied initially to hold the grid in position before a further 1kN was applied. Upon reaching the designated load, cyclic loading of 0.2kN at 3Hz was applied up to 100 cycles.

The rib profiles of the 30-65 and 45-65 grid are shown in Figure 3.20

Figure 3.18 Geogrid stiffness test arrangements in Instron

Figure 3.19 Clamp grip details for Grid Stiffness Test

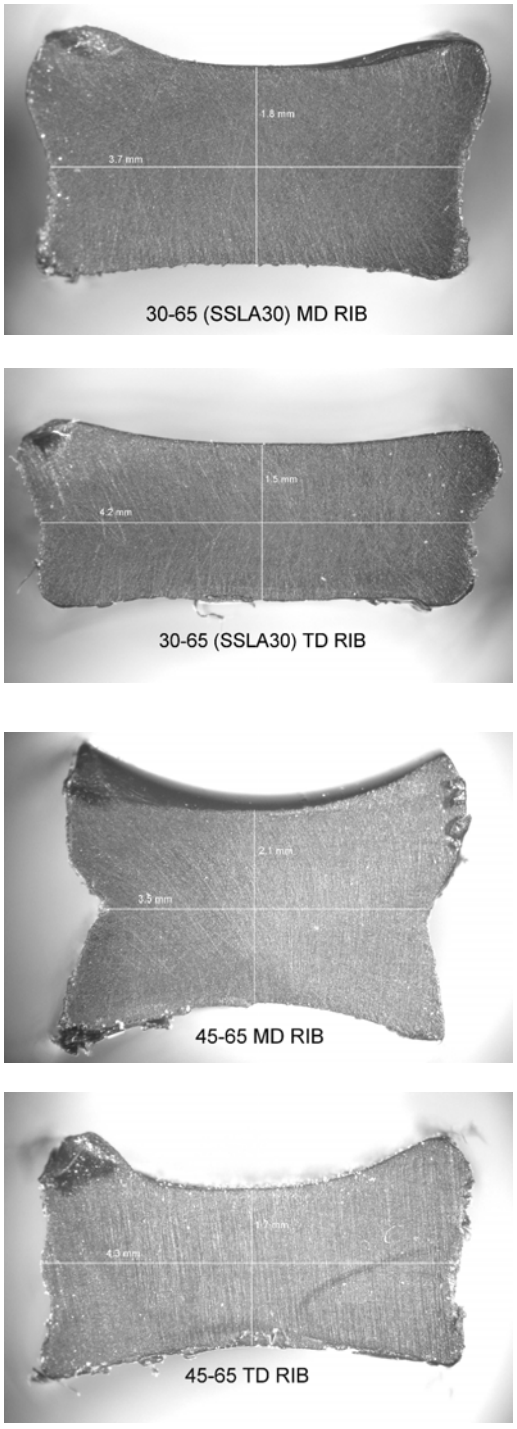

3.7x1.8mm

4.2x1.5mm

3.5x2.1mm

4.3x1.7mm

Figure 3.20 Rib cross sections for 30-65 and 45-65 grids

3.4.2 Test Results

A total of 4 grids namely the 15-65, 20-65, 30-65 and 45-65 grid, were tested. The stiffness was calculated by dividing the peak to peak load by the peak to peak strain. The graphical representation of the test results plots the tensile load (kN) and extension (mm) against the number of cycles. A typical output is illustrated in Figure 3.21 and Figure 3.22 shows the relationship between the measured stiffness and nominal tensile strength for the four 65mm aperture grids tested.

It can be seen from the results (Figure 3.22) that the relationship between measured stiffness and strength of the grid is not linear and that there is very little difference in stiffness between the 30-65 and 45-65 grid.

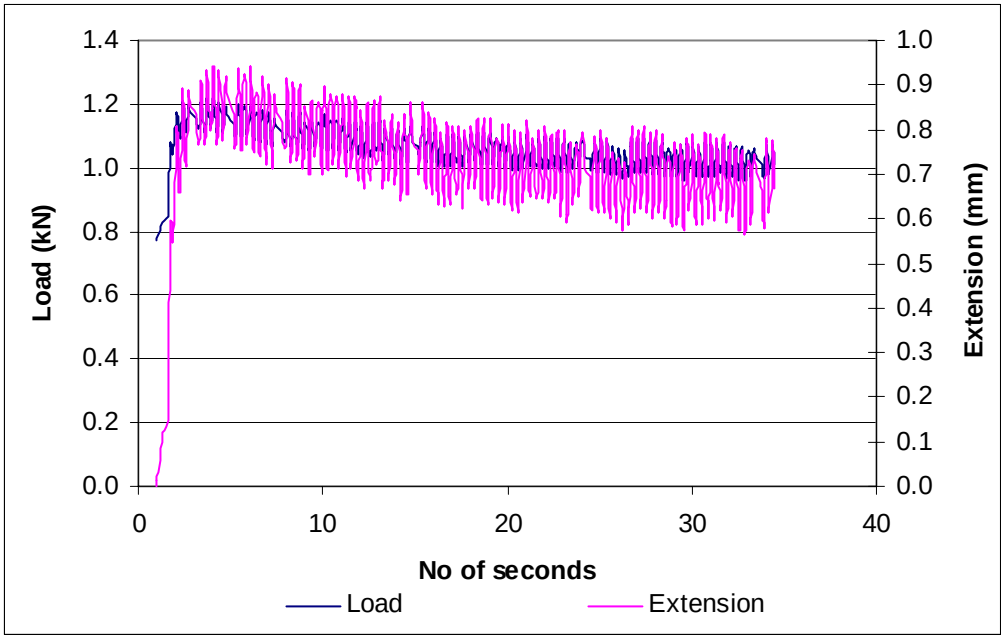

Figure 3.21 Typical output from Grid Stiffness Test

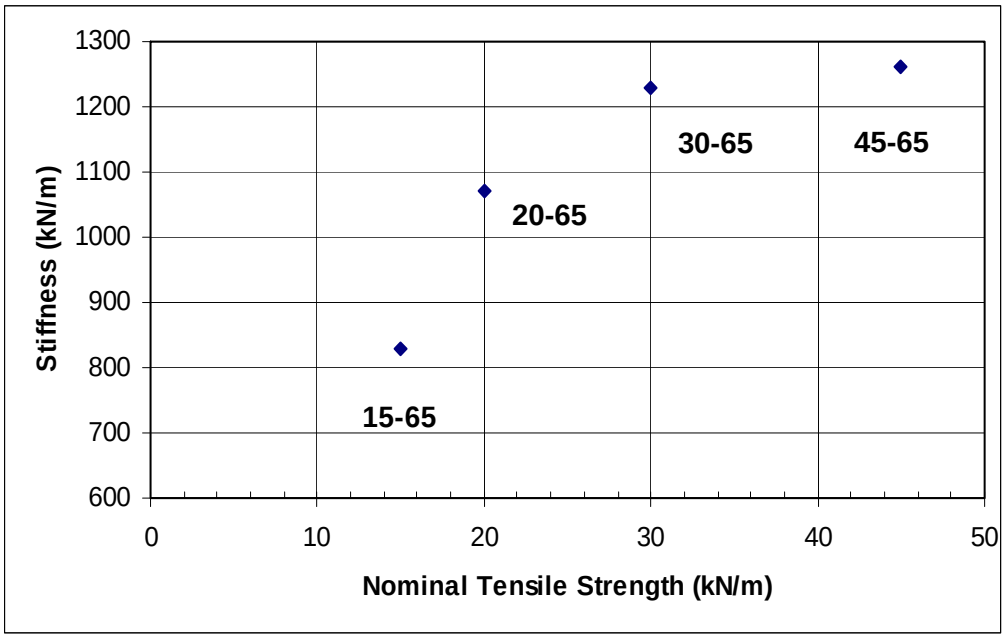

Figure 3.22 Relationship between tensile stiffness and strength for indicated grids

3.4.3 Discussion

The results from the Grid Stiffness Test showed the non-linear relationship between the strength and the stiffness of the grid. This information would be useful in the analysis of results from the CET tests.

It can also be seen from the results that the there is very little difference in stiffness between the 30-65 and 45-65 grid. However, as shown in Figure 3.20, there are significant differences in the cross sectional rib profiles of the two grids. This is likely to be one of the key parameters that contribute to any potential differences in the reinforcing quality of the grid.

3.5 Comparison with DEM

The DEM simulations of the ballast and grid described earlier were used in combination as shown in Figures 3.23 and 3.24. The DEM simulations, performed by Harrireche, replicate the dimensions of the pull-out box as well as grid aperture size. In Harrireche's pull-out model, the main features are:

- Creation of two separate samples of ballast above and below grid location. An eight-sphere cluster was used and the particles were randomly orientated as in the triaxial simulation. The sample plus grid was allowed to iterate towards equilibrium before the start of the test.

- Vertical stress was provided by the self weight of an artificially dense upper layer of spheres (shown in Figure 3.17). Penetration to the underlying ballast was prevented by the larger sized top layer spheres.

- A pull-out rate of 0.001mm/timestep was prescribed for the right end of the grid. Simulation was terminated at a total pull-out displacement of 60mm.

During simulation, the pull-out force, the axial deformation of the central ribs and the aggregate porosity were recorded. Harrireche repeated the simulation with 0kN, 0.5kN and 1.5kN confining load.

Figure 3.25 shows a comparison between 3 sets of experimental data for 20-65 grid with 11.6kPa (0.5kN surcharge plus self weight of ballast above grid level) vertical stress at the level of the grid. Figure 3.25 includes a simulation with grid stiffness multiplied by three but with geometry unchanged. The match between computed and measured resistance to pull-out is reasonably close. The reduced scatter shown by the simulated results is probably due to the lack of variability between particles.

It is interesting to note from Figure 3.25 that the effect of having a grid 3 times stiffer is not to increase the pull out force but to reduce the displacement necessary to activate that force.

Figure 3.26 shows the effect of increased grid thickness. The standard simulation grid is modelled based on the 20-65 grid. The experimental grid with twice the thickness of the standard grid represented the 30-65 grid. Again, it can be seen that the DEM results compare well with experimental data. Increased maximum pull-out force is accompanied by increased grid stiffness.

Harrireche's DEM model revealed another interesting observation. He investigated the effect of the ratio of geogrid aperture size to particle diameter (d=40mm). He performed the pull-out test under a surcharge of 0.5kN for values of aperture size ratio to particle diameter of 1.6, 1.4, 1.1 and 0.9 (denoted 'ratio' in Figure 3.27).

From Figure 3.27, as the ratio was decreased from 1.6 to 1.4, the peak resistance was mobilised at a much smaller displacement, though with little change to the peak force. As observed from the figure, with a reduced aperture/particle size ratio of 1.1, the peak resistance was similar to that with ratio 1.6 though it was mobilised at a smaller displacement. This is due to the effect of a stiffer rib which was thicker for the smaller aperture grid. However, the improvement of pull-out force mobilisation is only possible if the aperture size is big enough to induce effective ballast-geogrid interlock. A further reduction of size ratio to 0.9 gave an inferior pull-out resistance due to poor interlock.

It is interesting to note the relationship between the ballast particle size grading and the 65mm grid as shown in Figure 3.28. From the figure, it can be seen that the aperture size is slightly greater than the maximum particle size.

Harrireche's simulation on size ratio agrees well with the experimental work in which it was concluded that the 65mm aperture grid induces a better interlock than the 32mm aperture. The thickness of grid, as concluded in Section 3.2.2 is also an important factor in the optimisation of grid interlock as shown by the DEM simulation.

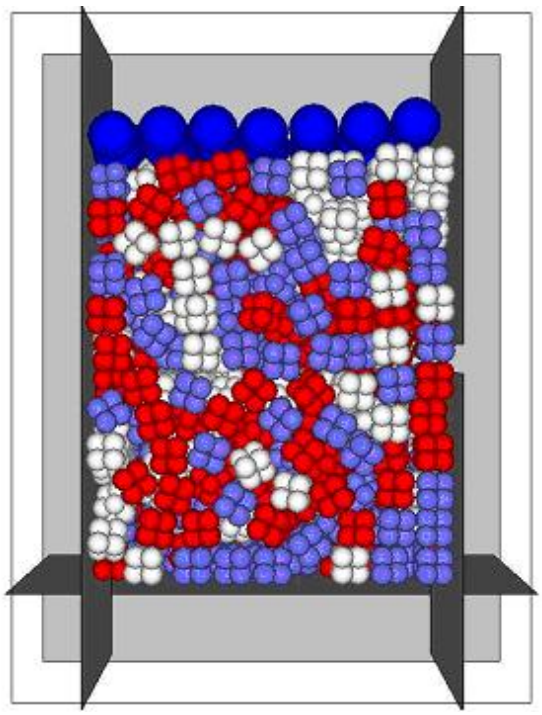

Figure 3.23 Simulation of a Pull-Out Test

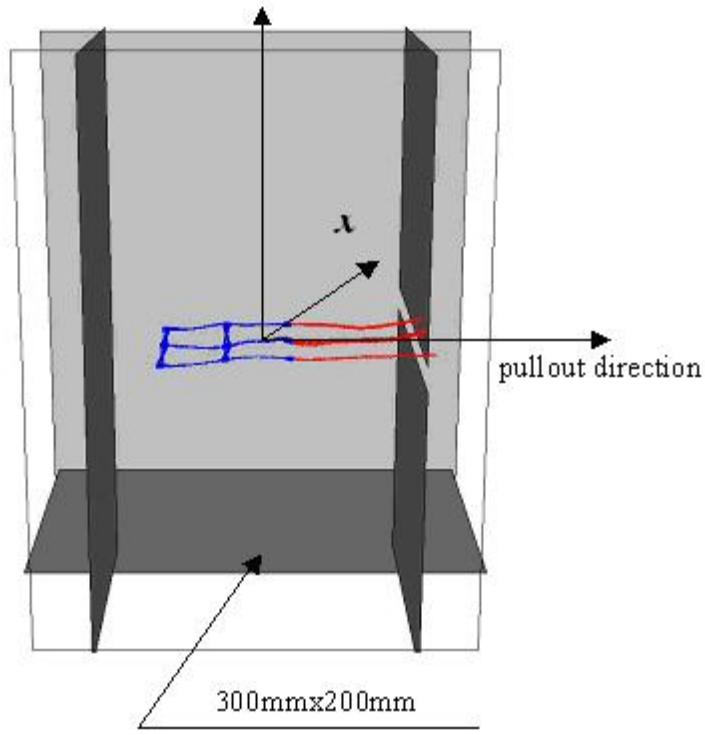

Figure 3.24 Geogrid deformation predicted in Pull-Out Test

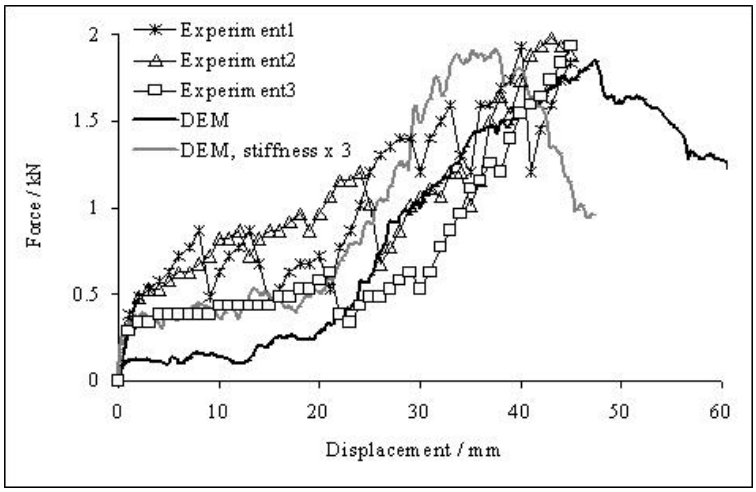

Figure 3.25 Comparison of DEM with laboratory results under 0.5kN surcharge

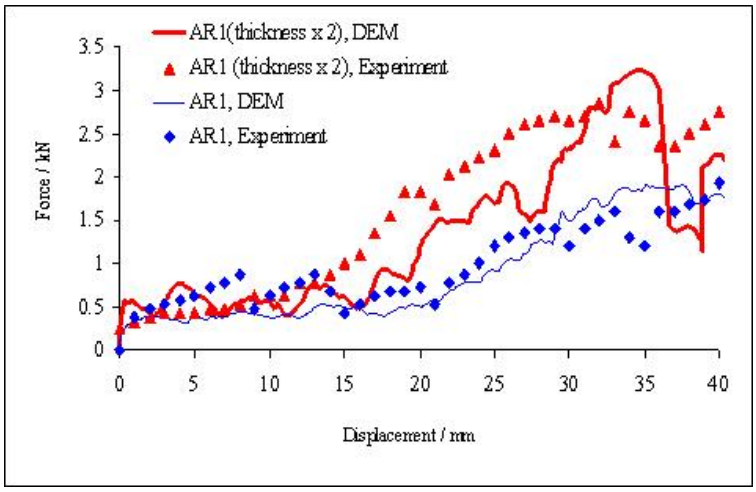

Figure 3.26 Effect of thickness in pull-out test simulation under 0.5kN surcharge

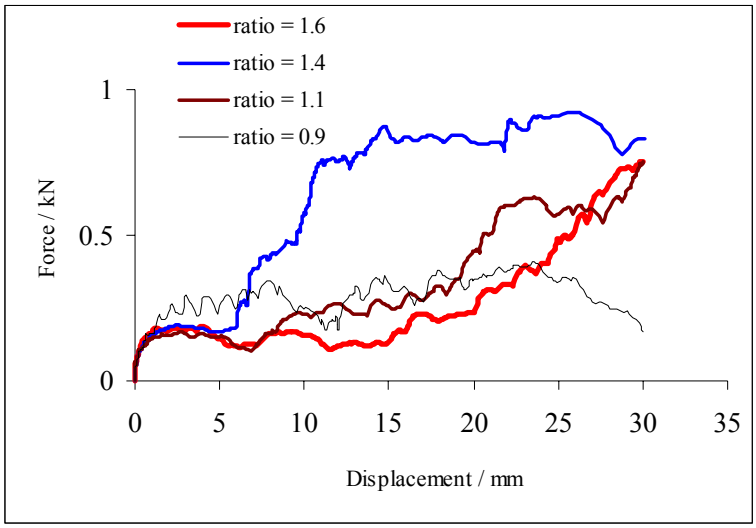

Figure 3.27 Effect of aperture size in pull-out test simulation under 0.5kN surcharge

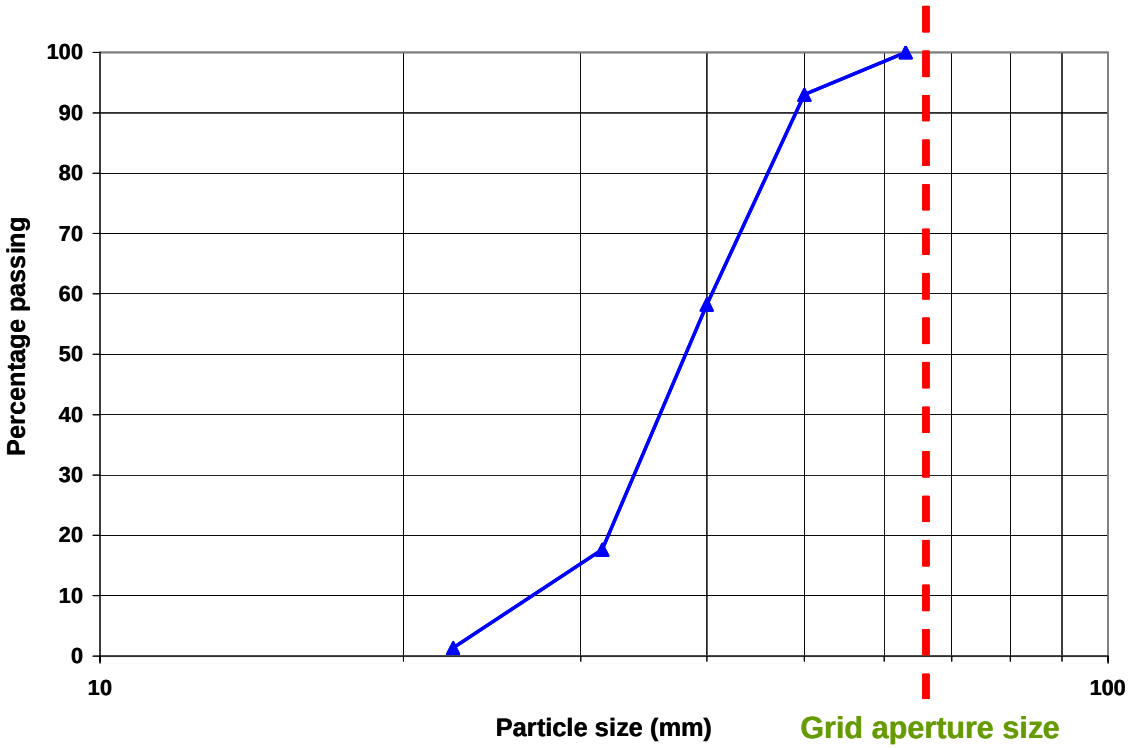

Figure 3.28 Optimum grid aperture size relative to ballast grading

3.6 Summary

The aim of the series of element tests described in this chapter was to provide data and information to assist the DEM modelling work performed by Harrireche.

A series of Particle Tests using a modified shear box test were performed to obtain the frictional properties of ballast particles to quantify one of the input parameters for computational modelling. A pull-out test was also developed to quantify the pull-out resistance of various grid types, as input data to the DEM simulation.

The results obtained from the Particle Test were fairly consistent with the literature with a frictional coefficient of 0.6. Results from the pull-out test were reasonably repeatable. Grid aperture and stiffness in terms of rib thickness were found to be the two critical criteria as proven in both laboratory (pull-out) tests and DEM simulation results.

The understanding of grid/ballast interlock gained from the work in this chapter helped in the planning of laboratory work for the Composite Element Test (CET) which will be presented in Chapter 4.

The understanding of the non-linear relationship between grid strength and grid stiffness would help in the validation of the results presented in the CET experiments.

An initial plan to model the CET using DEM was terminated due to the large number of clusters required to model the CET and the long computational time was found to be impractical.

4 COMPOSITE ELEMENT TEST

4.1 Introduction

This component of the project was designed to allow a relatively large number of simplified full scale tests to be carried out within a reasonable time frame. The aim was to investigate the various design variables (e.g. geogrid geometric properties, subgrade stiffness and geogrid location within a reinforced ballast and sub-ballast composite). The Composite Element Test (CET) provided an approximate simulation of the situation beneath a sleeper in a simplified format. The test provided meaningful direct data on the comparative performance of a reinforced and unreinforced composite and with grids of different characteristics. The intend was to use the CET to gather many more results which wouldn't be possible in the more refined but time consuming Railway Test Facility (RTF) which is a better representation of real railway track

The initial test was carried out in a trough-like enclosure with plan dimensions of 1.4m length x 0.7m width. This was to accommodate Tensar International's prototype grid size. The walls of the trough were made of wood with a covering of steel sheet to reduce friction. Subgrade stiffness variation was achieved through the use of rubber sheets. The rubber was overlain by a 50mm layer of graded 10mm maximum sized crushed stone sub-ballast. A 250mm thick ballast layer (from base of steel beam to geogrid) was placed above the sub-ballast for all tests. The reason being a minimum clearance depth of 200mm is required on a railway track for maintenance activities e.g. tamping. The ballast stone used in the CET was Glensanda ballast (see 3.2.1) and to ensure repeatability and validity of results, the same type of ballast was used throughout all the tests in this thesis. The test arrangement is as seen in Figures 4.1 and 4.2.

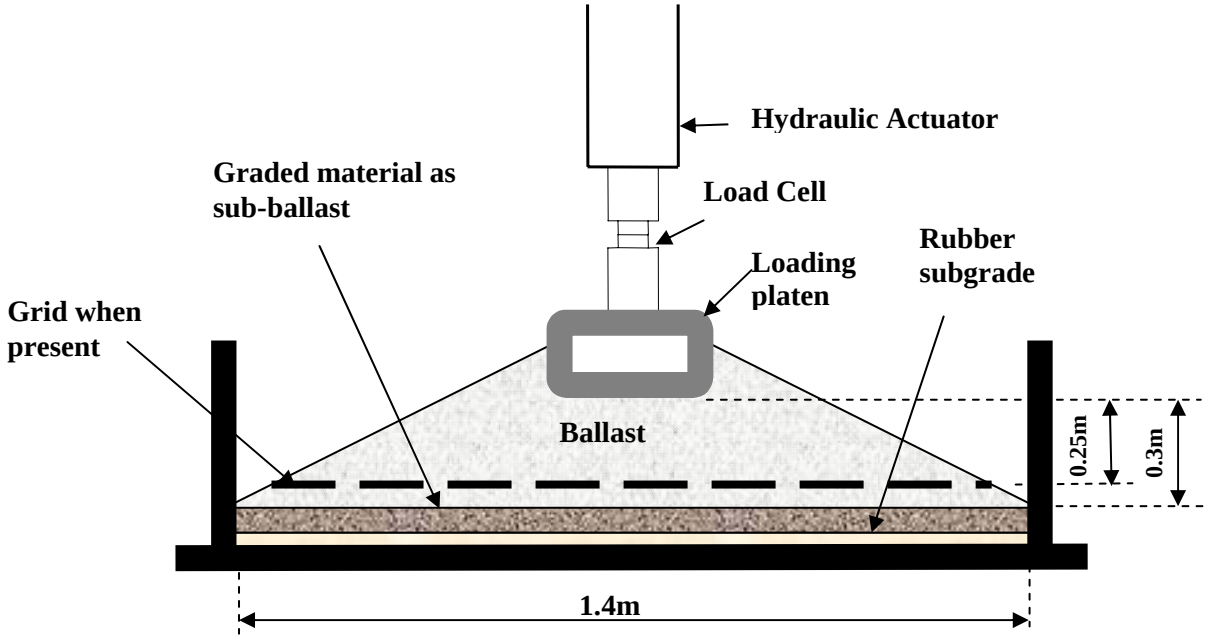

Figure 4.1 Section of CET

Figure 4.2 CET test arrangements

4.2 Test Procedures

In order to vary subgrade stiffness, 14mm thick sheets of shot-blast rubber were used. Tests were performed with two distinct subgrade conditions, namely stiff (with a single sheet of rubber) and soft (with three sheets of rubber). The shot-blast rubber has a shore hardness of 40/45 ShA (Tennant Rubber, 2002). Figure 4.3 and 4.4 show the details of the rubber subgrade. Figure 4.4 also shows the smooth steel plate surface of the trough wall, which was used to reduce friction with the ballast particles to allow more freedom for ballast movement.

Cyclic loading at 2 Hz was provided by the servo-hydraulic actuator which is capable of exerting a 50kN load. However, as the frame was not bolted to a strong floor, the facility provided an approximate safe working load of 30kN. A load of 20kN was selected for all CET set-ups. Loading was applied through a rectangular hollow steel beam which measures 0.7m long by 0.25m wide. This gives a stress of 114kPa beneath the beam which is approximately half of the maximum expected on an actual track. This is considered reasonable since the unsupported sloping ballast face gives a weaker structure than an actual track. Also, the role of the CET is not direct track simulation but an element test to assess the effects of the key variables. After initial experimentation, standard test duration of 30,000 cycles was adopted. This allows a relatively quick turn-around of tests and comparison of data with different variables.

Figure 4.3 Very soft subgrade conditions in CET

Figure 4.4 Rubber subgrade in CET

Vertical deformation was measured by means of Linear Variable Differential Transformers (LVDTs) placed either side of the loading ram on the upper side of the steel beam. This arrangement allowed compensation for the inevitable uneven settlement caused by the random packing nature of the ballast particles. The load cell measured vertical load. Load and deflection data was recorded from the control system and signal conditioning equipment as shown in Figure 4.5.

Figure 4.5 Control system for CET

In order to ensure repeatability and validity of comparable data, the same experimental sequence was maintained for the various test configurations discussed later in this section. The same volume of ballast was utilised and the compaction and profile of the slope was achieved by applying the same amount of vibration (compaction) to the ballast surface through the use of an electrical vibro-tamper. Before the placement of the loading beam, the same duration of compaction (1 minute on each side slope) was applied to the ballast surface to ensure even distribution of load to the ballast layer which in turn enhanced consistency. The angle of the slope was controlled by maintaining alignment with markings on the wall of the trough. A spirit level was used to ensure that there was minimum tilting on the loading beam.

In order to provide a consistent reference for the large number of grids tested in the CET, the nomenclature shown in Table 4.1 was adopted. The grids were referenced according to their nominal tensile strength (kN/m) and aperture size (mm) (e.g. a 20-65 grid will have a nominal tensile strength of 20kN/m and an aperture size of 65mm).

Table 4.1 Grid nomenclature and characteristics

Manufacturer ID	**New ID**	**Aperture Size (mm)**	**Manufacturer Quoted Tensile Strength (kN/m)**		**Grid Weight (g/m^2)**
			Machine Direction	**Transverse**	
SSLA 10	**15-65**	65	17.1	17.3	146
SSLA 20	**20-65**	65	20	20	220
SSLA 30	**30-65**	65	30	30	330
SSLA 40	**45-65**	65	46.1	46.8	414
SS20	**20-38**	38	20	20	220
SS40	**40-32**	32	40	40	530
NG 30 (100)	**30-100**	100	20.6	29.6	246
NG 90	**25-90**	90	27.4	27.2	220
BIAX 25	**25-50**	50	25.2	25.8	134
BIAX 47	**45-50**	50	45.5	47.3	237

In the first phase of the CET tests, two subgrade conditions were simulated, approximately equivalent to half spaces of stiffness 30MPa and 90MPa using three and one sheets of rubber respectively. The stiffness was defined using the conversion sheet provided by Tennant (2001). An unreinforced control test was performed under both subgrade conditions. 15-65, 20-65, 30-65 and 40-32 grids were also

subsequently tested. The grid sat on a single layer of ballast as shown in Figure 4.6. Resilient load-deflection responses were recorded at 100; 1000; 3000; 10,000; 30,000 cycles.

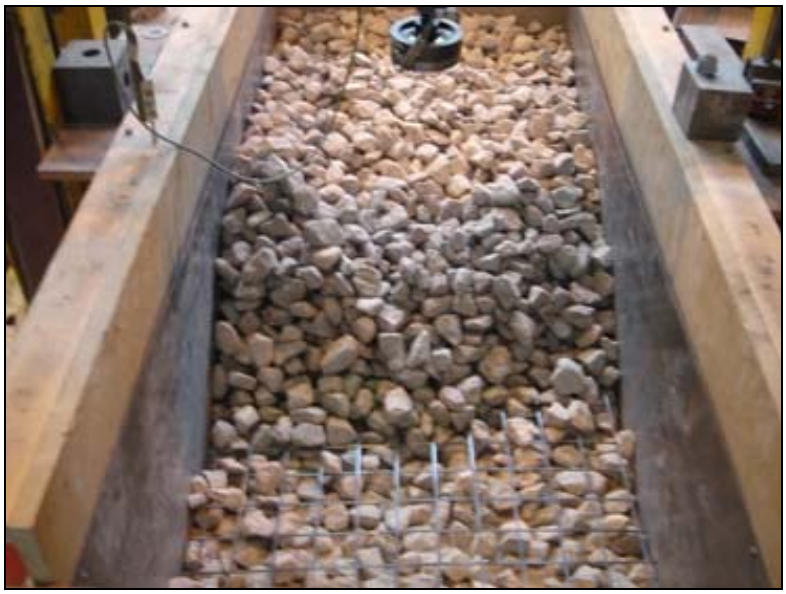

Figure 4.6 Grid sitting on a single layer of ballast (CET)

One potential problem with using the same batch of ballast for consistency is the loss of particle angularity. The used ballast, after five rounds of testing, was replaced with a new batch with approximately the same volume (1/2 of a one tonne ballast bag). Repeat tests were performed to ensure the validity of previous results.

The next stage of the CET testing saw the introduction of a higher overburden pressure by adding additional ballast over the sloping ends of the test elements. The purpose of this arrangement was to investigate the performance of selected grids under higher normal loads more closely representing in-situ conditions. This modification involved sealing the ends of the trough with wooden boards as shown in Figure 4.7. The end boards were securely fastened to the floor bolts to minimise any lateral movement exerted by the ballast during loading. Figure 4.8 shows the schematic diagram of the ‘overburdened’ CET.

After several rounds of testing, it was decided that to better compare the effects of reinforced and unreinforced composite, a 'soft' subgrade (e.g. 3 sheets of rubber) configuration was to be used for all the remaining tests.

Figure 4.7 'Overburdened' CET arrangements.

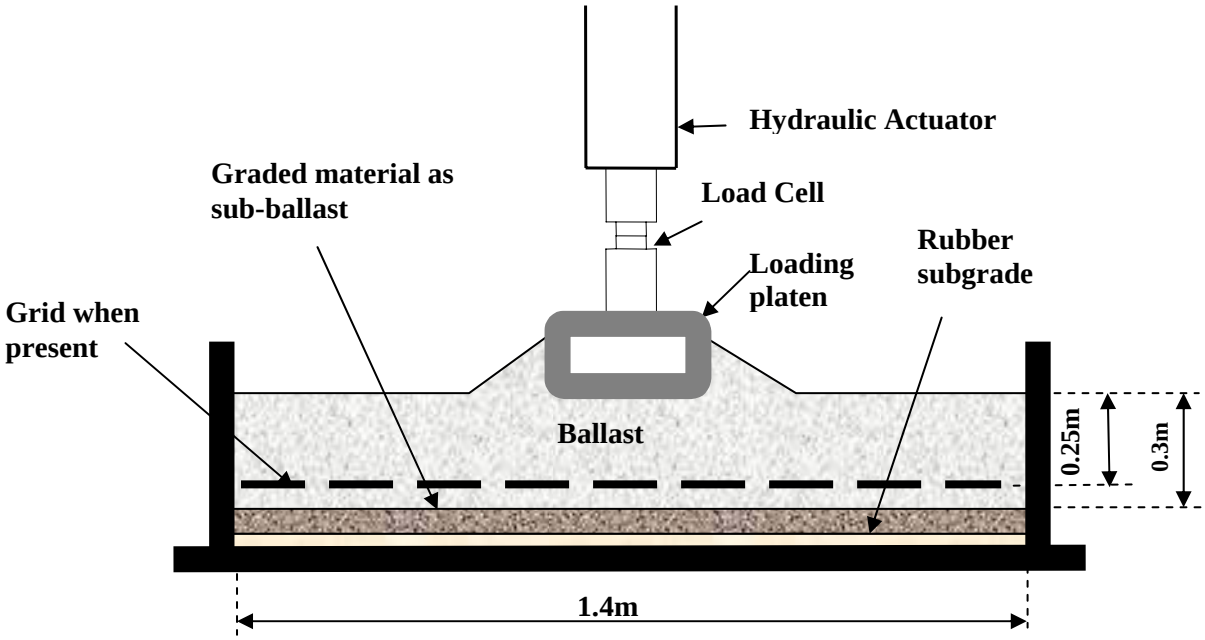

Figure 4.8 Schematic diagram of 'Overburdened' CET.

4.3 Results

Initial work on the CET was conducted to investigate the repeatability of the test. The deformation against the number of cycles for three unreinforced tests (soft subgrade) is shown in Figure 4.9. The total settlement was measured after 30,000 cyclic loads of 20kN at a frequency of 2Hz.

It can be seen that the 3 unreinforced CET tests demonstrated good repeatability as all three tests yield settlement in the region of 39mm to 44mm. However, the particulate nature of ballast could be seen in the initial stage of the test (less than 500 cycles) where there were some variations in settlement readings.

Similar control tests were performed with the stiff subgrade and the results are shown in Figure 4.10. The repeatability of the unreinforced tests with the stiff subgrade is once again very satisfactory and it can be observed that the random particulate nature of the ballast is less apparent under a stiffer subgrade due to the reduced freedom of movement. Overall the figures show that the settlement for the CET can be reproduced and comparisons with various reinforced grid arrangements can be made with an acceptable level of accuracy.

Table 4.2 presents the details of the CET tests achieved in this project. It can be seen from the table that most of the test results are obtained from a mean of 2 or 3 tests.

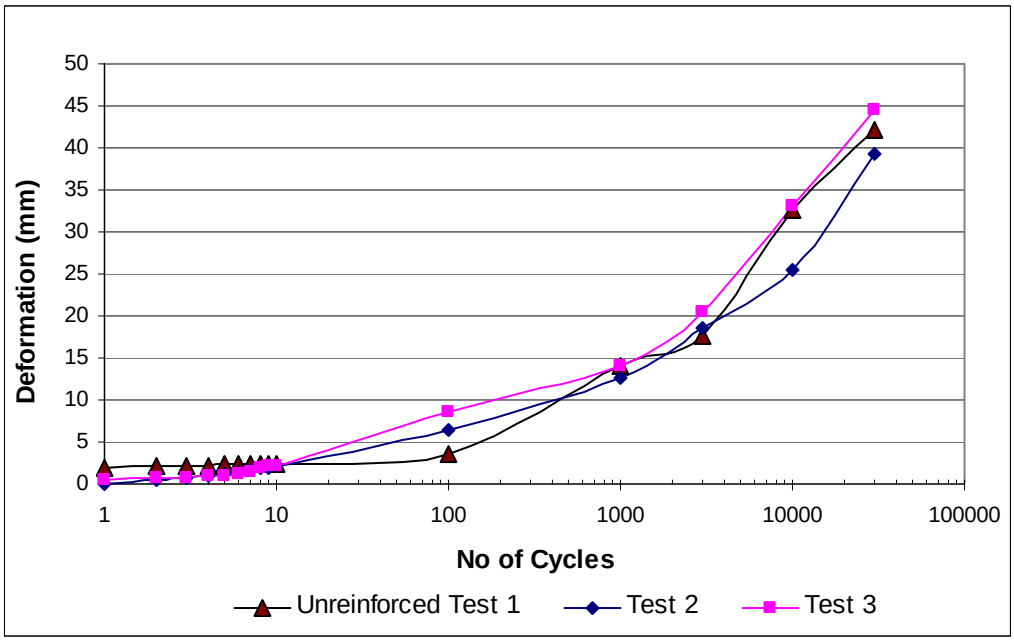

Figure 4.9 Repeatability of CET demonstrated by 3 control tests (unreinforced on soft subgrade)

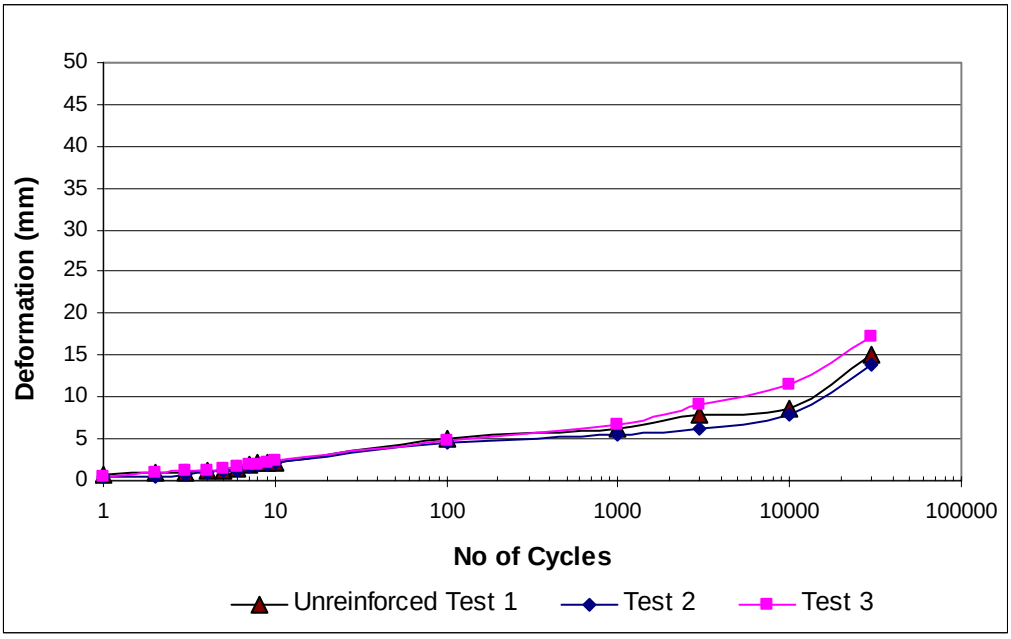

Figure 4.10 Control tests on stiff subgrade (unreinforced)

Table 4.2 Details of all CET tests

Grid Types	New ID	Aperture Size (mm)	Support Condition/ Grid Placement	CET		CET + Overburden	
				No of Tests	Mean Settlement (mm)	No of Tests	Mean Settlement (mm)
SSLA 10	15-65	65	Sub ballast on 3 layers of rubber/ Grid on single layer of ballast	3	31.73	2	10.34
			Sub ballast on 1 layer of rubber/ Grid on single layer of ballast	2	9.87	-	-
SSLA 20	20-65	65	Sub ballast on 3 layers of rubber/ Grid on single layer of ballast	3	10.25	-	-
			Sub ballast on 1 layer of rubber/ Grid on single layer of ballast	2	7.70	-	-
SSLA 30	30-65	65	Sub ballast on 3 layers of rubber/ Grid on single layer of ballast	3	12.12	2	7.79
			Sub ballast on 1 layer of rubber/ Grid on single layer of ballast	2	7.90	-	-
			Sub ballast on 3 layers of rubber/ Grid direct on sub ballast	0	-	2	8.99
SSLA 40*	45-65	65	Sub ballast on 3 layers of rubber/ Grid on single layer of ballast	2	23.04	2	6.08
SS40	40-32	32	Sub ballast on 3 layers of rubber/ Grid on single layer of ballast	2	46.94	2	13.27
SS20	20-38	38	Sub ballast on 3 layers of rubber/ Grid on single layer of ballast	2	38.03	-	-
NG 90*	25-90	90	Sub ballast on 3 layers of rubber/ Grid on single layer of ballast	2	27.5	-	-
NG 100*	25-100	100	Sub ballast on 3 layers of rubber/ Grid on single layer of ballast	2	22.34	-	-
BIAX 47*	45-50	50	Sub ballast on 3 layers of rubber/ Grid on single layer of ballast	2	39.80	-	-
BIAX 25 *	25-50	50	Sub ballast on 3 layers of rubber/ Grid on single layer of ballast	2	27.08	-	-
Double 30-65	30-65	65	Sub ballast on 3 layers of rubber/ Grid on single layer of ballast and mid-depth of ballast	-	-	1	8.63
Mid-depth 30-65	30-65	65	Sub ballast on 3 layers of rubber/ Grid on single layer of ballast	-	-	1	8.66
Steel Mesh	-	65	Sub ballast on 3 layers of rubber/ Grid on single layer of ballast	-	-	1	5.81
30-65 Geotexile	30-65	65	Sub ballast on 3 layers of rubber/ Grid on single layer of ballast	-	-	1	12.75
30-65 unbonded geotexile	30-65	65	Sub ballast on 3 layers of rubber/ Grid direct on sub ballast	-	-	1	11.42
Non-Junctioned Grid	30-65	65	Sub ballast on 3 layers of rubber/ Grid on single layer of ballast	-	-	1	16.05
Unreinforced	-	-	Sub ballast on 3 layers of rubber	3	42.11	3	11.72
			Sub ballast on 1 layer of rubber	3	15.06	-	-
			Sub ballast on no rubber	3	11.55	-	-

* Specially made Tensar geogrid for the purpose of this project.

The effect of reinforcement was explored with the installation of a 20-65 grid, seated on a single layer of ballast stones. Figure 4.11 shows the comparison of two subgrade stiffnesses namely stiff and soft, governed by the layers of rubber utilised. The plots are the average of three tests performed in the CET.

From Figure 4.11, there is a marked reduction in settlement with a 20-65 reinforced composite under both subgrade conditions. The Aperture size to Ballast size (A/B) is also shown. The improvement is most apparent in the reinforced composite with a soft subgrade. In that case, total settlement reduces by approximately 75% (from 42mm to 10.2mm) over 30,000 cycles under a 20kN cyclic load. The results are consistent with Hamed (1987)'s observation where he stated in his report that the benefit of reinforcement is most noticeable under soft subgrade conditions. In his experiment, he also utilised rubber to mimic a soft subgrade. Raymond (2001) published a similar observation.

On a stiff subgrade, the comparative reduction in ballast settlement is less at approximately 50% (from 15.4mm to 7.7mm). From Figure 4.11, it can be seen that the reinforced and unreinforced setup only differs at high load cycles. This is likely to be due to the reduced rate of particle orientation; hence, it is only at high number of load cycles that sufficient plastic strain has developed for the interlock to develop between ballast and geogrid, resulting in reduced deformation.

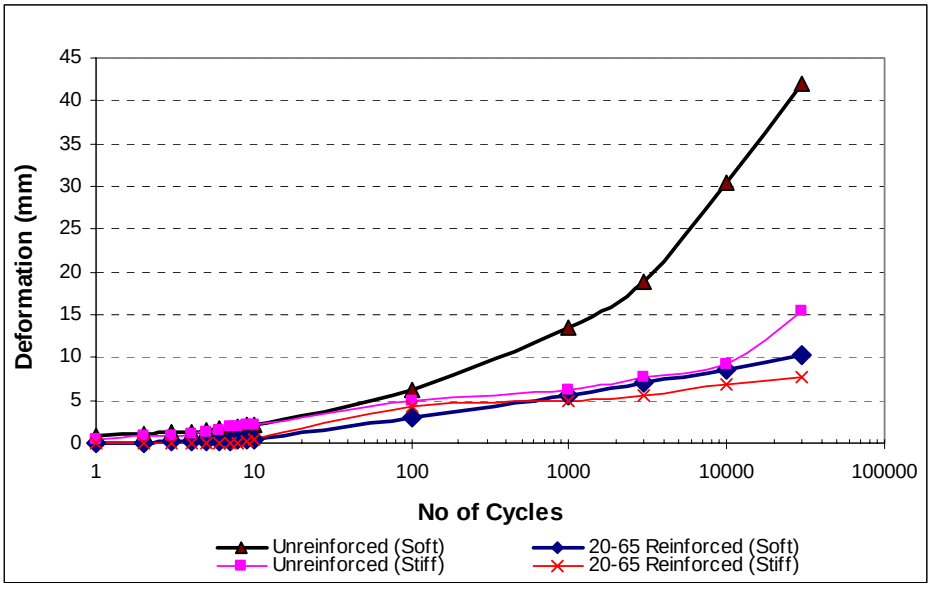

Figure 4.11 Effect of reinforcement on stiff and soft subgrade (A/B: 1.6)

The geogrid's aperture size has a direct influence on the settlement characteristic of a reinforced composite (see section 3.2.3). This was investigated with a series of tests involving Tensar 40-32 and 20-65 grids. Due to the amplified improvement observed in tests using the soft subgrade, all later CET tests were conducted using the soft subgrade (3 rubber sheets). The results are shown in Figure 4.12, including unreinforced case as a reference for comparison. The 20-65 grid with a relatively larger aperture size (65mm and of medium stiffness of 20kN/m) outperformed the stiffer 40-32 grid (32mm aperture). This is in agreement and correlates well with Harrireche's DEM results (see Section 3.5). The results also highlighted the relative importance of aperture size compared to stiffness of the grid. One grid has either twice the stiffness or twice the aperture size of the other.

Figure 4.13 and 4.14 illustrate the typical load deflection responses of 40-32 and 20-65 reinforced composite's recorded under very slow loading during testing.

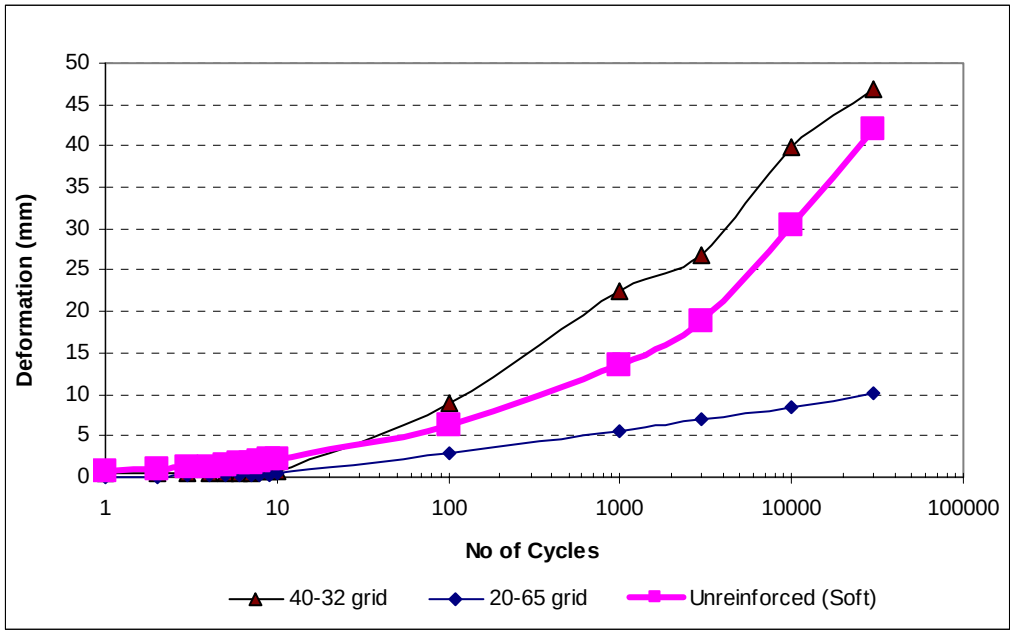

Figure 4.12 Comparison in performance of 40-32 (A/B: 0.8) and 20-65 (A/B: 1.6) grid.

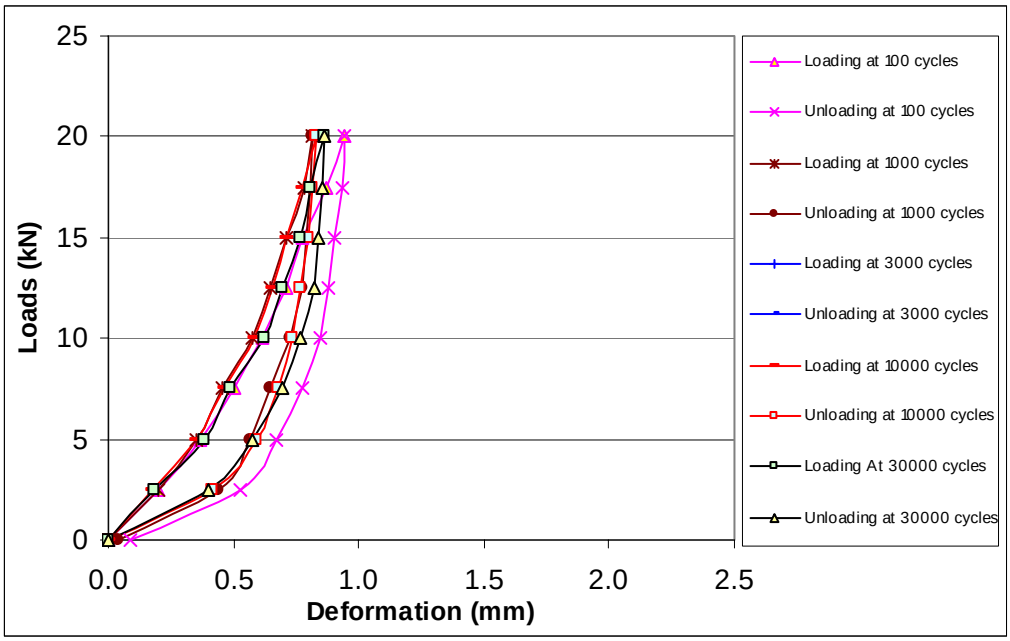

Figure 4.13 Load-deflection Hysteresis Loops – 20-65 grid (A/B: 1.6); soft subgrade

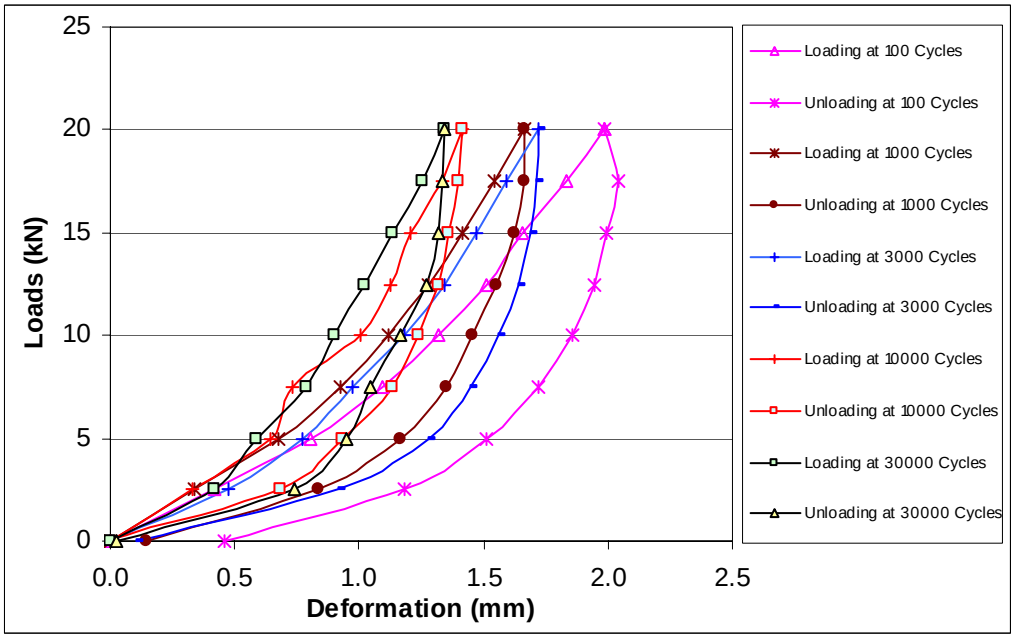

Figure 4.14 Load-deflection Hysteresis Loops – 40-32 grid (A/B: 0.8); soft subgrade

It can be seen from Figure 4.13 that there was minimal change in the stiffness response in the 20-65 reinforced composite. Comparatively, as observed from Figure 4.14, larger hysteresis loops were recorded for the 40-32 reinforced system and stiffening continued during the course of the test; it was significantly less stiff than the 20-65 reinforced system. This reinforces the belief that grid stiffness is much less significant than geometry. A photograph taken after the test showed the inefficiency of grid interlock in a 40-32 reinforced system as seen in Figure 4.15.

From Figure 4.15, it can be concluded that the apertures in the 40-32 grid are too small to allow proper interlock with the ballast particles to take place. In fact, 'voiding' occurred and it created a shear failure plane. This effectively compromised the composite and is deemed to be the key reason for its poorer performance where total settlement surpassed that in an unreinforced test.

Figure 4.15 Shear failure plane in 40-32 (A/B: 0.8) reinforced CET

The aperture size effect was further investigated with the testing of more grids. Tensar International provided a series of novel grids with a wide spectrum of aperture sizes. The additional grids tested were 20-38, 25-90, 25-100 and 25-50, and had similar tensile strengths (and possibly similar stiffness, see Section 3.4.2) in order to make a comparison based on aperture size only. Again, tests were conducted using the 'soft' subgrade condition and the results are presented in Figure 4.16.

All the grids generally reduced deformation but the variation in aperture size produced a wide spectrum of results. There is a consistency in the data collected as the smaller grid (20-38) performed poorly as expected. In addition, the larger grids did not perform as well as the 20-65 grid. The relationship between aperture size and resistance to deformation is more clearly shown on Figure 4.17, and it can be seen that the optimal grid aperture size appears to be at around 60- 80mm.

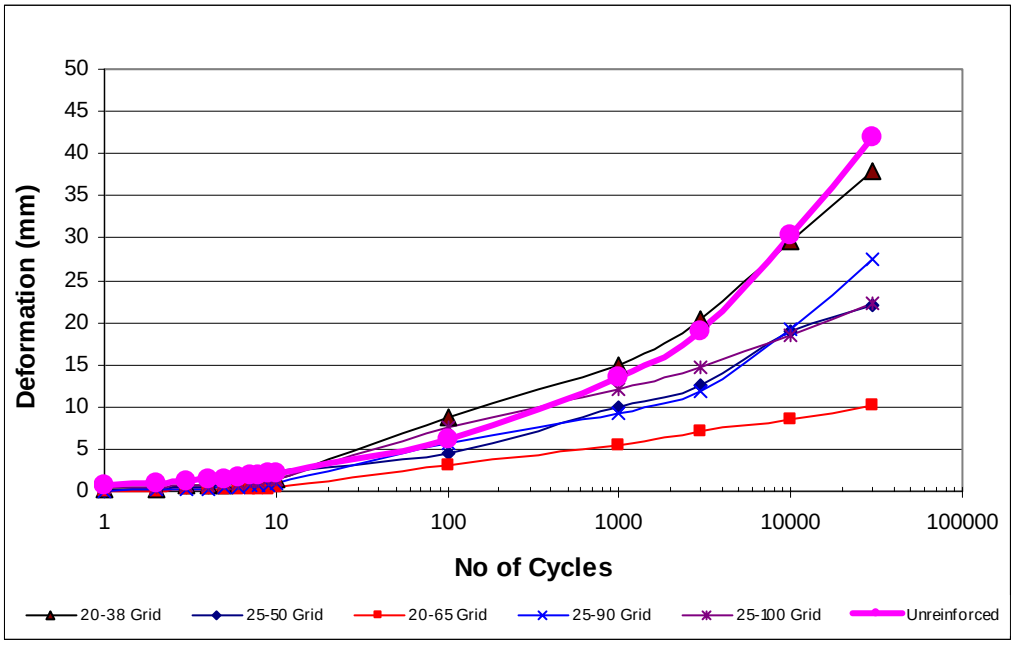

Figure 4.16 Aperture size effect [20-38 (A/B: 0.95), 25-50 (A/B: 1.25), 20-65 (A/B: 1.6), 25-90 (A/B: 2.25), 25-100 (A/B: 2.5)]

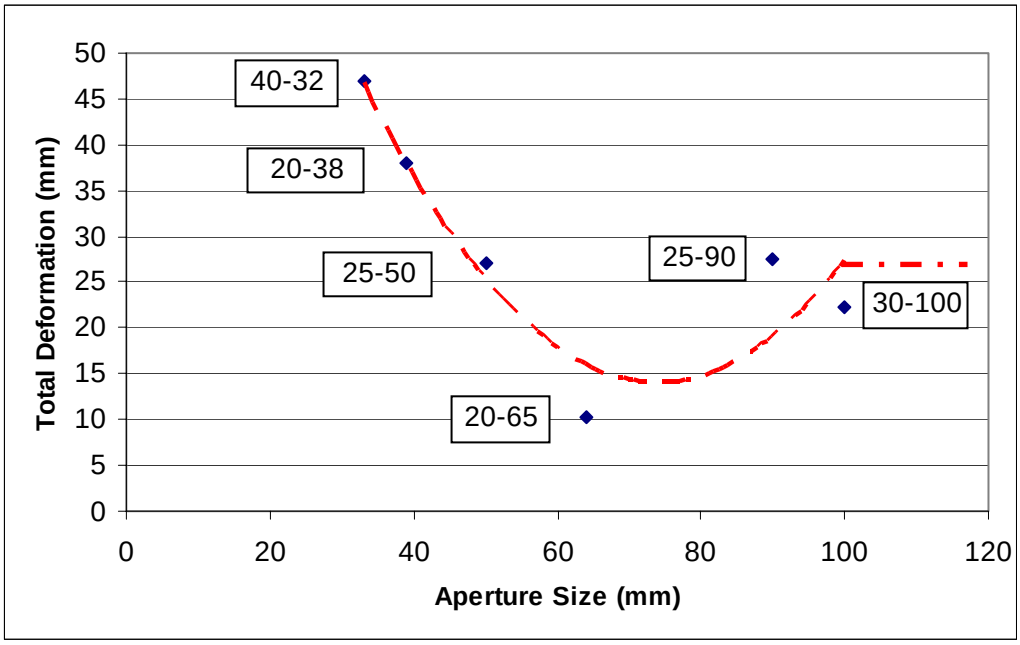

Figure 4.17 Permanent deformation after 30,000 cycles as a function of grid aperture size (showing probable best fit line compared with Figure 2.25)

In order to quantify the optimal mechanical properties of the grid, a range of Tensar 65mm aperture grids with different stiffnesses were tested in the modified CET with a higher vertical confining stress. The results are presented in Figure 4.18.

It can be seen from Figure 4.18 that the general level of permanent deformation was significantly lower than in the earlier tests. The deformation after 30,000 cycles for the unreinforced test as shown in Figure 4.16 is 42mm compared to 12mm in the modified CET. The reason is likely to be due to the increased confinement of particles with the additional ballast. The major difference in this 'overburdened' version of the test was that the level of permanent deformation consistently decreased as the tensile strength and therefore stiffness of the grid increased. Figure 4.19 summarises all the data for both types of test and illustrates the points.

It had been observed from the earlier version of the 45-65 reinforced CET test that there was a formation of a shear failure plane, similar to that seen in the 40-32 reinforced CET, hence the high deformation shown in Figure 4.19. This led to the conclusion that bending stiffness of the grid plays a part in the failure plane

formation. The effect was however not seen in the 'overburdened' CET due to the additional normal stress. The additional overburden is likely to have increased contact between ballast and grid resulting in better interlock even if the grid has a high bending stiffness.

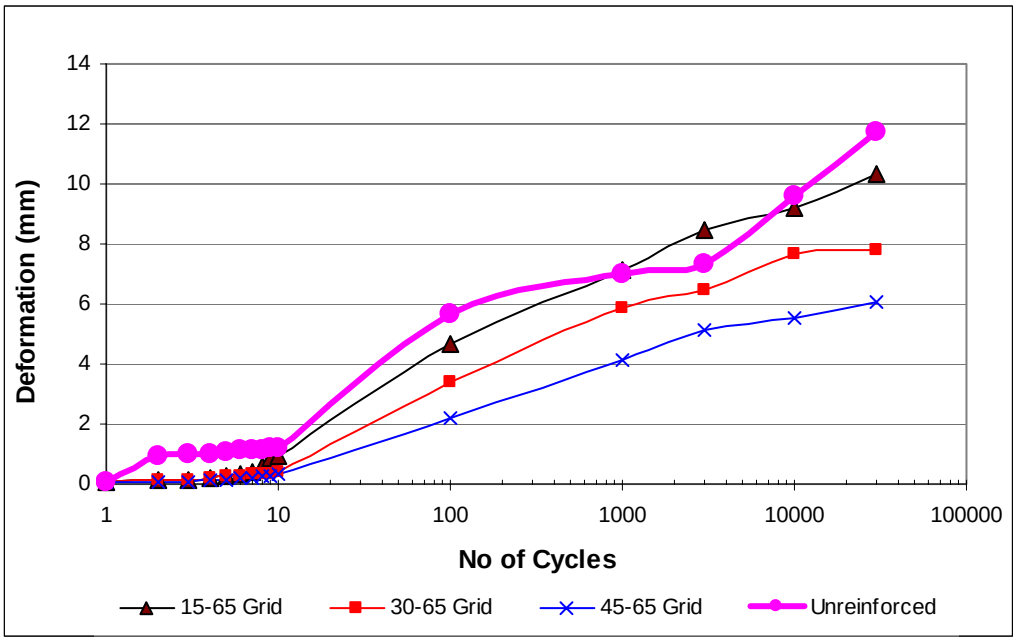

Figure 4.18 'Overburdened' CET test of 65mm (A/B: 1.6) aperture size grid

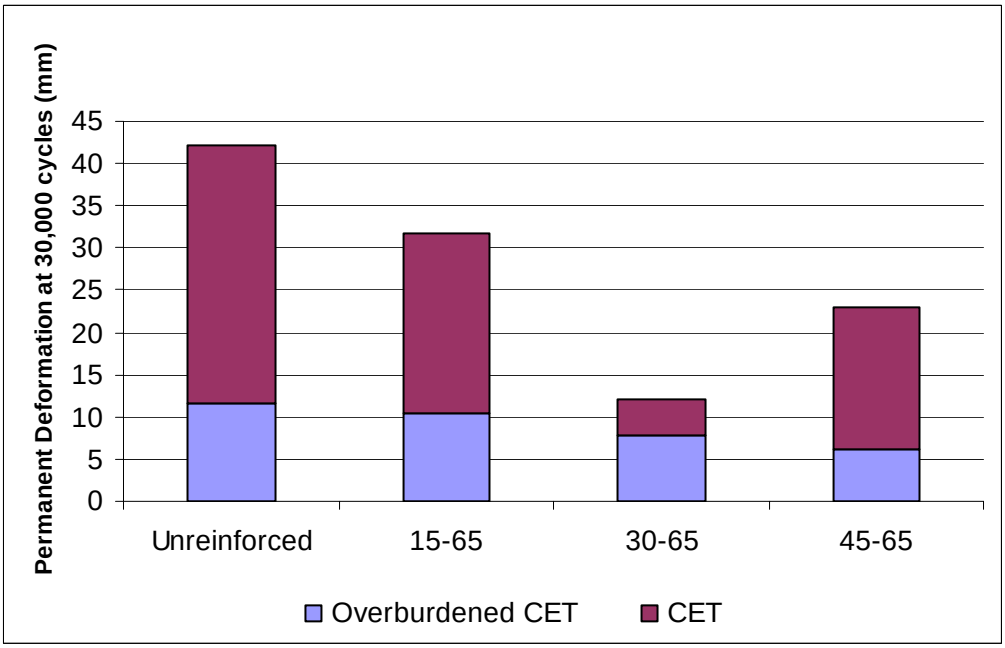

Figure 4.19 Comparison of CET and 'Overburdened' CET

The data from the CET tests suggest that a 65mm aperture size and high stiffness to strength ratio provides the most effective reinforcement. This is supported by the results shown in Figure 4.18 where all 3 variants of the 65mm range performed better than the unreinforced test, with the stiffest 45-65 recording the least permanent deformation. The 45-65 clearly outperformed the less stiff 15-65, reducing final settlement by around 50% compared to the unreinforced case.

To further investigate the effect of stiffness, a steel grid was fabricated in the laboratory with a 65mm aperture size but with a different rib shape relative to the Tensar grids. The steel grid (Figure 4.20) was subjected to the same test regime in an 'overburdened' CET test. From Figure 4.21, it is clear that the steel grid exhibited much better performance over the initial part of the test, up to 1,000 cycles; however, the final settlement was similar to Tensar's 45-65 grid. This indicates the importance of grid stiffness, particularly in the early stages of loading, with rib profile becoming more prominent in the latter stages of loading at higher strains.

The rib profile effect can be derived from the results shown in Figure 3.22. The figure shows the grid stiffness results obtained from a series of grid stiffness tests performed using the Instron machine. It can be seen that the stiffness of the 45-65 grid (1260kN/m) was not very much higher than the 30-65 grid (1230kN/m), and the improvement in performance is therefore likely to be due to the difference in rib profile with 45-65's thicker rib providing a better lateral restraint (improved interlock) of the ballast. The rib profiles are shown in Figure 3.20.

The resilient response of a variety of grids tested in the modified 'overburdened' test was presented in Figure 4.22. It can be observed that the resilient deflections do not follow any distinct pattern and it is not related to the recorded deformation. It can be concluded from the results that geogrid reinforcement has very little influence on the stiffness of the ballast-grid composite.

Figure 4.23 shows CET results involving various installation arrangements for the 30-65 grid, the material which was regarded as the best compromise for practical use, not least because it is a current production material. The figure shows a comparison of the performance of the grid in its usual position at the bottom of the ballast layer

sitting on a single layer of ballast particles, versus one located at mid-depth and a system with two layers of grid (one at the bottom and one at mid-depth). The results showed that neither of the alternative systems were any more effective at reinforcing the ballast. The results indicated that once effective interlock is achieved, the grid will reinforce the whole layer as an entity to a certain depth or zone of influence. Hence, having a grid at mid-depth or a multi layer system will not influence the performance of the composite in terms of settlements as shown in Figure 4.23.

Figure 4.20 Steel grid (A/B: 1.6)

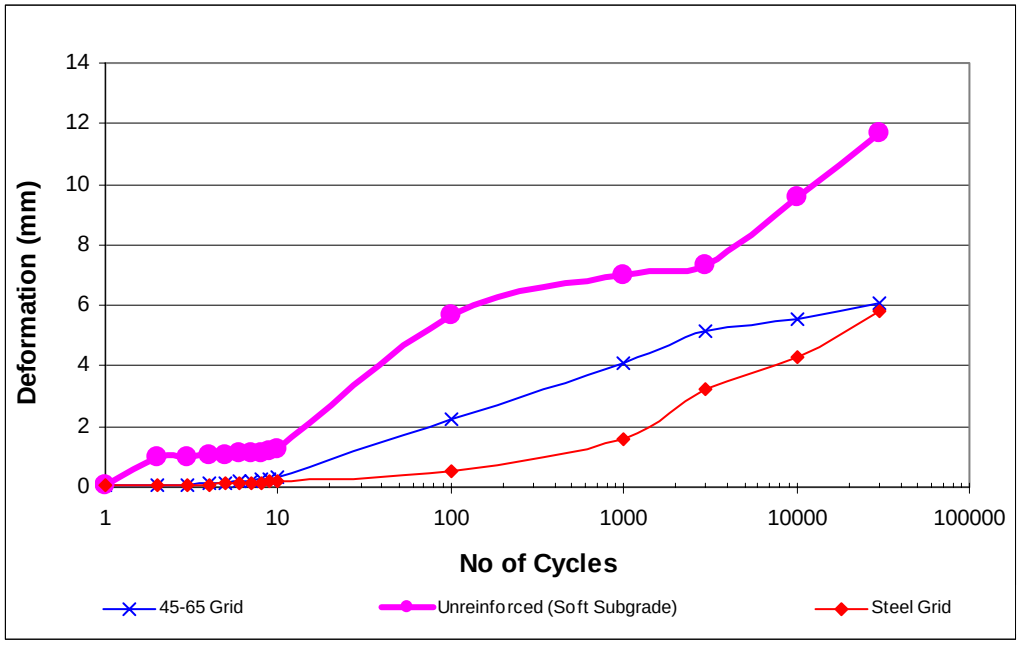

Figure 4.21 Effect of grid stiffness on settlement

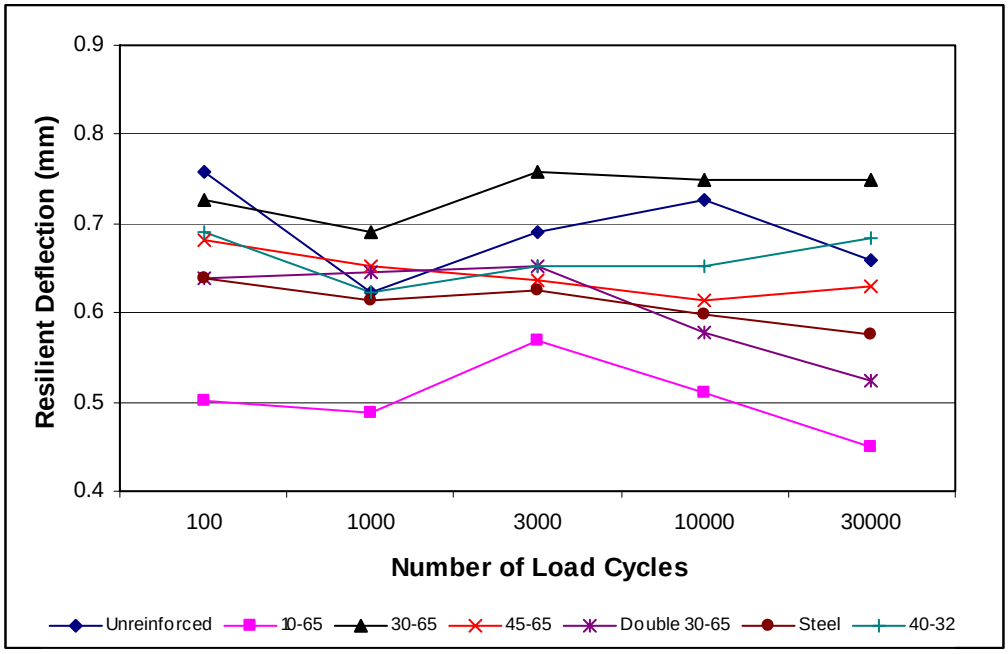

Figure 4.22 Resilient responses of grids in 'Overburdened' CET

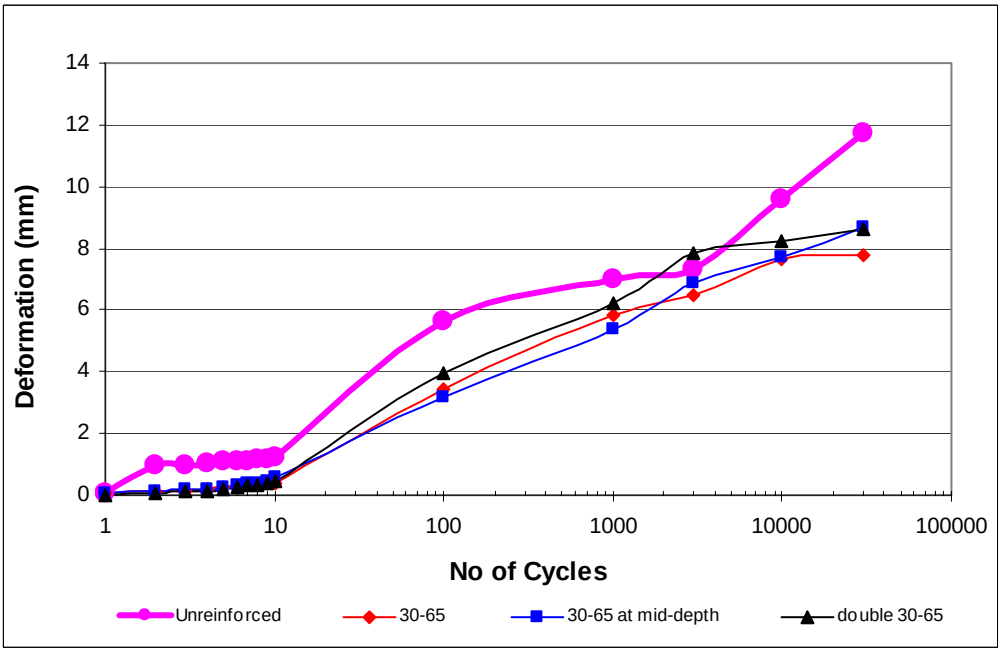

Figure 4.23 Effects of two grid layers and installation depth

The performance of a geo-composite, geogrid heat bonded to a non-woven geotexile separator (Figure 4.24) was investigated. Figure 4.25 shows the comparison in performance between the geo-composite and the same geogrid (30-65) without the geotexile. Both the geo-composite and 30-65 grid sits direct on the subgrade material . As seen in the figure, the composite failed to improve the system and its performance was equivalent to the unreinforced system, whereas the 30-65 grid becomes effective after 3,000 cycles. This is likely to be due to the ineffective interlock between the ballast particles and the grid. The presence of the geotexile may have inhibited the penetration of the particles into the grid apertures. The comparison is made with a 30-65 grid positioned directly over the graded material in the same arrangement as shown in Figure 4.24.

To further investigate the effect of 'subdued' grid/ballast interlock due to the presence of a geotexile, a 30-65 unbonded geotexile was tested in the modified CET. The results were compared with the unreinforced and 30-65 grid findings and are presented in Figure 4.26. From the figure, it can be confirmed that the presence of geotexile does inhibit effective interlock between the grid and ballast. In this case, the 30-65 grid was not heat bonded to the geotexile yet the performance was equivalent to that of the unreinforced.

Figure 4.24 Geo-composite tested in CET

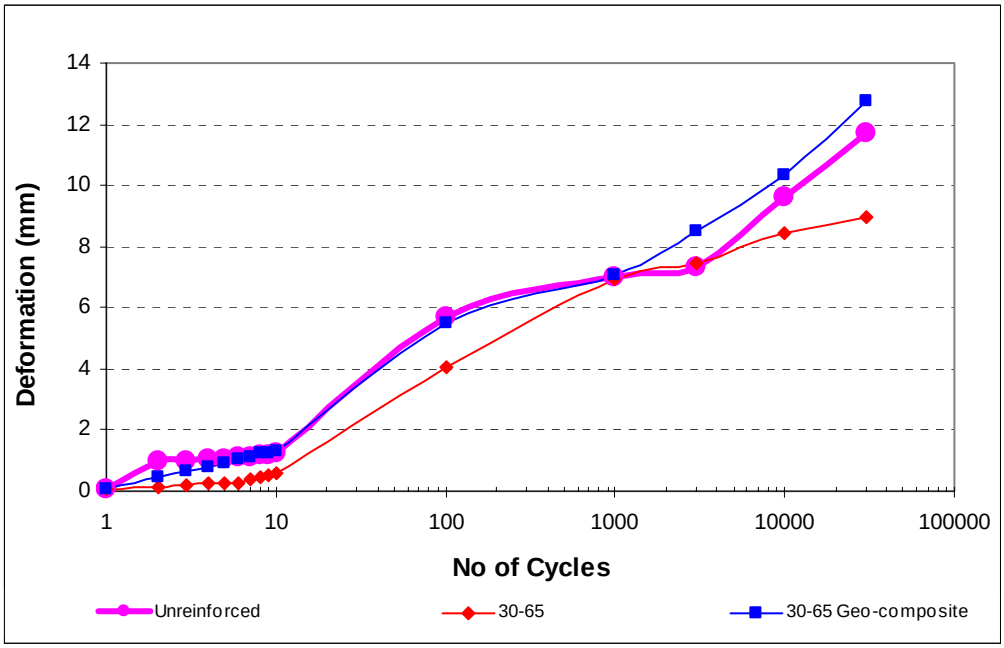

Figure 4.25 Performance of unreinforced, 30-65 grid reinforced and 30-65 grid + bonded geotexile reinforced

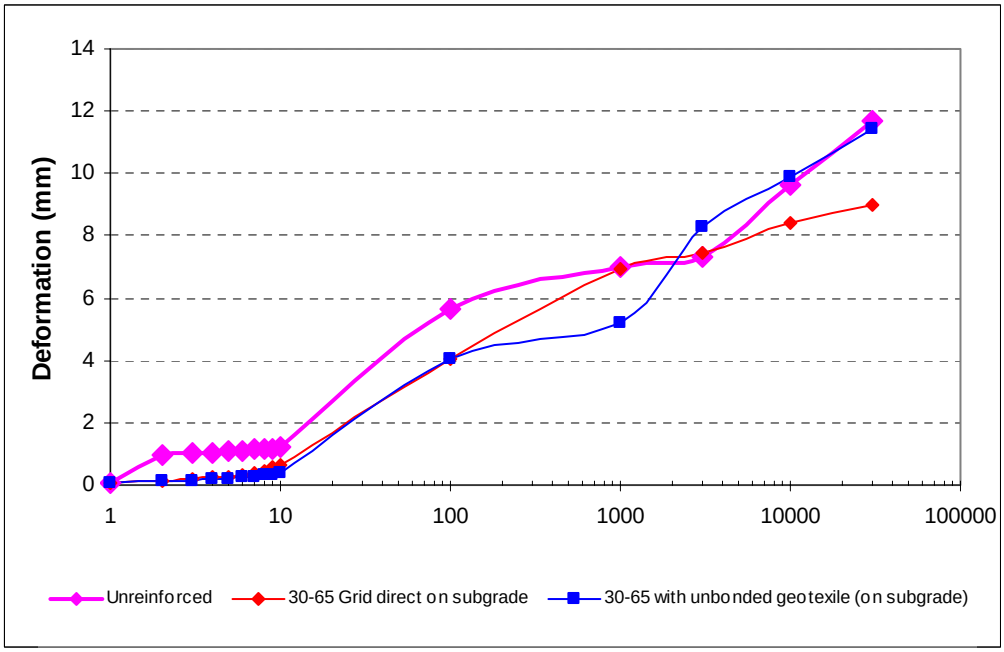

Figure 4.26 Performance of unreinforced, 30-65 grid with unbonded geosynthetic, 30-65 bonded geosynthetic

The importance of junction strength was investigated using a Tensar specially produced grid. The grid (Figure 4.27) has the same rib stiffness as a 30-65 but with a different cross-sectional profile. The ribs were heat bonded resulting in negligible junction strength. The grid was subjected to the same test regime as a standard 30-65 grid and the performance in the CET is compared in Figure 4.28.

From the graph, it is evident that the weak-junctioned grid performed poorly compared with both the 30-65 grid and the unreinforced cases. To achieve effective reinforcement, the ribs have to resist lateral stress exerted by the ballast particles; the reduced junction strength compromised effective interlock resulting in the poor performance. The difference in cross-sectional profile is unlikely to be the cause of the increase in settlement; clearly junction strength is an important parameter as shown by the figure. At the end of the 30,000 cycles of loading, all junctions of the weak-junctioned grid were observed to be broken as shown in Figure 4.29.

Figure 4.27 Grid with heat bonded junctions in the CET

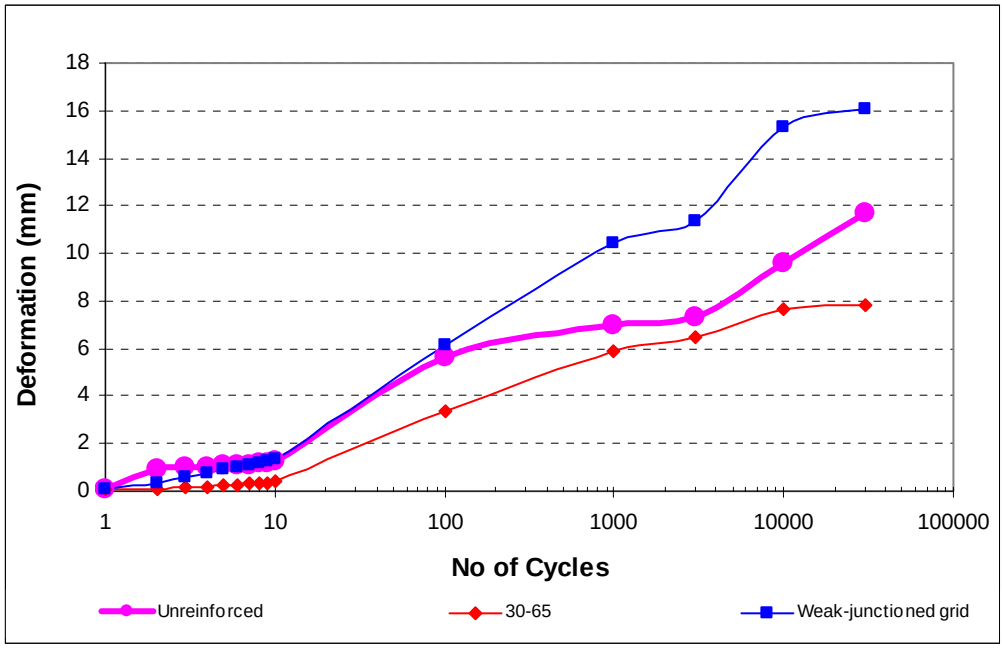

Figure 4.28 Effect of junction strength

Figure 4.29 Broken grid junctions

4.4 Discussion

The repeatability of the CET tests was demonstrated in Figures 4.9 and 4.10 where there was good experimental agreement shown by the plots under 2 different subgrade conditions. Several variables had been kept constant to ensure good repeatability. Volume of ballast, amount of compaction to the ballast and the obtained slope (for the earlier version of the CET) were all kept constant.

There was a significant reduction in permanent settlement in both the 20-65 reinforced CET tests as shown in Figure 4.11. The benefit of the grid reinforcement increases with a softer subgrade. This is consistent with Raymond (2001)'s findings where he noted a larger improvement to his grid reinforced composite when the foundation was weak. In fact, Tensar (2001) reported that an efficient grid reinforcement system can increase bearing capacity. This is exemplified in Figure 4.11 where the 20-65 reinforced (soft subgrade) CET performed as well as its counterpart for a stiff subgrade. In addition, further observation showed that both the 'unreinforced' plots are displaying an upward trend while the plots depicting the reinforced composite are reaching a constant state. This implies that the benefit of the reinforcement is likely to increase with each additional cycle.

Effective grid interlock is widely regarded to be a key feature of geogrid reinforcement. One of the governing criteria for such is the aperture size of the geogrid. Figure 4.12 presents the results of two contrasting grids in terms of aperture size and stiffness. Clearly, the figure indicated a considerable improvement in the 20-65 reinforced composite over the unreinforced compared to the 40-32 reinforced composite. The load-deflection hystersis loops shown in Figures 4.13 and 4.14 show the change in stiffness for the two tests over 30,000 cycles. While the 40-32 composite stiffened up over the course of the test, the 20-65 composite was always much stiffer. This is supported by Figure 4.15 where a shear failure plane was visually observed during excavation. Such a formation indicates the lack of ballast/grid interlock which will consequently reduce the stiffness of the composite.

The poor performance of the 40-32 grid could either be due to its aperture size or its stiffness. However, the results shown in Figure 4.30 indicate that the influence of aperture size is likely to be greater than the stiffness of the grid. The figure shows the comparative results from an overburdened CET of a 45-65 and a 40-32 reinforced composite. Both the grids have similar stiffnesses but the 45-65 has twice the aperture size of the 40-32. The 40-32 reinforced system settled twice as much as the 45-65 system (13mm vs 6mm). The findings are consistent with the data shown in Figure 4.12 where the 40-32 reinforced composite also performed worse than the unreinforced case. Again, it must be noted that the results was achieved under the specific test conditions stated earlier in this chapter.

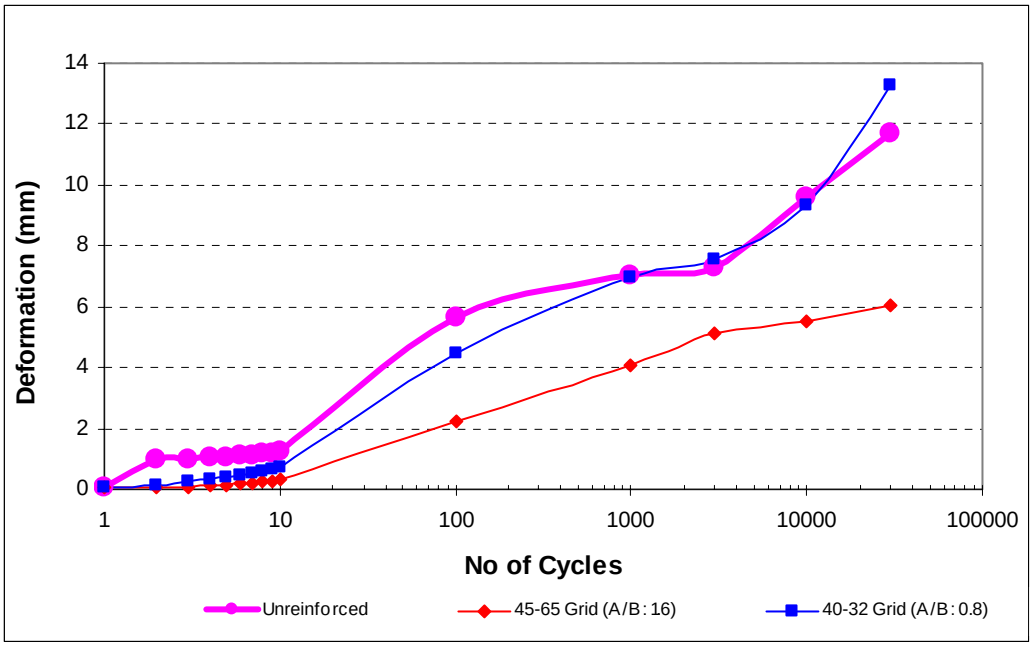

Figure 4.30 Aperture size effect where aperture to ballast (A/B) ratio of 1.6 is found to be superior compared to a ratio of 0.8 (overburdened CET)

The optimal aperture size shown in Figure 4.16 and 4.17 was found to be between 60-80mm. The results compares well with those of Jewell (1985) observations (see Figure 2.25), although there is some uncertainty about the relationship at high aperture size. The results were concluded after subjecting a series of grids with similar tensile strengths to the CET using a soft subgrade condition. The 20-65 grid yielded the least settlement at approximately 14mm. The reduced settlement is likely

to be due to the better interlock between the grid aperture and ballast particles. The findings are in agreement with the Pull-Out Test (see Section 3.2.2) as well as Harrireche's DEM simulation on size ratio where a ratio (geogrid aperture size to particle diameter) of 1.6 gave the best performance with the aggregate size at 40mm. It is noted that the best performer out of the optimal 65mm aperture sized grid is the stiffest 45-65 grid. In fact, according to the plots shown in Figure 4.18, it can be concluded that the optimal aperture size coupled with a high stiffness provides the best reinforcing effect. When the results were compared to those of the steel grid (also with 65mm apertures), the steel grid's better performance in the first 1,000 cycles indicated the importance of stiffness. However, it is possible that the rib profile of the Tensar grid (see Section 2.5.3) became more effective in the latter stages, as seen in Figure 4.21.

Using a multiple layer of geogrid or installation of a grid at mid-depth has little effect on the performance as shown in Figure 4.23. It is likely that once effective interlock is achieved it will reinforce the entire zone. Hence, there is very little difference in the performance with the various arrangements. Attempts to investigate the zone of influence of the grid were performed. A series of coloured ballast particles were placed at two marked layers which were 100mm and 200mm from the bottom of the steel beam. The tests were meant to quantify the amount of settlement contributed by different layers above the grid reinforcement. Due to the random nature of the obtained results, there was no conclusion. The CET will have to be modified to perform such a task.

Figure 4.25 and 4.26 shows that geo-composite weakens the whole system. This is likely to be caused by the lack of ballast punch depth due to the presence of the geo-textile heat-bonded to the grid. The lack of proper interlock created a shear failure plane which is likely to be one of the reasons for the poor performance. Another possibility would be the influence of the rubber subgrade. The rubber subgrade is unlikely to have behaved in the same manner as soil and would have inhabited effective indention of particles into the sub-ballast layer directly above it.

The lack of junction strength exhibited by the heat bonded grid (see Figure 4.26) prevented effective interlock due to the lack of lateral restraint. The inability of the

grid to hold its shape allowed the grid strands to break off (see Figure 4.29) and interfered with the interlock between particles. The reduction in ballast contact points explained the poor performance of the weak junction grid as shown in Figure 4.28.

The main problem working with the CET was that of ballast handling. The procedure was labour intensive and access under the portal frame was awkward. The poor access created a problem in the lifting and placing of the steel beam as well as in the replacement of the ballast. However, the CET was a prototype arrangement and modifications could be made to improve ballast handling and access. The test will also benefit from the possible inclusion of visual aids such as a perspex wall to observe interlock between the grid and ballast particles.

4.5 Summary

The CET was designed and set up to simulate the situation beneath a sleeper in a simplified and controlled manner. The simple format allows tests to be conducted quickly and it provided comparative data that allowed analysis of grid performance. The initial setup involved loading the ballast in a trough-like enclosure under a cyclic load of 20kN at a frequency of 2Hz over 30,000 cycles. This provided a stress of 114kPa beneath the beam which is considered to be about half of the maximum expected on an actual track. This is deemed to be adequate as the role of the test is not direct track simulation but an element test to assess the effects of the key variables. Subgrade stiffness variation is achieved through the use of rubber sheets. Loading was applied through a rectangular hollow steel beam and settlement measured by Linear Variable Differential Transformers (LVDT) placed on either side of the beam. Systematic compaction of the ballast's surface profile ensures that the test is repeatable.

Initial tests on the CET showed good repeatability with the general trend of plots and total settlement in good agreement. The simulated loading was found to be sufficiently large to differentiate between different test conditions. The benefit of working under a relatively low load ensures minimum ballast breakage which

preserves repeatability. However, to guarantee consistency, a new batch of ballast was used in the fifth repeat test.

There is a marked improvement in terms of settlement reduction with the use of the 65mm aperture size grid range. The improvement was evident in both subgrade conditions with the improvement particularly noticeable with the soft subgrade. It was also concluded that grid stiffness appeared to be less significant than geometry. The optimal aperture size was found to be between 60-80mm. The 65 mm aperture size range was found to be the best performing grid in terms of reduced deformation.

The vertical confining stress was later increased to better simulate in-situ conditions with the elimination of the ballast surface slope. Subsequent tests in the CET were all performed with the extra overburden.

Resilient response results from the modified CET with extra overburden show that grid reinforcement has very little influence on the stiffness of the composite. The geogrid is therefore likely to be useful for the limitation of plastic strain but not resilient strain.

A laboratory fabricated steel grid with 65mm aperture but with different rib profile later showed the importance of grid stiffness, especially in the initial stage. However, the final settlement was similar to that of Tensar 45-65 grid. The results highlighted the importance of rib profile.

A geo-composite performed poorly in the CET. The lack of 'punch' depth in the geo-composite due to the rubber foundation was the likely reasons for the poor performance. This effect is also apparent in geogrid with unbonded geotexile.

The importance of junction strength was exemplified from the results of the test involving a specially produced Tensar heat bonded grid which had negligible junction strength.

5 RAILWAY TEST FACILITY

5.1 Introduction

Following analysis of the data from the early Composite Element Tests (CET) and associated laboratory work, the knowledge was used to plan into a realistic rail track environment as planned. The Railway Test Facility (RTF) is a full-scale test facility which simulates the passage of a train at a speed of 28km/hr and an axle load of 250kN over a sequence of three sleepers. The facility is housed in an existing 1.8m deep concrete pit which is 4.1m long x 2.1m wide. A dynamic load of 92kN is applied to the three full scale sleepers with the reaction provided by a self contained frame fitted in the pit. A schematic diagram of the frame is shown in Figure 5.1.

The pit was filled with a consistent, relatively soft, subgrade to provide a known stiffness. The effect of geogrid reinforcement can be analysed through the comparison of settlement readings from the various tests performed, with and without geogrid. Vertical settlement readings were provided by the displacement transducers attached to the actuator as well as a Linear Vertical Displacement Transformer (LVDT) attachment on each end of the middle sleeper. Stress transmitted from the ballast was recorded via three strain gauges installed at 50mm subgrade depth.

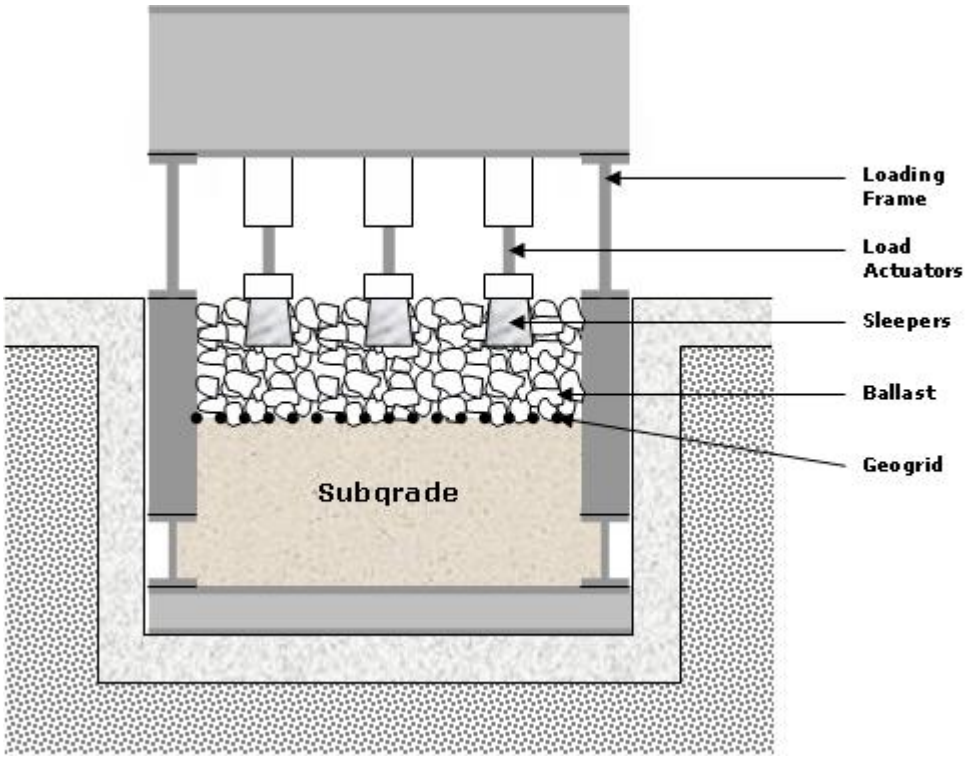

Figure 5.1 Schematic diagram of frame in pit

5.2 Test Equipment

Trackbed Construction

The loading frame, designed by Chief Experimental Officer Barry Brodrick, was fabricated and positioned in the 4.1m long by 2.1m wide and 1.8m deep concrete lined pit as shown in Figure 5.2. Concrete slabs covered the base of the frame to provide continuous support for the subgrade. Waterproofing of the floor and walls was achieved with the use of polythene sheets. In addition, vertical perforated tubes were placed in each corner to provide the option of adding water to the subgrade and to control the water table if required.

Figure 5.2 Steel frame in concrete lined pit for RTF

The pit was filled with silt from a local gravel pit. It was placed in 120mm layers to ensure material consistency and was compacted with a plate vibrator to a depth of 875mm. The silt material used in the RTF has a compacted wet density of 1768kg/m^3 and moisture content of 15.5% when it was finally placed in the RTF. Based on the Cone Penetration Method, the Liquid Limit of the silt was found to be 0.33 while a Plastic Limit of 0 was found.

Three strain gauge diaphragm type pressure cells were installed at a depth of 50mm in the subgrade as shown in Figure 5.3. They were placed at strategic locations to measure the stress transmitted to the subgrade by the ballast. The configuration of the test pit is shown in Figure 5.4. Two cells were positioned under the alignment of the central sleeper and one cell placed at the halfway point between the central sleeper and one of the outer sleepers. A schematic diagram of the positions of the instruments is shown in Figure 5.5

Measurements of subgrade stiffness were taken using a Zorn ZGF-01 (the 'German Dynamic Plate' in the UK) on the surface at several positions. The GDP, as shown in

Figure 5.6, has an accelerometer in the centre of its loading plate. The load is dropped 3 times onto a 300mm diameter steel base which transmits the stress to the surface of the subgrade material. Extra care was taken to ensure the plate rested on a level and smooth surface to ensure the accuracy of the test. The average of three responses of the material to the impact load measured by the surface deflection is used to calculate the stiffness of the material. The problem with the German Dynamic Plate is that it tends to under-read in comparison with other dynamic test devices. The lack of results accuracy was tolerated as the data are mainly for comparative purposes.

Moisture content of the subgrade material at various depths was measured on samples obtained through the use of a steel tube. The 1m long steel tube, with a diameter of 30mm, was driven into the subgrade at two arbitrary positions to obtain an average figure for the moisture content across the subgrade at different depth. It should be noted that a temporary polythene sheet was used to cover the surface of the subgrade to prevent atmospheric moisture loss. The polythene sheet was then removed and a thin non-woven geotexile was positioned over the subgrade surface to act as a separator. This was to facilitate the collection of fines from ballast degradation, required for a companion project.

Figure 5.3 Pressure cells in the RTF

Figure 5.4 Instrumentation in the RTF pit

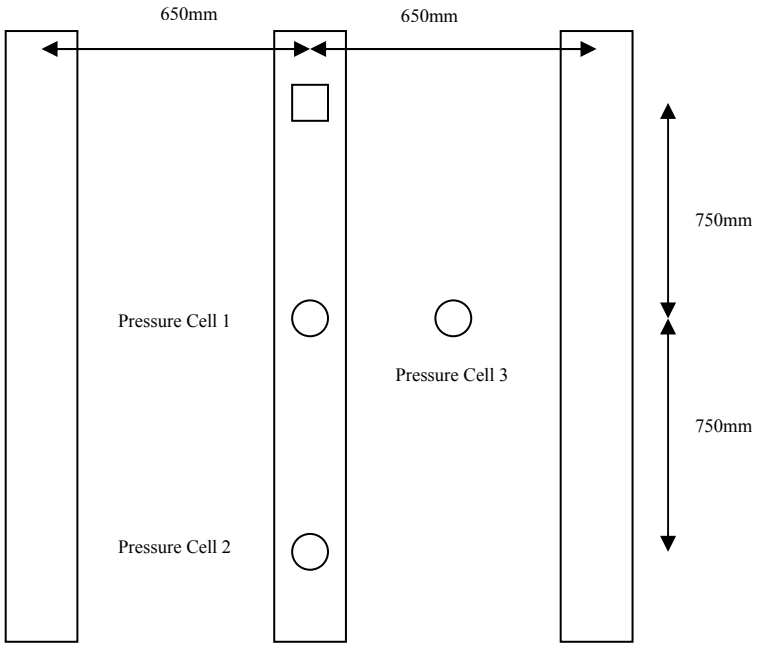

Figure 5.5 Plan view of instrumentation just below subgrade surface

Figure 5.6 German Dynamic Plate measuring subgrade stiffness

Ballast, supplied by Foster Yeoman in one-ton bags, was hoisted over the pit using the laboratory crane. The bags were carefully split to allow the ballast to fall into the pit in a controlled manner. The material was placed and compacted in 100mm layers using the same plate vibrator as used for the subgrade, to a depth of 300mm. The three sleepers were then lowered by crane into their respective positions and even seating on the ballast surface was achieved by working a vibrating chisel into the ballast under the sleeper. Special attention was given to the levelling of the sleeper at the position where the rail would have been. Additional ballast was then added to the sides and ends of the sleepers to provide restraint as shown in Figure 5.7.

According to RT/CE/S/102 (Railtrack PLC, 2002), the minimum ballast depth and sleeper spacing for mainline track are 300mm and 600mm respectively. The ballast depth and sleeper spacing in the RTF are 300mm and 650mm respectively. The G44 sleeper used in the RTF is also the standard concrete sleeper used on United Kingdom mainline track. Figure 5.8 depicts a G44 sleeper.

Figure 5.7 Sleepers level with the top of ballast

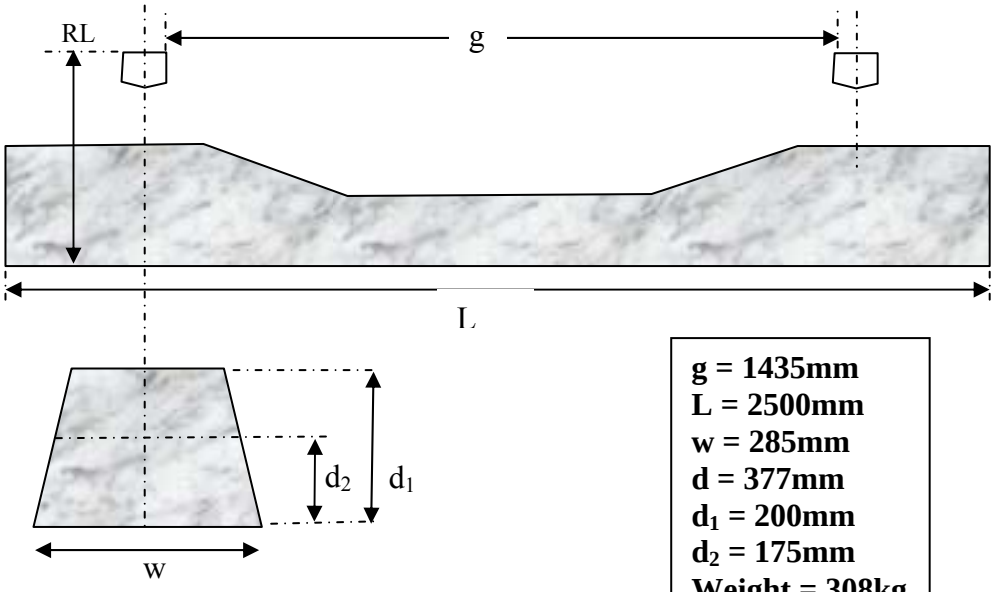

Figure 5.8 Dimensions of a G44 sleeper used in RTF

The Test Facility Equipment

The loading frame already shown in Figure 5.2 was designed to constrain three 100kN vertical loads which mimic the dynamic loading of a passing train. The three servo actuators were bolted to cross plates under the top two beams of the loading frame. A load cell was screwed to the end of the actuator shaft and a displacement transducer was built within the actuator body to measure shaft movement (stroke). The in-built displacement transducer gave an indirect measurement of sleeper displacement once the load cells came into contact with the spreader beam. The actuators were aligned with reference to the spacing of the three sleepers. The actuator load was applied through load cells onto the centres of the spreader beams which rested on two cylindrical rollers, located on the sleepers at the position where the rails would be attached. The test arrangement is shown in Figure 5.9. The simply supported arrangements of the spreader beams ensured a spacing of 1.5m between loads.

Figure 5.9 RTF loading arrangement

The hydraulic actuators were fitted with a servo valve which directed oil through the actuator so as to allow precise shaft response to an electrical command signal. Figure 5.10 shows the servo controlled hydraulic actuators. The servo valve, load cell and displacement transducer for each actuator are connected to a three channel controller housed in a clean room adjacent to the RTF. This stand-alone controller was connected to a computer which stored control functions and acquired data and this is shown in Figure 5.11. The controller was tuned regularly and calibration of the feedback transducers was also checked on a regular basis to minimise errors. An LVDT was attached to each end of the middle sleeper to record its vertical displacement.

The sleepers were linked to the frame using thin wire rope to ensure that they remained vertical during testing. The wire rope would not interfere with sleeper settlement as the wire has sufficient slack to react to any downward movement.

In order to replicate realistic traffic loading, load transfer to the sleepers must be simulated in a controlled manner using phase related loadings. Phase lags of 0, 90

and 180 degrees for actuators 1, 2 and 3 were used. This meant actuator 1 would start its loading cycle first and actuator 2 would be activated once actuator 1 completes a quarter of the loading cycle. This pattern would continue to actuator 3 and hence achieve sequential loading across the three sleepers as shown in Figure 5.12.

Figure 5.10 Servo controlled hydraulic actuators

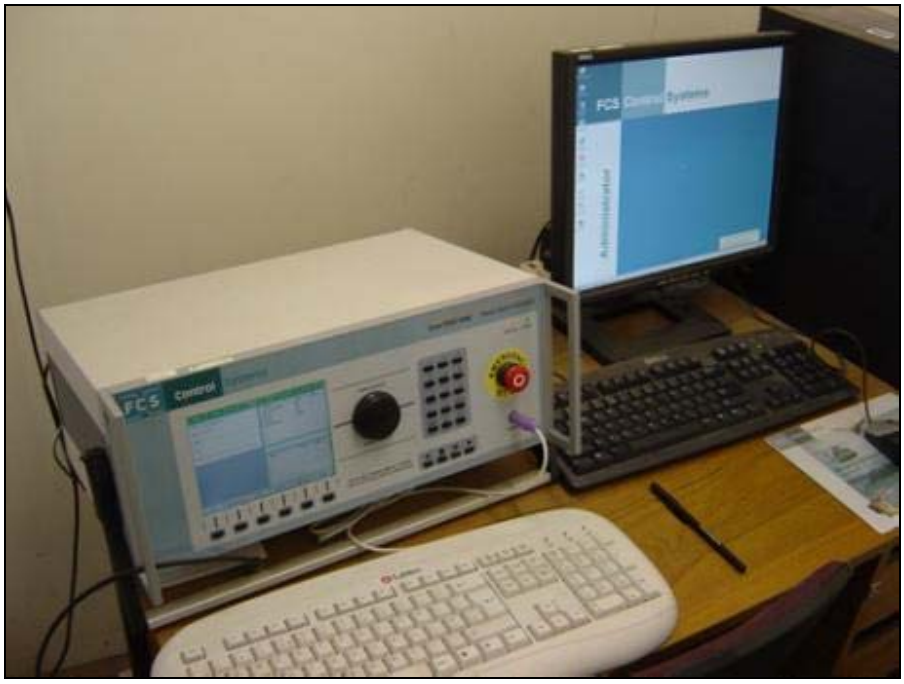

Figure 5.11 Three channel controller

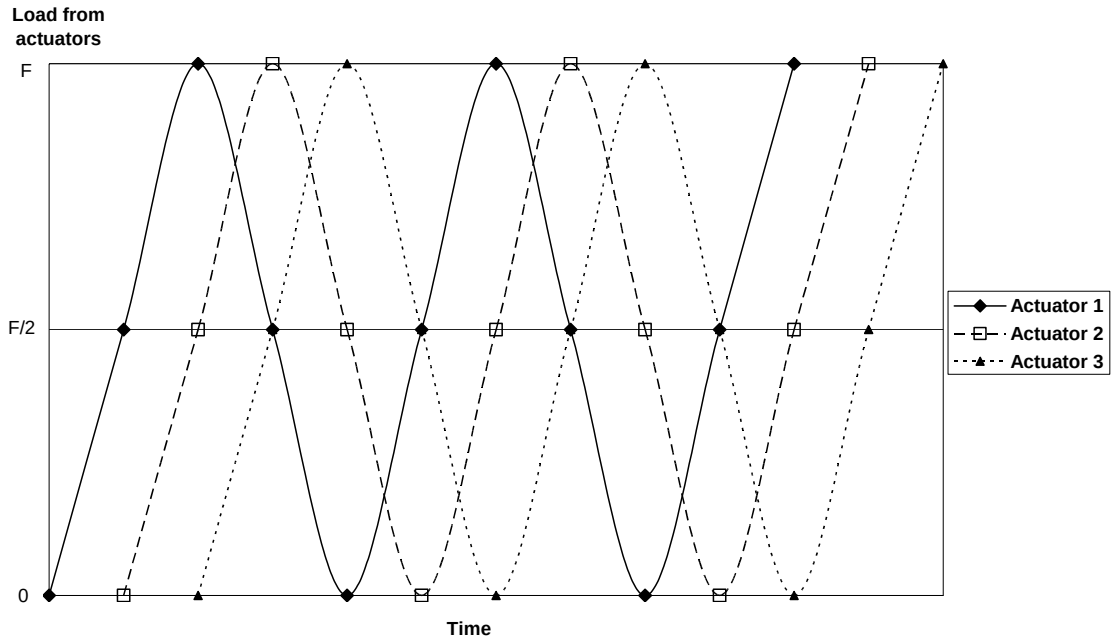

Figure 5.12 Phase loading used in the RTF

Figure 5.13 shows a schematic diagram comparing load distribution in the RTF and that of a real track. The loading pattern of the real track was calculated based on a simplified approach to track deflection analysis commonly known as the 'Beam on Elastic Foundation' analysis. This analysis replaces individual sleepers with a continuous support and the expression is as shown:

$$y = (P\lambda / 2k)\, e^{-\lambda x} [\sin \lambda x + \cos \lambda x] \qquad (5.1)$$

In which:

E = Young's modulus of the steel rail

I = 2nd moment of area.

k = modulus of subgrade reaction

y = deflection

x = length of track from P

P = axle load

Where: $\lambda = (k / 4EI)^{0.25}$ (5.2)

The calculation for the loading distribution is based on a modulus of subgrade reaction of 50MN/m^3, 'I' value of (2 x 3950) cm^4, 'P' value of 18 tonnes.

From the figure, it can be seen that the loading pattern in the RTF is very similar to that in the real track. The two loading arrangements show that the load on the central sleeper is approximately twice as large as the next adjacent sleeper. The good replication of load distribution in the RTF indicates a relatively good simulation of real track. The effects of rotating principle stresses is not known but have had to be ignored in this study. Another effect which is not being modelled is the uplift of adjacent sleeper (see Figure 2.3). In reality, a greater vertical movement might cause faster settlement development.

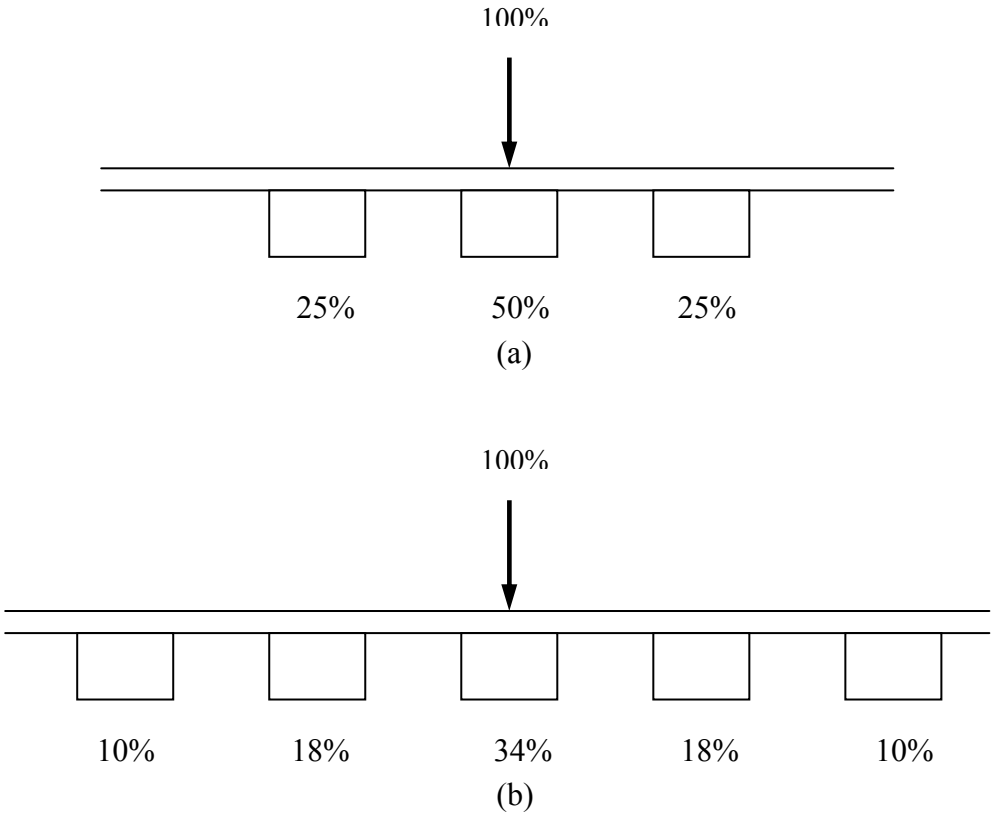

Figure 5.13 Load distributions along successive sleepers (a) in the RTF and (b) on a real track based on elastic beam on foundation calculation.

A tamping facility was also constructed to meet the requirements of a companion project. The facility, as shown in Figure 5.14, is a modified Plasser tamping bank with its independent hydraulic pump and linear actuator to provide vibration. The tamper works by insertion of its vibrating arms (fitted with tamping tools) into the ballast (to either side of the central sleeper at the location of the rail seating) and squeezing them together. Two large accumulators connected to the pump ensure sufficient oil flow and that pressure is maintained during the tamping operation. The tamping procedure is fully automatic with options to operate it manually. The tamping bank had to be mounted onto a frame which spans across the pit. Two out of the four tests performed in the RTF involved the tamping facility.

Figure 5.14 The tamping bank facility

5.3 Test Procedure

Testing commenced as soon as load cell calibration and incremental proof loading of the frame was completed as part of the testing protocol and risk assessment. Testing comprised a million dynamic loads on each sleeper. This is equivalent to 50 MGT, approximately 2 years traffic load on a UK main line. This is based on a report by Esveld (2001), where he stated that 1 MGT = 8896MN of traffic. The dynamic load used was a sine wave with an amplitude of 45kN (90kN peak to peak) and on intital mean load of 47kN operating at a frequency of 3Hz. The seating load of 2kN, which ensured the load cell remained in contact with the spreader beam allowing closed loop control, was later discovered to be insufficient, generating excessive vibration. The mean load value was later increased to 49kN with a seating load of 4kN. Although the actuators are designed to achieve 100kN, the safety trip was set at 97kN.

Settlement readings were taken at intervals for which the cyclic loading would be stopped and the load would be held at 1kN. Readings from the LVDTs were also taken and compared with those obtained from the displacement transducer. Readings from the pressure cells and accelerometer were also taken at the same time. The intervals were set at 100; 1000; 2000; 5000; 10,000; 20,000; 50,000; 100,000; 150,000; 200,000; 250,000; 300,000; 400,000; 500,000; 600,000; 700,000; 800,000; 900,000; and 1000,000 cycles.

Tests were initially performed in a one-stage format where cyclic loading was applied cumulatively to the million cycle mark, and displacement readings would be taken at intervals. The final two tests of the RTF involved a two-stage format where 500,000 cyclic loads were applied to each sleeper; this was followed by tamping on the central sleeper and the test was concluded with another 500,000 cyclic load applications. The two-stage application was performed to satisfy the requirement of the companion test project which was primarily interested in ballast degradation.

The contribution of subgrade settlement to the overall settlement registered by the displacement transducer and LVDT readings was investigated. To achieve this, a

datum was set by placing a steel rod with regular intervals marking on it across the pit. The distance from the datum to the surface of the subgrade at various intervals was measured with the use of a steel ruler. Visual inspection ensured that the ruler was perpendicular to the ground at the points of measurement. Measurements were taken before and after each test. The process is shown in Figure 5.15. It was concluded from this investigation that there were minimal settlements within the subgrade layer with a maximum settlement recorded at 4mm.

Figure 5.15 Measurement of subgrade settlement

5.4 Results

The commissioning of the RTF began with the calibration of the load cell and proof loading of the test facility. It was important to keep a record of the ballast settlement as it was known to settle significantly under loading. The settlement reading for each

sleeper is shown in Figure 5.16. From the figure, it can be seen that sleepers 1 and 3 settled more than sleeper 2 (central sleeper). However, settlement was low (less than 1.3mm) and it only represents a small part of the overall settlement on completion of the repeated load tests. The difference between sleepers is likely to be due to the uneven compaction of the ballast and subgrade. As sleepers 1 and 3 lie nearer to the edge of the pit, it was harder for the plate vibrator to achieve good even compaction in such areas.

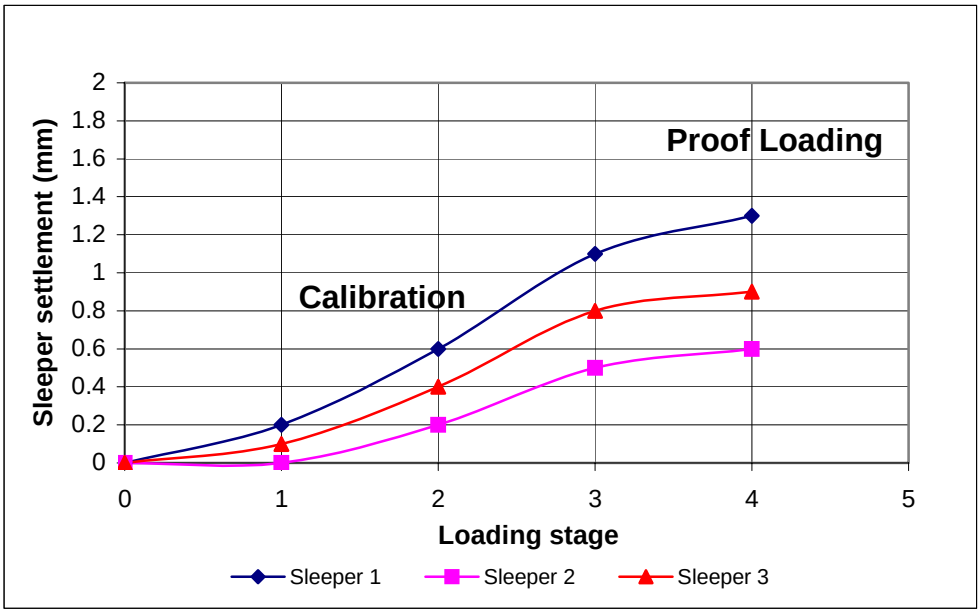

Figure 5.16 Loading history before testing

Figure 5.17 shows the subgrade stiffness readings, obtained from the German Dynamic Plate Test, of the subgrade material just prior to the first cyclic loading test. An average of 10MPa was obtained from the 15 GDP readings obtained across the RTF pit. GDP readings were taken at similar positions before and after each of the four RTF tests performed. Table 5.1 summarises the subgrade stiffness and moisture content for each installation including the loading regime.

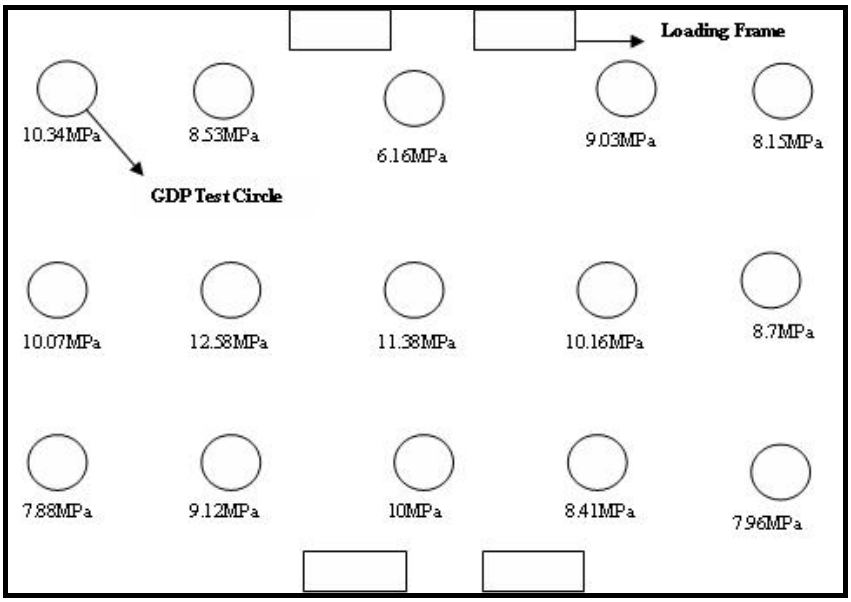

Figure 5.17 Initial GDP readings of RTF subgrade

Table 5.1: Summary of RTF tests

Test	Test Description	Pre-Test Subgrade Stiffness (MPa)	Pre-Test Subgrade Moisture Content at mid-depth of test pit (%)	Loading Regime
1	**Unreinforced**	10	15	1 million cycles
2	**Reinforced (30-65 sitting on a single layer of ballast)**	14	14.7	1 million cycles
3	**Reinforced (30-65 sitting direct on geotexile)**	16	15.3	0.5 million cycles- Tamp – 0.5 million cycles
4	**Unreinforced**	18	17.4	0.5 million cycles- Tamp – 0.5 million cycles

Figure 5.18 shows the settlement measurements at the 3 sleeper positions for the first unreinforced RTF test. Position 2 which represents the centre sleeper recorded less settlement than each of the side sleepers. This is consistent with the calibration and proof loading readings achieved and shown in Figure 5.16. Silt and ballast material were unlikely to be well compacted at sleeper positions 1 and 3, since both sleepers

are positioned near to the side walls of the RTF pit. This is the likely reason for the increased settlement compared to the central sleeper. For the first RTF test, only a single LVDT was employed at one end of the central sleeper and from Figure 5.18, there is large difference in the settlement readings obtained from the displacement transducer and the LVDT readings for the central sleeper. The disparity in results is likely to be caused by tilting of the central sleeper. An additional LVDT was added to the other end of the sleeper for the remaining three RTF tests.

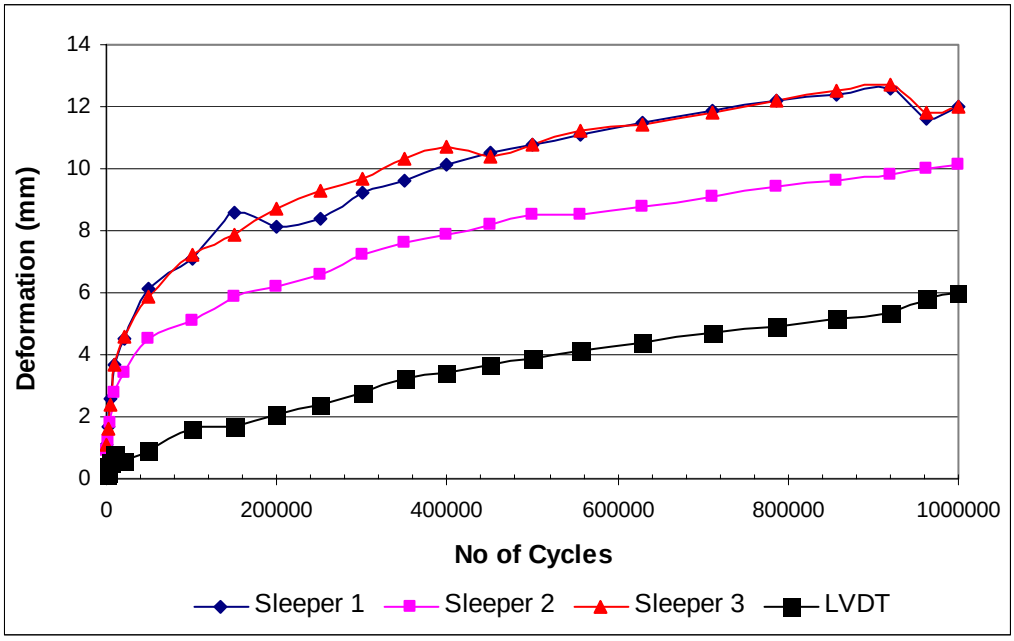

Figure 5.18 Stroke and LVDT readings from Test 1 (Unreinforced)

The results for Sleeper 2 are the main focus of the testing and the outer sleepers were included primarily to represent the restraint and loading distribution representative of in-service conditions. A final settlement reading of 10.1mm was recorded for Sleeper 2. This magnitude of settlement was considered sufficient to assess the effectiveness of the geogrid reinforcement, assuming that there will be a reduction in settlement over a million cycles. From Figure 5.18, it can also be seen that Sleepers 1 and 3 experienced some deviations at various points of the experiment, most notably near to the million cycle mark. This deviation is a result of relevelling of the spreader beams to compensate for the tilting of the sleepers.

The pressure cell data shown in Figure 5.19 shows the measurements recorded by the pressure cells buried 50mm underneath the surface of the subgrade. These vertical stresses are transmitted to the surface of the subgrade from the cyclic loading over the full duration of the test. The readings followed the sinusoidal loading waveform and the peak readings are shown in the figure. Pressure cell 1 is directly under the centre of the middle sleeper (see Figure 5.3); the large variations in the waveform are likely to be due to an electrical fault as zero output indicates a short circuit in the signal. The higher (peak) readings can therefore be assumed to be the actual stress readings for this pressure cell.

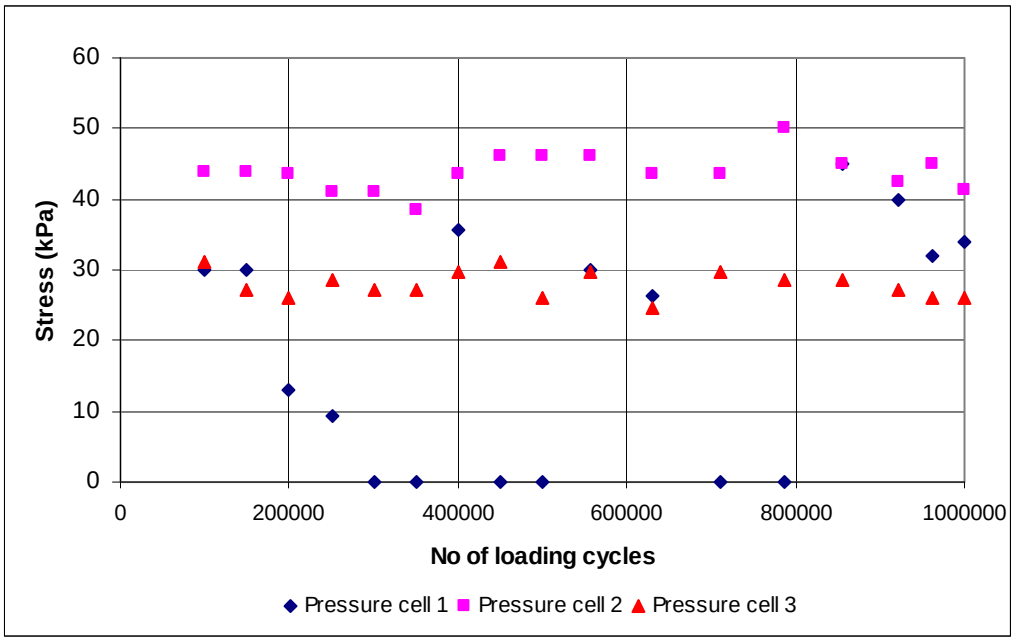

Figure 5.19 Pressure cell readings just below the subgrade surface (Unreinforced- Test 1)

The 2nd test performed in the RTF explored the effect of geogrid reinforcement with the inclusion of a 30-65 Tensar grid at a depth of 250mm. It was the best performing production grid (see Section 4.3) according to the Composite Element Test (CET). The 30-65 grid was installed over a single layer of ballast, similar to the placement of the grid in the CET. Figure 5.20 shows the settlement measurements for the 30-65 reinforced RTF test. Deviation can be seen once again in the settlement plot of Sleeper 3; again it is the result of relevelling of the spreader beams to compensate for the tilting of the sleepers. The LVDT readings are now the average of two LVDTs

attached to each end of Sleeper 2 and the readings were almost identical to that from the displacement transducer.

A final settlement reading of 7.7mm was recorded for Sleeper 2 for this reinforced RTF test. Figure 5.21 indicates the effect of a grid reinforced installation by comparing the two plots from the 1st and 2nd tests over a million cycles. The results indicated a reduction in total settlement of over 2mm. More importantly, it illustrated the potential increased time between maintenance intervals through the lateral difference between the two curves. The arrow at a settlement value of 6mm, a conservative estimate which assumes 6mm to be the settlement limit which triggers maintenance on track, showed a potential life extension factor of over 3 times in terms of number of load cycles under these specific test conditions.

Table 5.2 and Table 5.3 show the average pressure cell readings and resilient deflection readings respectively at various locations. The pressure cell readings under the centre of the sleeper in Table 5.2 show a possibility of interference in particle contact hence a higher than average readings (64kPa and 69kPa). The stroke readings in Table 5.3 showed very little difference in the resilient modulus of the reinforced and unreinforced RTF tests. This indicates that the grid reinforcement has no stiffening effect and it is ultilised principally to reduce accumulation of plastic rather than resilient strain. The obtained pressure cell readings would be used to help validate the design analysis presented in Chapter 7.

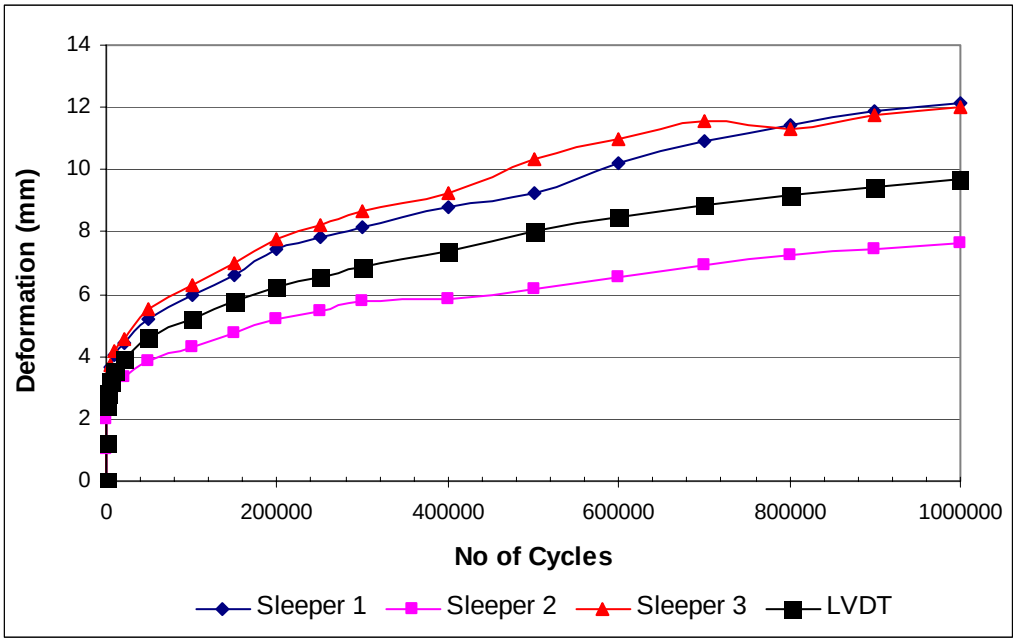

Figure 5.20 Stroke and LVDT readings from Test 2 (30-65 reinforced)

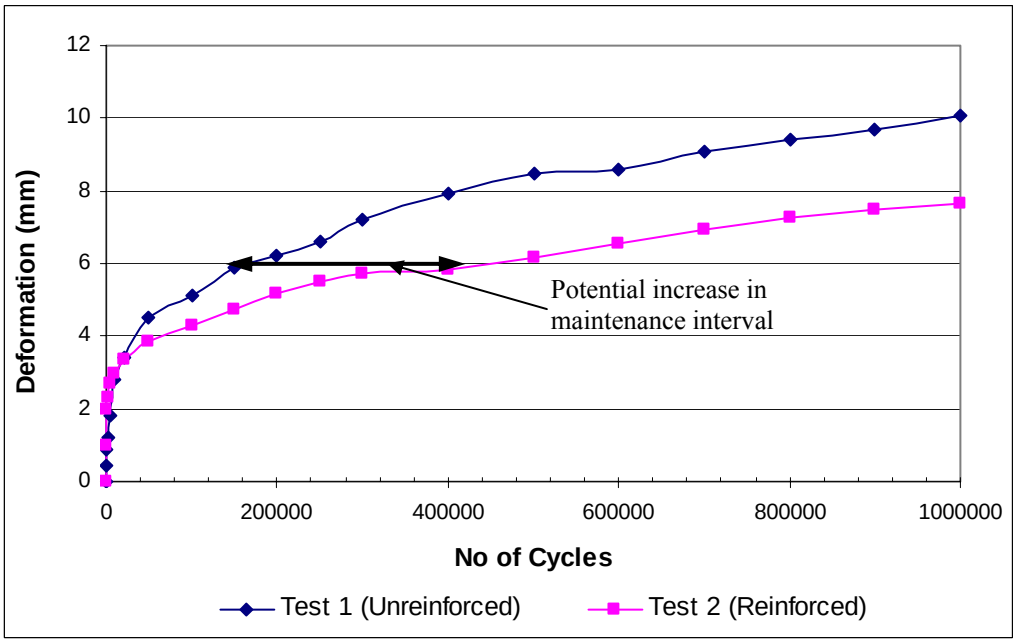

Figure 5.21 Effect of reinforcement over a million cycles

Table 5.2 Pressure cells readings for Test 1 and 2

Test No	**Cycles (10^6)**	**Average Pressure Cell Readings (kPa)**			**Comment**
		Sleeper End	**Centre of Sleeper**	**Between Sleepers**	
1	0.5	45	30	30	Unreinforced
	1.0	44	36	27	Not Tamped
2	0.5	41	64	32	Reinforced at a depth of 250mm
	1.0	43	69	31	Not Tamped

Table 5.3 Resilient deflection of sleepers for Test 1 and 2

Test No	**Cycles (10^6)**	**Average Resilient Deflection Readings (mm)**		**Comment**
		Stroke	**Sleeper**	
1	0.5	1.2	0.5*	Unreinforced
	1.0	1.1	0.5	Not Tamped
2	0.5	1.2	1.1+	Reinforced at a depth of 250mm
	1.0	1.3	1.1	Tamped

* Readings of LVDT at only one end of sleeper

+ Average reading of an LVDT at each end of the sleeper

For Test 3 and Test 4, the structure was subjected to 0.5 million cycles, followed by tamping and a further 0.5 million cycles of load. Test 3 involved the installation of the 30-65 grid directly above the geotexile at a depth of 300mm while Test 4 was an unreinforced test. Figures 5.22 and 5.23 show the total settlement for Tests 3 and 4 respectively.

Figure 5.24 summarises all the settlement measurements for the four tests. From the plots, there was good repeatability for the two reinforced installations up to the 0.5

million cycles mark even though the geogrid was installed on a layer of ballast in the first case and placed directly over the geotexile in the second case.

It can also be seen from the figure that in Test 4 (unreinforced), there is an increase in post tamping settlement when compared to those of Test 3 (reinforced). The increased settlement is likely to be due to a tilt of the central sleeper, observed visually during the tamping process. This has created an increased disturbance in the ballast under the sleeper resulting in the increased initial settlement.

It must be noted that the difficulty experienced in holding the sleeper in position during tamping has influenced, to a certain extent, the results of both Tests 3 and 4.

The average pressure cell readings and resilient readings of Test 3 and Test 4 are shown in Tables 5.4 and 5.5 respectively. It can be seen that the average pressure cell readings, for both the reinforced and unreinforced test, for the central sleeper reduced by approximately 50% after tamping. This is likely to be due to the 'hump' effect as discussed in Section 5.5. The resilient readings shown in Table 5.5 show a good consistency for both tests and a reduction in the resilient deflection is recorded in the reinforced tests. This will be discussed in Section 5.5.

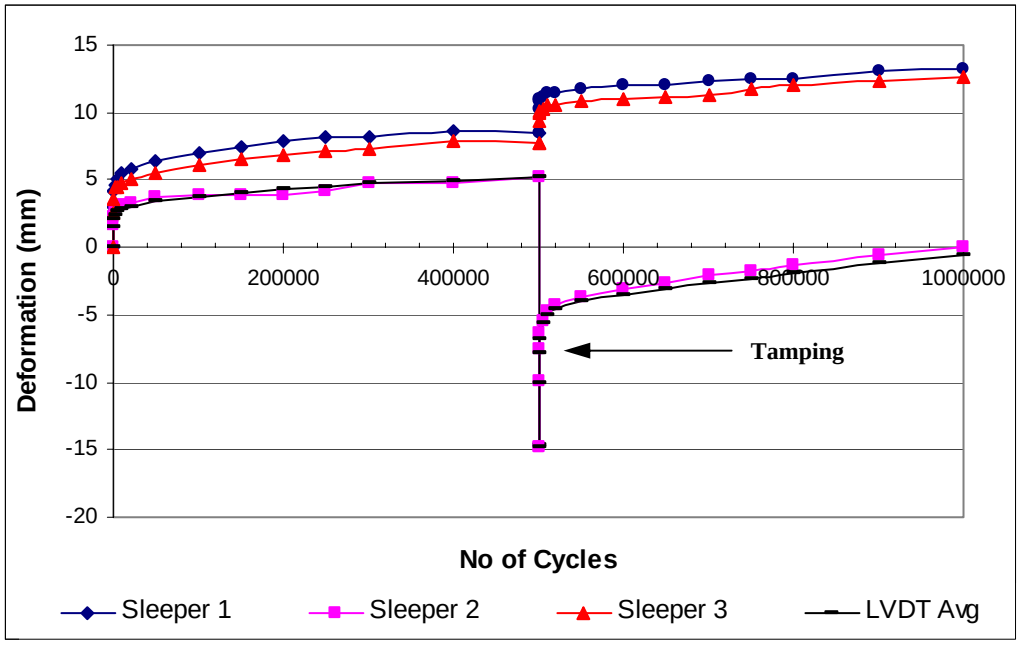

Figure 5.22 Stroke and LVDT readings from Test 3 (Tamped and reinforced)

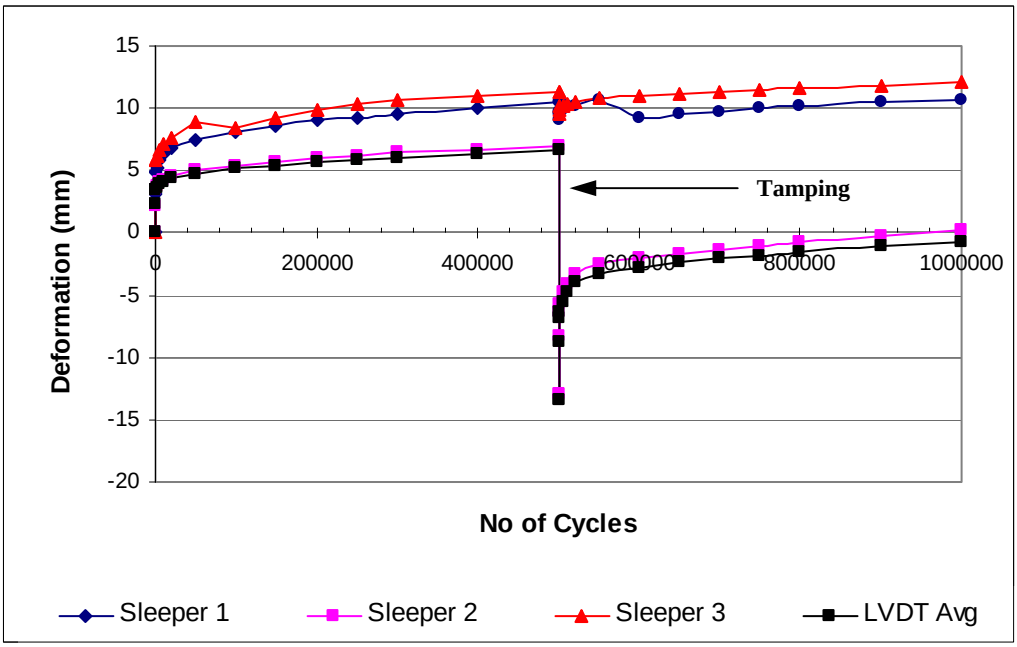

Figure 5.23 Stroke and LVDT from Test 4 (Tamped and unreinforced)

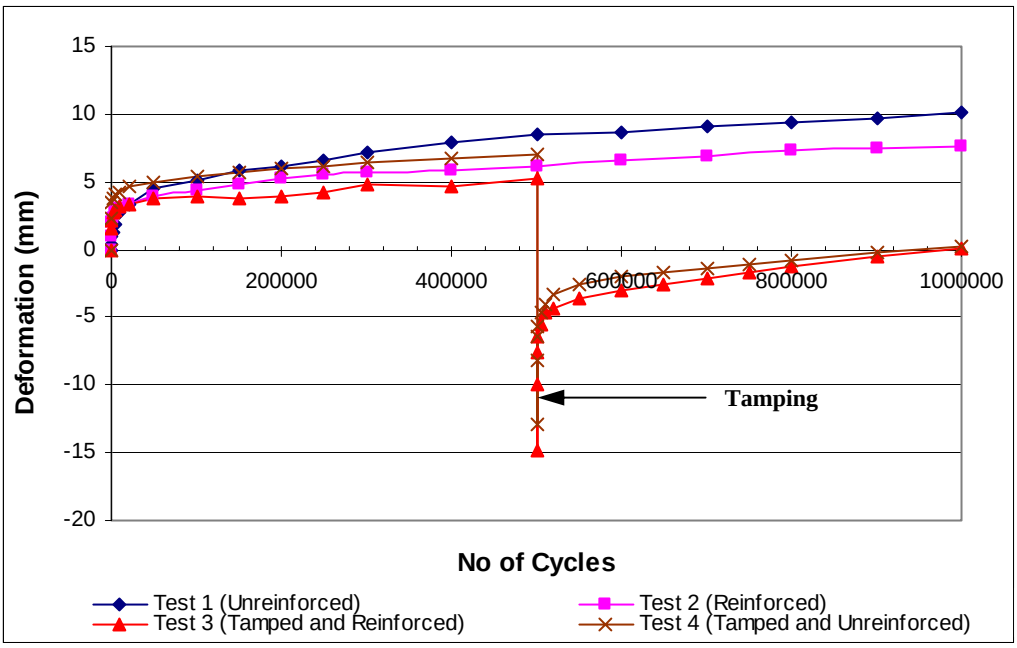

Figure 5.24 Settlement accumulations in the 4 RTF tests

Table 5.4 Pressure cells readings for Test 3 and 4

Test No	**Cycles (10^6)**	**Average Pressure Cell Readings (kPa)**			**Comment**
		Sleeper End	**Centre of Sleeper**	**Between Sleepers**	
3	0.5	52	44	14	Reinforced at 300mm depth
	1.0	72	22	14	Tamped
4	0.5	31	54	18	Unreinforced
	1.0	45	23	14	Tamped

Table 5.5 Resilient deflection of sleepers for Test 3 and 4

Test No	**Cycles (10^6)**	**Average Resilient Deflection Readings (mm)**		**Comment**
		Stroke	**Sleeper**	
3	0.5	1.3	1.1	Reinforced at 300mm
	1.0	1.3	0.7	Tamped
4	0.5	1.4	1.3	Unreinforced
	1.0	1.3	1.0	Tamped

5.5 Discussion

A consistent, relatively soft subgrade was required in order to compare performance of various test set-ups in the RTF. The chosen silt material, from a local gravel pit, has a known stiffness and would allow sufficient settlement to develop in order to explore the potential benefit of grid reinforced ballast. The silt had the advantage of ready availability and relative ease of placement and compaction. Though the silt material stiffened over the course of the 4 RTF tests, the progressive increase is large enough to affect the results though not by much (from 10MPa to 18MPa). The order of the reinforced and unreinforced tests though (Test 3 and 4) was reversed to show

that any improvement due to reinforcement was not due to the increased silt stiffness. Glensanda ballast was used throughout the four tests to reduce variability.

The pressure cell readings for the 4 RTF tests were shown to vary slightly from test to test. The accuracy of the pressure cells very much depends on the consistency of the material, frequency of data collection as well as the quality of the installation. The pressure cell should be securely seated on a level and firm foundation for accurate readings. Usually a minimum of three cells are used in pavements to obtain replicate readings which would then provide a mean value. In the RTF, although three cells were used, they were positioned differently relative to the loading points hence they should not be compared directly.

From Tables 5.2 and 5.4, the average pressure cell reading under the centre of the sleeper in Test 2, in particular, is higher than the rest. The difference is likely to be due the 'hump effect' where there is a concentration of stress under the sleeper due to imperfections in levelling; the sleeper was likely to be sitting on a ballast 'hump'. Pressure cell malfunction is also a possibility but it must also be noted that a result variation of +/-10kPa is commonly expected for this type of equipment especially when it involved 4 different installations. The results shown in Table 5.4 are a better illustration of the effect of tamping on the stress condition at just below the surface of the ballast.

The lower stress at the position at the centre of the sleeper represents the loose state of ballast material under the centre of the sleeper. It can also be seen that there is an increase of stress at the end of the sleeper after tamping in both tests 3 and 4. This is likely to be due to the 'hump effect' after tamping. It is likely that the tamping effect dominated the post tamp 0.5 million cycles and due to the loosened state of the ballast particles, the geogrid would not be able to immediately induce effective interlock and influence the settlement although it must be noted that this is unlikely to have lasted over the 0.5 million cycles. It is hence likely to be due to disruption caused by tamping (and the sleeper is likely to be tilted when held during tamping) that made it impossible to replicate the test precisely This caused the geogrid reinforced system in Test 4 post tamping failing to show any significant reduction in settlement.

The resilient readings from the displacement transducer are higher than those recorded by LVDTs. This is likely to be due to the flexure of the loading beam. In general, the resilient readings from the two sources were very consistent.

It was observed during the tests that there is a tendency for the outer sleepers to tilt away from the centre. This is likely to be due to poor compaction and reduced particle interlock nearer to the smooth polythene covered walls.

The effect of reinforcement was clearly illustrated in Figure 5.21 in a straight forward one stage test. As shown, the settlement reduces from 10.1mm to 7.7mm with the inclusion of geogrid reinforcement. More importantly, this represent a 2.5 times extension in maintenance interval for track renewal work. It must be noted that this estimation is based on the assumption that a settlement of 6mm on track will trigger maintenance and also that this results was obtained under the specific test conditions. In reality, it should be based on a track settlement standard deviation figure which triggers maintenance. The lack of data on the relationship between standard deviation and vertical settlement means that an empirical judgement had to be made in this instance.

The benefit of reinforcement was further emphasised in the initial 0.5 million cycles of Tests 3 and 4. The 'reinforced' test recorded a settlement of 5mm in the 0.5 million cycles compared to 7mm in the unreinforced test. This was achieved despite of a stiffer subgrade for the unreinforced test. Both reinforced tests reduced vertical settlement by approximately 26% in the first 0.5 million cycles; this demonstrates the repeatability and likely validity of results.

The difficulty in holding the sleeper in position for tamping is best illustrated in the results as shown in Figure 5.24. From the figure, it can be seen that the post tamp reinforced trackbed in Test 3 recorded a higher total settlement that the corresponding unreinforced trackbed in Test 4. It was observed during the test that the sleeper in Test 3 (reinforced) tilted. This affects the stress distribution onto the ballast and is likely to have an effect on the settlement characteristics.

The tilt of the sleeper in Test 3 is illustrated by the LVDTs reading in Figure 5.22. It is larger than the tilt experienced by the sleeper in unreinforced Test 4. It can be seen that tamping will disturb ballast and cause the track to degrade rapidly before it reaches a stable state. It is only when the track approaches a stable state that the grid would start to influence particle interlock and improve the system. Hence, the effect of reinforcement is not likely to be represented on the plot in Test 3. The test would be better concluded if it was allowed to run for another 0.5 million cycles.

5.6 Summary

The magnitude, frequency and distribution of load in the RTF represent a train speed of 28km/hr and an axle load of 250kN. The RTF is a basic representation of a heavily trafficked main line and it has successfully completed four tests investigating the effect of geogrid reinforcement based on the total settlement.

Loading was applied through a loading frame fabricated in the laboratory and positioned in the 4.1m long by 2.1m wide and 1.8m deep concrete lined pit.

Three hydraulic actuators provided the 94kN vertical loads applied in phase to mimic the dynamic loading of a passing train.

Three strain gauge diaphragm type pressure cells, placed at strategic locations, were installed at a depth of 50mm in the subgrade to measure the stress transmitted to the subgrade by the ballast. The stress readings were of good consistency. The settlement readings were obtained from the displacement transducers mounted on the actuators as well as Linear Vertical Displacement Transducers (LVDT) placed at each end of the central sleeper.

The settlement plots from the two reinforced tests up until the 0.5 million mark showed that the test is repeatable. There was also a well defined difference in settlement readings when a geogrid was used to reinforce the ballast. From the first two tests, in a one stage format, geogrid reinforcement reduced total settlement from

10.1mm to 7.7 mm. It can be concluded that geogrid reinforcement is likely to increase the maintenance interval quite substantially.

The reinforced composite in Test 3 settled more than the unreinforced case in Test 4. The accelerated settlement happened after tamping and is likely to be due to the sleeper being tilted when held during tamping. From the results, it can be seen that tamping caused an immediate deterioration of the track with accelerated settlement. However, densification is expected with additional loading and the effect of geogrid reinforcement is likely to be more apparent at that stage.

6 FIELD TRIALS

6.1 Introduction to Site

A major trial of the 30-65 grid was carried out at a heavily trafficked site along the West Coast Main Line, in Lancashire, near Wigan. The work was commissioned by Network Rail. The renewal work took place during October 2004. Network Rail agreed to include a trial of the 30-65 grid based on the findings of the CET experiments.

The site (Coppul Moor) is on an embankment where the upper 0.41m layer (directly underlying the ballast) was described as dark grey, slightly silty, sandy ash. A ground investigation was carried out in April 2004 and the water table was found to be just 0.2m beneath the bottom of the ballast, within the ash layer. The site was chosen for renewal work as it had a history of relatively rapid track deterioration which requires regular tamping to correct track alignment and restore track quality.

The site was determined to be suitable as it had similar track bed conditions throughout and this would allow the assessment of the effect of grid reinforcement. Figure 6.1 shows a photograph of the work on site. A close-up of the installed 30-65 grid is shown in Figure 6.2.

Figure 6.1 Renewal work at Coppul Moor

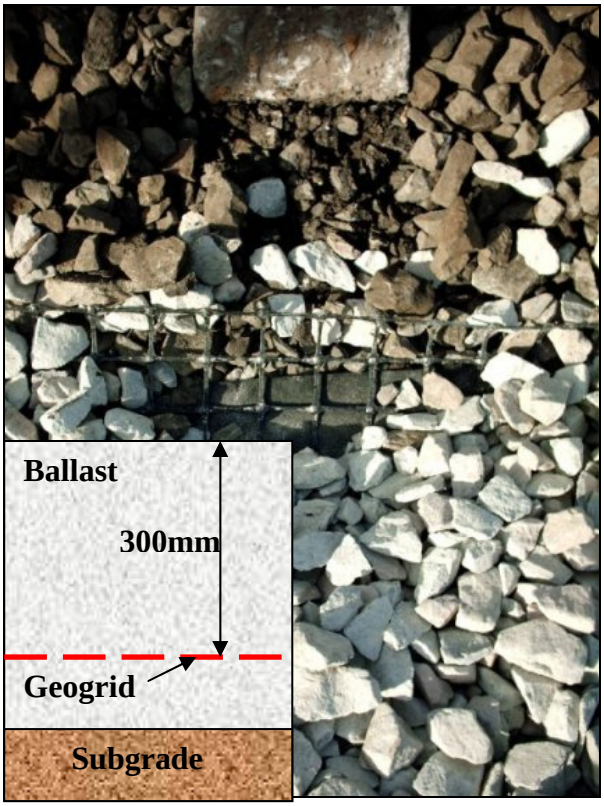

Figure 6.2 Close-up of the installed 30-65 grid and a schematic diagram of grid position

The length of track that was put up for renewal was at 1100 yards, 0.625 miles. The 30-65 grid was installed from the first 440 yards of the section. The installation was successfully carried out and has been monitored by the High Speed Track Recording Car (HSTRC). The HSTRC indicates the ride quality of the track in terms of a standard deviation of the rail over a moving 35m length. The data from the HSTRC would indicate any improvement following renewal and any subsequent change in standard deviation under traffic.

A track bed stiffness survey was carried out by Scott Wilson Pavement Engineering by means of a Falling Weight Deflectometer (FWD). The FWD works on the principle of applying a measured stress to the surface of the subgrade by utilising a weight falling onto a platen. The resulting deflection of the surface is recorded and the results analysed to give a stiffness value. The survey was performed some months after the installation in order to provide background information on the subgrade and to identify any possible influence on track bed stiffness with the presence of grid reinforcement.

The data obtained from the HSTRC and the FWD provides important evidence of the viability of grid reinforcement in the reduction in the rate of track deterioration. The results obtained from the site trial will be compared to the laboratory findings, e.g. Composite Element Test (CET) and Railway Test Facility (RTF) to validate the work performed through the course of this project.

6.2 Results from Site

The HSTRC data shown in Figure 6.3 was obtained between early March 2004 and the end of June 2005. The figure clearly indicates the improvement of ride quality after renewal. It can also be observed that on sections where the 30-65 grid was installed, a lower standard deviation was achieved and maintained despite having higher standard deviation values prior to renewal. This conclusion is supported by Table 6.1 where it showed the average standard deviation values before and after renewal work. The updated results were gathered from March 2004 to early 2006.

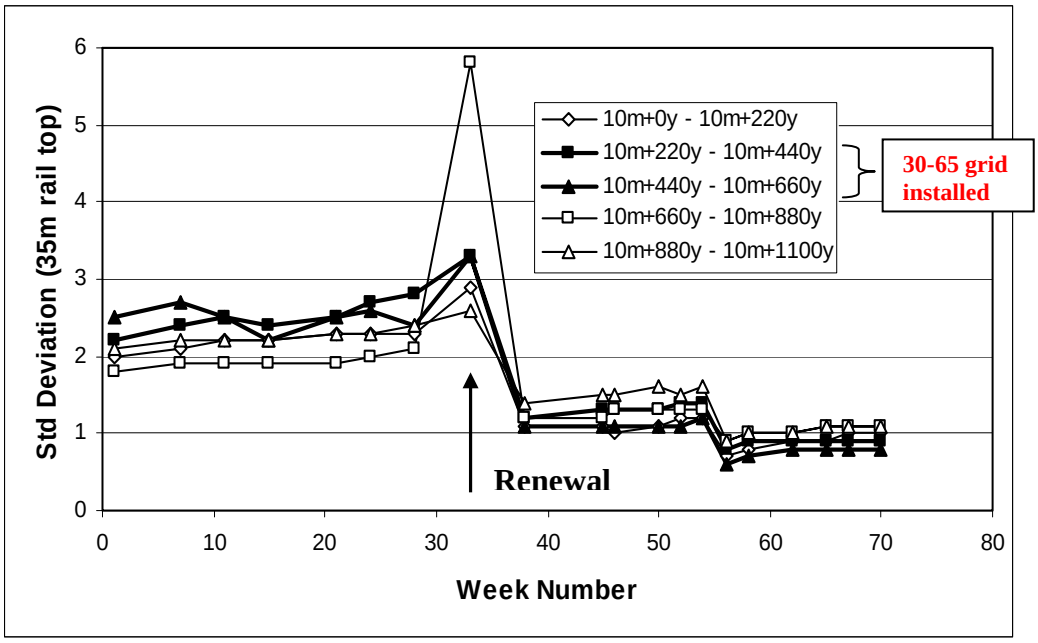

Figure 6.3 HSTRC Data

Table 6.1 HSTRC comparison data

	30-65 Grid Reinforced		No Grid	
	220 - 440 (yards)	440 – 660 (yards)	660 - 880 (yards)	880 onwards (yards)
Av SD before renewal (mm)	2.58	2.44	1.96	2.28
Av SD after renewal (mm)	1.16	0.98	1.16	1.20
Av SD improvement (mm)	1.41	1.46	0.8	1.08
Rate of deterioration before renewal mm/yr	1.4	2.2	1.0	1.2
Rate of deterioration after renewal mm/yr	0.4	0.7	0.6	0.7

Table 6.1 shows that the 30-65 grid section registered the highest average standard deviation improvement. It can also be seen that the grid was installed on the section with the worst ride quality but the standard deviation, after the installation of the grid, was restored to a level equal or better than the rest of the track. More importantly, there was a considerable reduction in the rate of deterioration for the grid reinforced section after renewal. This indicated a potential life extension in terms of increased maintenance intervals, an important track performance measurement explained in Chapter 7's design guide.

Further evidence for the reduction in track deterioration can be seen in the historical (11 years) rate of deterioration data shown in Figures 6.4 and 6.5. Figure 6.4 depicts the reinforced section while the unreinforced section is represented in Figure 6.5. The gradients of the plots in the figures show the annual rate of deterioration. Based on the standard deviation gradient plot shown in Figures 6.4 and 6.5, it is interesting to note that the grid reinforced track has a history of inferior track record in terms of rate of deterioration compared to that of the unreinforced section. However, the reduced post renewal rate of deterioration, measured in annual increase in standard deviation, in the reinforced section (0.25 / year against 0.4 / year in the unreinforced track) highlighted the benefit of grid reinforcement in improving and retaining track geometry, allowing a better ride quality

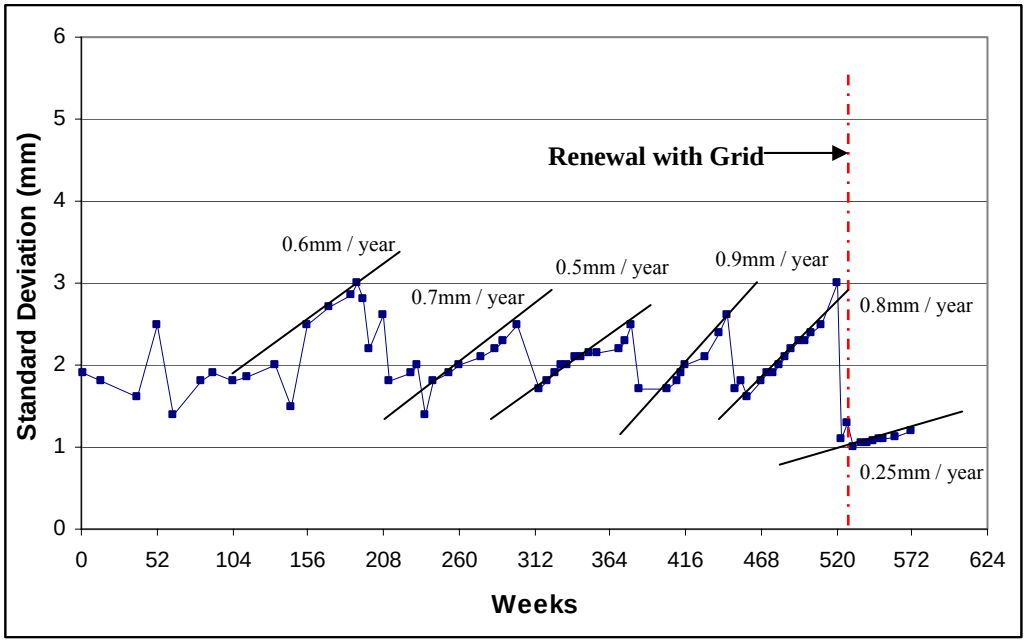

Figure 6.4 Historical rates of deterioration and deterioration post renewal with grid installed (Network Rail)

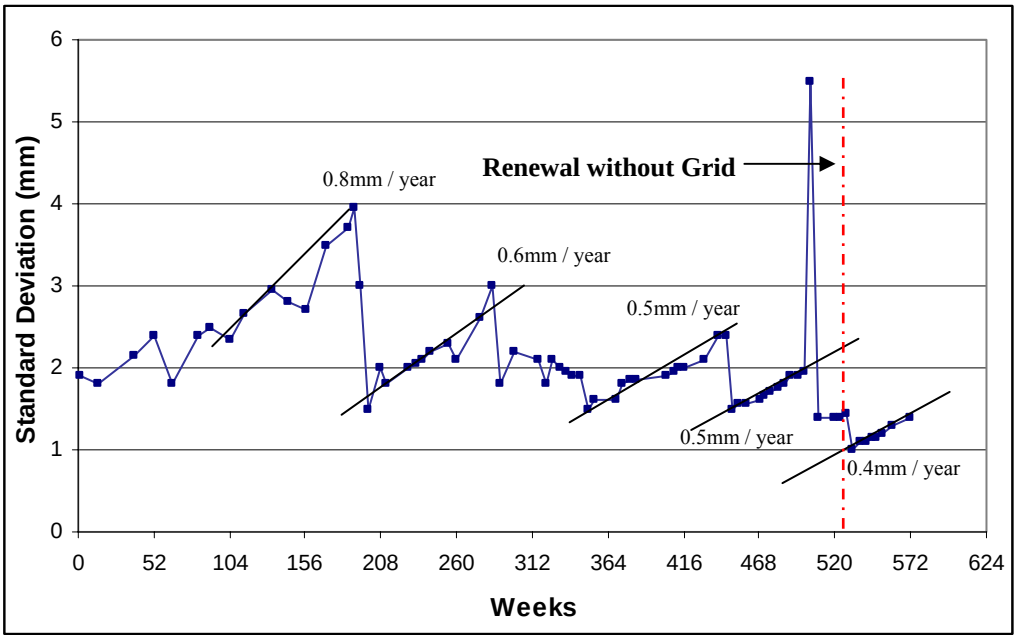

Figure 6.5 Historical rates of deterioration and deterioration post renewal with no grid installed (Network Rail)

A FWD survey was conducted by Scott Wilson Pavement Engineering some months after renewal to provide background information on the site subgrade and to investigate the effect of grid reinforcement on the trackbed stiffness.

The FWD data is expressed as deflection of a loaded sleeper (D0) and deflections measured on the surface of the ballast at distances of 300, 1000 and 1500mm from the centre of the sleeper. Figure 6.6 shows typical FWD deflection readings on UK track. Figure 6.7 shows the FWD readings on the Coppul Moor site after the renewal work. The deflection is an average from at least two measurement points. The re-ballasted section is stiffer than the untreated section but the reinforced section is less stiff than the unreinforced. This is likely to be due to the presence of the grid which possibly hinder the compaction process. However, the difference in value is still very small. Comparing the plots from Figure 6.6 with the FWD data obtained from the Coppul Moor trial site, it can be concluded that the trial site has FWD readings equivalent to those of a poor UK main line.

The outer deflections, D1000 and D1500, correlate with the quality of subgrade at depth and no significant difference was detected between the reinforced and the remainder of the track. Deflections D0 and D300 are related mainly to the ballast and the uppermost subgrade layer. It can be seen from the figure that the section with the grid reinforcement is actually less stiff which is likely to be due to the continuing presence of a poor sandy ash layer at the top of the subgrade, where the water table was previously found to be relatively high. It can be concluded that the grid did not have any stiffening effect; the grid is utilised to limit the accumulation of plastic strain rather than resilient strains. This is shown by the reduction in standard deviation (lower differential settlement) and rate of deterioration hence enabling a better ride quality.

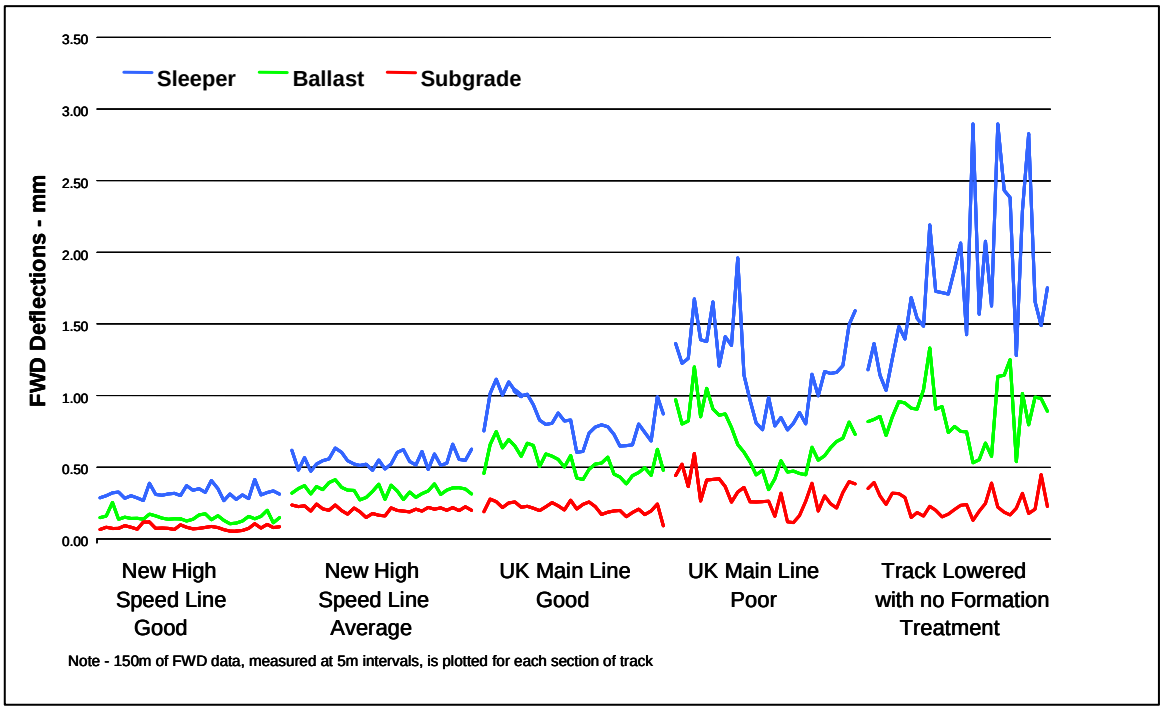

Figure 6.6 Classification of UK tracks based on FWD results
(Scott Wilson Pavement Engineering)

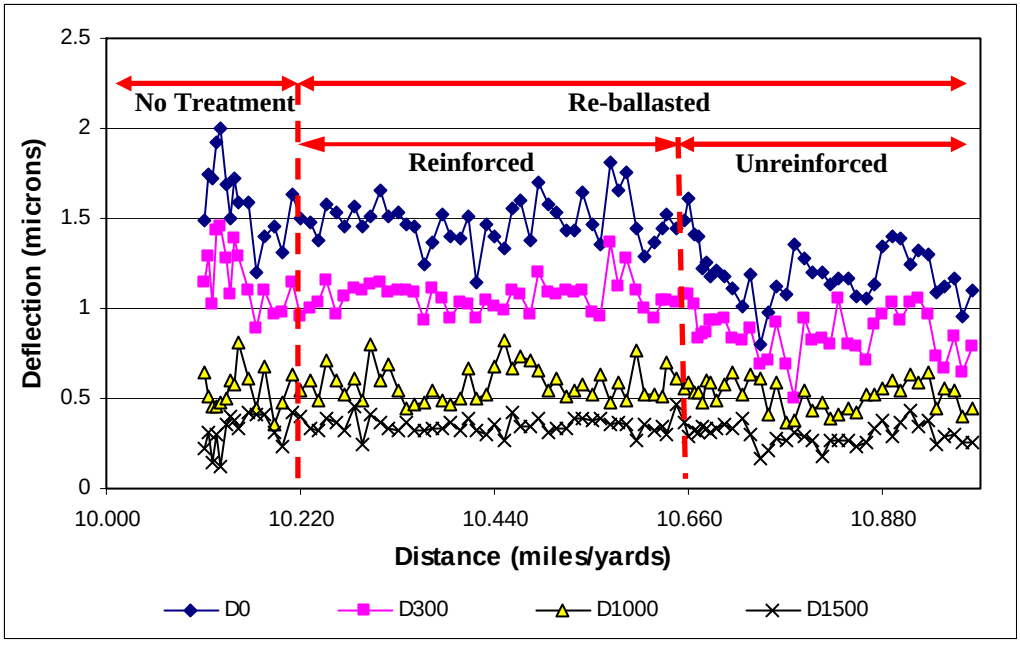

Figure 6.7 FWD readings from Coppul Moor
(Depth of reinforcement at 300mm depth)

6.3 Comparison with RTF and CET

The Composite Element Test (CET) was designed to provide comparative data that allowed the analysis of grid performance. The CET tests established the influence of geogrid reinforcement on the settlement of ballast under repeated loading. The CET also successfully identified several major parameters (e.g. optimum grid aperture size, importance of grid stiffness and junction strength) that influenced the reinforcing mechanism of the geogrid.

The CET data helped in the planning of the larger full-scale Railway Test Facility (RTF). The RTF as described in Chapter 5 allows full-scale testing of a track section. The RTF underlined the benefits of geogrid reinforcement in terms of reduced ballast deformation and extension of service life as shown by the results from geogrid reinforced track.

The results from the field trials, in the form of the FWD and HSTRC data, showed that the 30-65 geogrid registered the highest standard deviation improvement compared to unreinforced sections. Results from the field trial, when compared with historical rate of deterioration for the site, revealed that the 30-65 reinforced grid section showed a much reduced rate of deterioration translating to longer maintenance intervals.

Direct comparison of the field trials to the experimental work is not applicable as it is not possible to measure performance of the grid in the laboratory in terms of track standard deviation. There is also a lack of information on relationship between standard deviation and absolute settlement. However, it may be possible to do an approximate comparison in terms of rate of deterioration.

To summarise, the similarity in findings between the 3 tests that can be drawn from this research are:

- Results from the CET, RTF and field trials suggest that a geogrid reinforced (30-65 grid) track performs more effectively than the unreinforced section in terms of the rate of track deterioration.

- Based on the results from the RTF (see Figure 5.22, Section 5.4) and field trials, there was a similar trend in the increase in track life by a factor of 2.5 and 1.9 times respectively. The life extension factor of the field trial is derived from Figure 6.4 where historical data shows the average rate of track deterioration (in Standard Deviation) to be around 0.7mm / year. The rate of track deterioration post renewal and with the installation of grid is 0.25mm / year. On the other hand, from Figure 6.5, the average rate of deterioration before renewal is 0.6mm / year and the rate of deterioration post renewal without the installation of grid stands at 0.40mm / year. The ratio of the post renewal SD with grid reinforcement over the unreinforced track (hence isolating the effect of fresh ballast) gives the LEF which is approximately 1.9. The results provided a good appreciation on the reduction in the rate of deterioration due to geogrid reinforcement even though the two tests involve various other different parameters, e.g. traffic loadings, effect of weathering, fouling etc.

- Resilient data from the RTF (see Tables 5.3 and 5.5) showed similar subgrade resilient response for the 30-65 reinforced and unreinforced tests. The FWD results for the Coppul Moor site as seen in Figure 6.7 indicated that there was very little difference in trackbed stiffness after renewal between the reinforced and the unreinforced section. Both tests indicate that the grid is utilised to limit the accumulation of plastic strain rather than resilient strains.

6.4 Summary

The full scale field trial of a geogrid-reinforced rail track section performed at Coppul Moor served to validate the other results presented in this thesis.

The field trials showed that the rate of deterioration is reduced where the 30-65 grid is installed even when compared to sections with a stiffer subgrade. The maintenance interval for the reinforced section is likely to be increased and this represents a significant economic benefit.

The CET, RTF and field trials revealed similar findings; most notably that geogrid reinforcement can potentially reduce the rate of track deterioration and improve ride quality. Resilient response data from the RTF and field trials also concluded that geogrid reinforcement has very little influence on the trackbed stiffness as the grid is utilised principally to limit the accumulation of plastic strain rather than resilient strains.

The results from the field trial reconfirmed the validity of the experimental work performed in the laboratory. The consistency in findings from both the CET and RTF tests demonstrated the ability in this project, to simulate reasonably realistic rail track conditions in a controlled laboratory environment. This indicates that further RTF tests can be performed with confidence in the future to investigate the role of different grid parameters.

The validation of the experimental work through the field trial justified some of the assumptions made from the findings of the CET and RTF in the development of the design method. The development of the design method for reinforced rail track is discussed and presented in the next chapter.

7 DEVELOPMENT OF DESIGN METHOD FOR REINFORCED RAILTRACK

7.1 Introduction

The purpose of this chapter is to describe the development of a guide, providing the basis for the design of a ballasted rail track incorporating high tensile polymeric geogrid reinforcement. The guide is based on a 'mechanistic-empirical' model (i.e. an engineering model + calibration factors). Results from the Composite Element Test (CET) and Railway Test Facility (RTF) were used to calibrate and evaluate the design guide. Structural analysis using the Shell BISAR multilayer linear elastic layered system program provided the background for the design method. .

The analysis has been performed in two stages. The first is a pseudo non-linear elastic computation of stresses in the ballast and the second computes the vertical plastic strains resulting from these stresses.

The model allows exploration of the effect of various variables, e.g. subgrade stiffness, geogrid reinforcement etc, on the settlement characteristics of the track.

The model provides the basis for predicting extension to track life when grid reinforcement is used. This then allows an estimate to be made of the cost saving from reduced maintenance activity on rail track. This chapter concludes with comparison charts for different track variables and the effect of reinforcement on track settlement

7.2 Design Approach

The theoretical analysis is a two stage process. In the first stage, stresses induced by wheel loading and self weight of ballast were determined. The second stage saw the computation of plastic strains based on the computed stress regime from stage one. The surface settlement was determined by the summation of vertical plastic strains with depth.

The Shell BISAR computer program was used to compute the stresses, elastic strains and deflections in the structure from the application of one or more circular uniformly distributed loads to the surface which assumes infinite extent horizontally. The overlapped circular loads were used to simulate a rectangular loading area. Initial stress analysis was carried out by assuming the ballast and subgrade to be a series of linear elastic layers subjected to surface loading. Non-linearity of ballast was introduced by means of a successive iteration approach used to compute the stress regime from surface loading. The procedure is summarised in Figure 7.1.

Due to a lack of experimental data for the ballast used in this project, the non-linear resilient characteristics of the ballast were modelled using the repeated load triaxial test data from Selig and Waters (1994) as shown in Figure 7.2. This figure shows the relationships between the applied stress levels and the vertical resilient strains for tests on granite ballast. To compute permanent strain, repeated load data from Selig and Waters (1994) were again used to relate permanent strain to applied stress as shown in Figure 7.3. The figure shows representative results of constant-amplitude repeated load tests with full unloading.

.

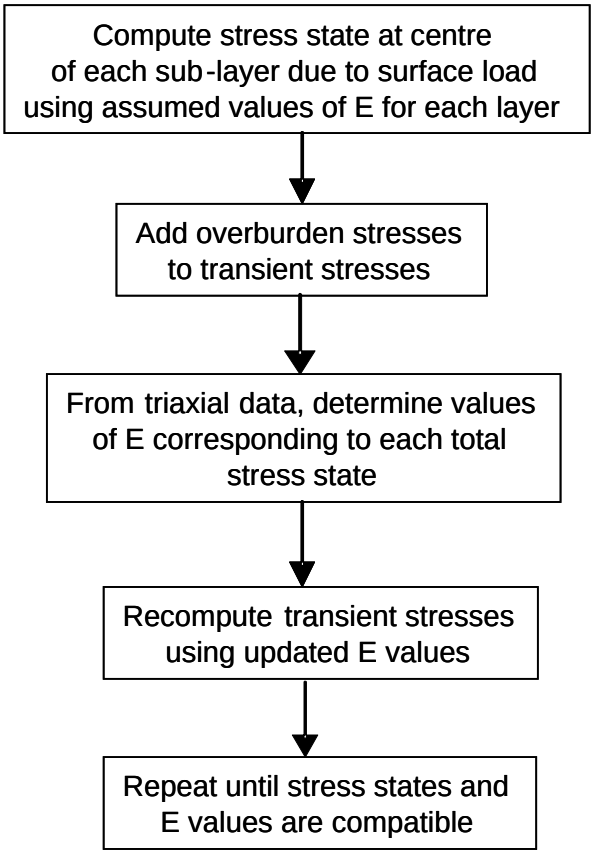

Figure 7.1 Procedure for computing stress in ballast

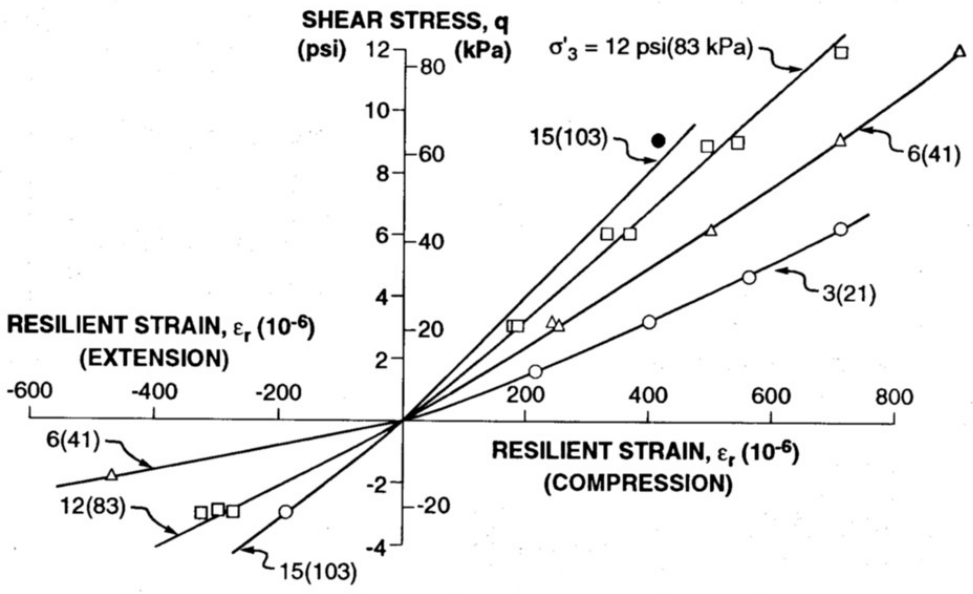

Figure 7.2 Relationship between applied stresses and resilient strain for granite ballast (Selig and Waters, 1994)

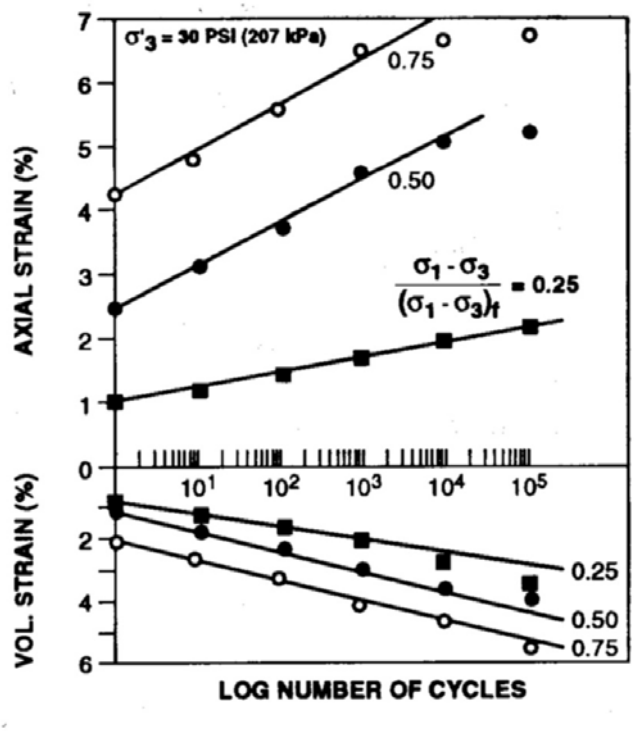

Figure 7.3 Relationship between applied stress and permanent strain for granite ballast (Selig and Waters, 1994)

7.3 CET Model

Initial work focused on the modelling of the Composite Element Test (CET). This was done as a means to determine the appropriate means of accounting for the grid reinforcement effect which could then be used in modelling the Railway Test Facility (RTF). As discussed in Chapter 4 of this thesis, the CET is a simplified element test which allows the ballast and grids to be tested at full scale with approximate simulation of the situation beneath a sleeper. Two configurations were used, one with the extra overburden which was deemed to be more realistic. The test was carried out in a box-like structure and the cross section is as shown in Figure 7.4.

In the BISAR structural model of the CET, a series of surface loads were applied to simulate loading on ballast via the sleeper, as shown in Figure 7.5. These circular loads were arranged and assigned a load (6.67kN) to simulate the load distribution in the CET. Since BISAR assumes infinite extent horizontally, in order to reproduce the

boundary effect, additional circular loads were added to produce zero the lateral horizontal displacement at the location of the wall.

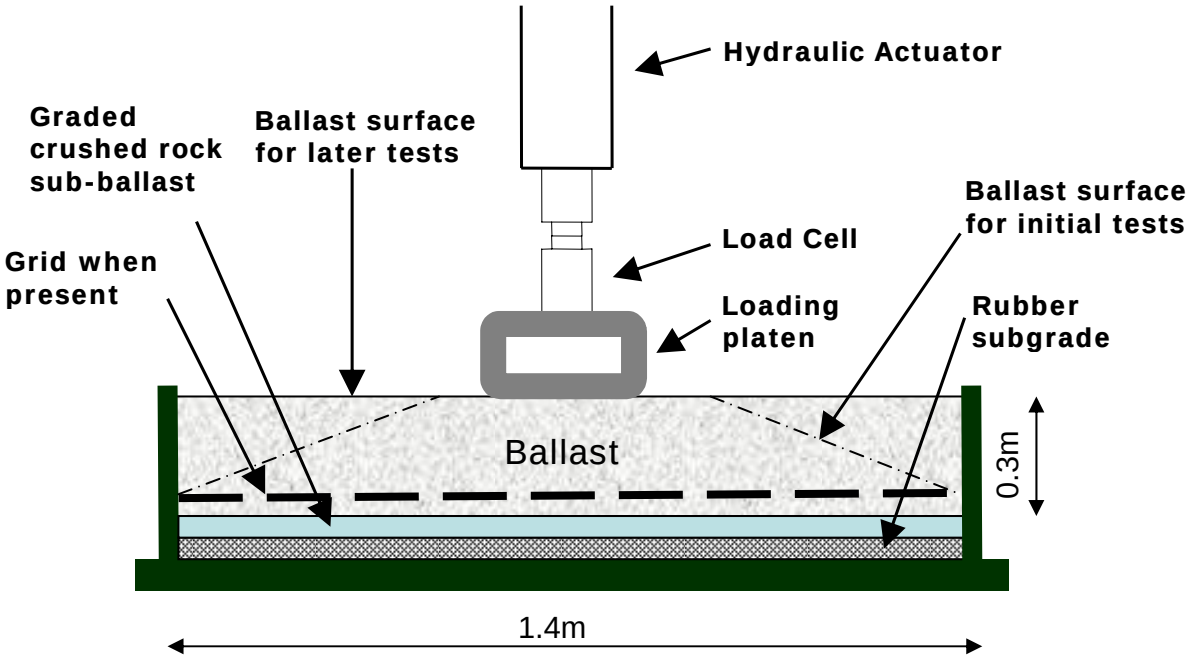

Figure 7.4 Composite Element Test (CET)

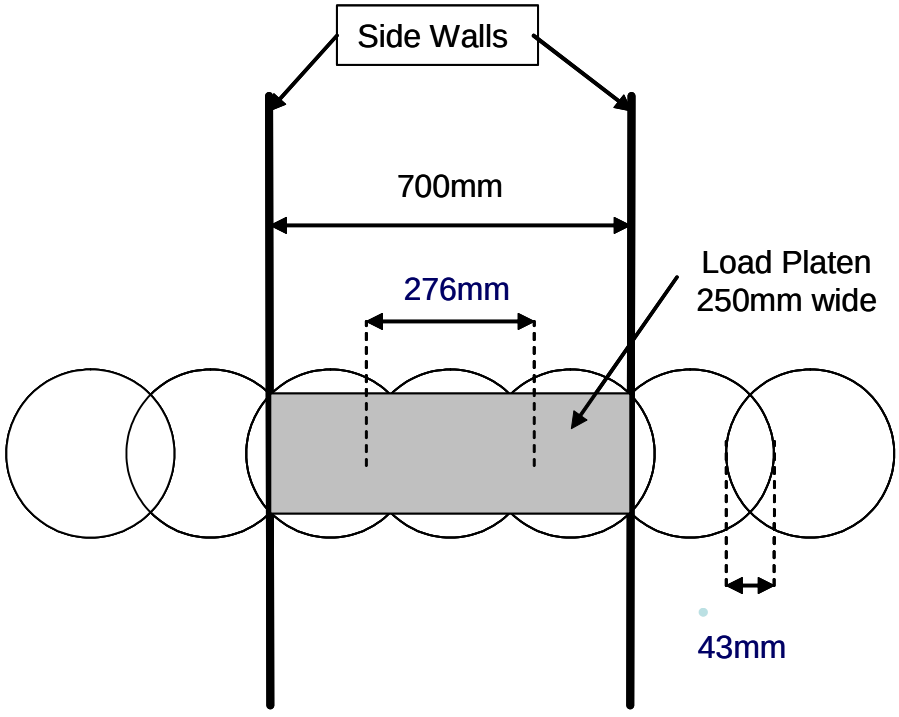

Figure 7.5 Loading arrangements for analysis of CET

The BISAR program allows the foundation to be analysed in layers and in the case of the CET, the ballast was divided into 3 sub-layers of 100mm sitting on top of a subgrade material. In the CET, the subgrade condition was simulated through the use of rubber sheets over a rigid base. An equivalent subgrade stiffness value was deduced based on the resilient data from the CET; a subgrade stiffness of 80MPa was found to produce the best match. The modulus of elasticity of the ballast was set initially at 100MPa. The structural details are as shown in Figure 7.6. The exact locations for stress and strain computation are as shown in Table 7.1.

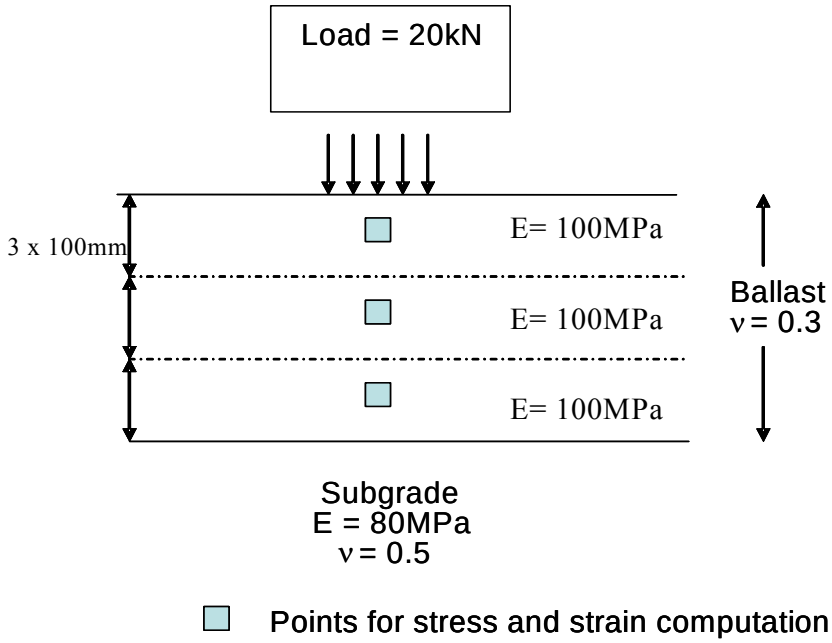

Figure 7.6 Structural details for CET analysis

Table 7.1 Coordinates for stress and strain computations

Position	X-Coordinates	Y-Coordinates	Depth (m)
1	0	0	0.05
2	0	0	0.15
3	0	0	0.25

The computed vertical deflection under the centre of the loading beam (at ballast surface) compared favourably with the measured values.

Example of CET Permanent Strain Calculations

i. Set up structural model in BISAR

ii. Commencement of iteration. Using Selig and Waters (1994)'s model for railway ballast shown in Figure 7.2, the non-linear model E = f (q, p), the iterated Young's Modulus E can be derived from

$$\varepsilon = 1/E\ (\sigma_v - 2\upsilon\sigma_h) \qquad (7.1)$$

Where ε = resilient strain, and is obtained from Figure 7.2.

σ_v = vertical stress (from BISAR calculation),

σ_h = confining stress (from BISAR calculation),

υ = Poisson's Ratio,

q = deviatoric stress, $(\sigma_v - \sigma_h)$,

p = mean normal stress, $1/3(\sigma_v + 2\ \sigma_h)$.

iii. Repeat until E values are compatible

iv. Based on the assumption that ballast angle of friction, $\emptyset = 50^o$ (Selig and Waters, 1994) , the ratio of maximum applied deviator stress to failure deviator stress can be found, the axial strain for each 100mm ballast layer after 30,000 cycles performed in the CET could then be obtained from Figure 7.3.

v. Adjustment factors of 0.7 to be applied to the computed results to match the measured data obtained from the CET. Table 7.4 illustrate an example of the use of CET Adjustment Factor (AF).

Table 7.2 Calculation of plastic strain

	Calculation of Total Plastic Strain
Layer 1 (100mm)	Computed strain ε_1 x AF
Layer 2 (100mm)	Computed strain ε_2 x AF
Layer 3 (100mm)	Computed strain ε_3 x AF
Total plastic strain	Σ (ε x AF)

vi. For reinforced ballast, apply Grid Reinforcing Factor (GRF) as shown in Table 7.3.

vii. Summation of plastic strain of all three layers with grid reinforcement, Σ (ε x AF x GRF).

Finally, in order to model the benefit of reinforcement in the CET model, an approach using factored values was introduced. The magnitude of the permanent strain was reduced through the introduction of a 'Grid Reinforcing Factor' (GRF). The GRF is a factor assigned to different layers in the ballast structure representing the potential benefit in terms of reduced permanent strain with the use of geogrid reinforcement. The GRF was obtained through the calibration against the CET results and based on the assumption that the reduction of permanent strain will be most apparent in a ballast layer near to the grid with a diffused effect at increasing distances. There is no literature which quantifies this hypothesis but from an engineering point of view, such an approach seems logical. Table 7.3 summarises the magnitude of GRF selected for different grids for the three sub-layers to achieve a match to the CET results. The CET measured values can be found in Figure 4.19.

Although the model includes many assumptions and an approximate calculation methodology, the CET model has allowed a platform to be derived which can be calibrated and applied to model the RTF tests.

Table 7.3 Grid Reinforcing Factors for CET simulations and comparison of calibrated computed settlement with measured values for grid at 250mm installation depth within ballast

Grid Type	**Grid Reinforcing Factor (GRF)**			**Settlement (mm)**	
	Layer Depth (mm)			**Measured**	**Computed**
	0-100	**100-200**	**200-300**		
Unreinforced	1.00	1.0	1.0	11.7	11.2
15-65	0.95	0.9	0.8	10.4	9.7
30-65	0.90	0.8	0.6	7.8	8.2
45-65	0.85	0.7	0.4	6.1	6.7
Steel	0.80	0.6	0.2	5.8	5.2

7.4 RTF Model

The Railway Test Facility (RTF) is a full-scale test facility which simulates the passage of a train at reasonable speed. Vertical loads of 92kN were applied at 3Hz by each of the three actuators in a programmed manner to simulate moving traffic. The vertical settlement of the central sleeper was monitored along with the pressure cell readings at the surface of the subgrade. Comparison of the unreinforced and reinforced construction was done and is presented in Chapter 5. Figure 7.7 shows the RTF test setup.

To reproduce the loading effect of the rigid sleeper of the RTF facility in BISAR, the load distribution was arranged in such a way that the outermost circular loads was of the highest magnitude as shown in Figure 7.8. This arrangement ensures approximately even vertical displacement simulating the rigid nature of a sleeper. The exact locations for stress and strain computation are similar to those in the CET model as shown in Table 7.1.

Figure 7.7 Aerial photo of the Railway Test Facility (RTF)

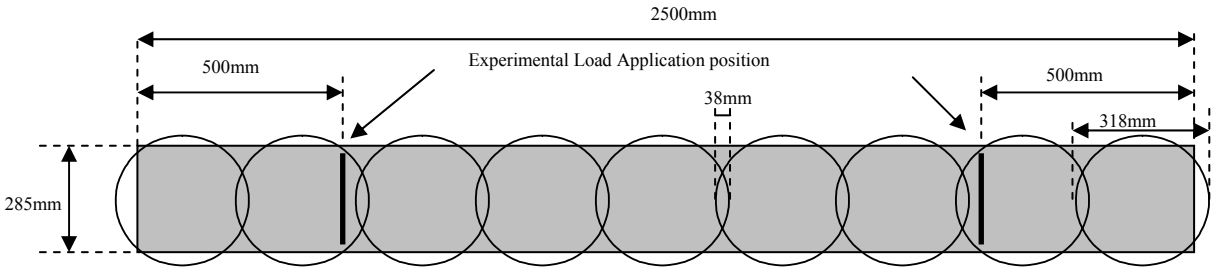

Load (kN)	14.95	8.89	8.832	8.56	8.98	8.56	8.832	8.89	14.95

Figure 7.8 Loading arrangements for analysis of RTF

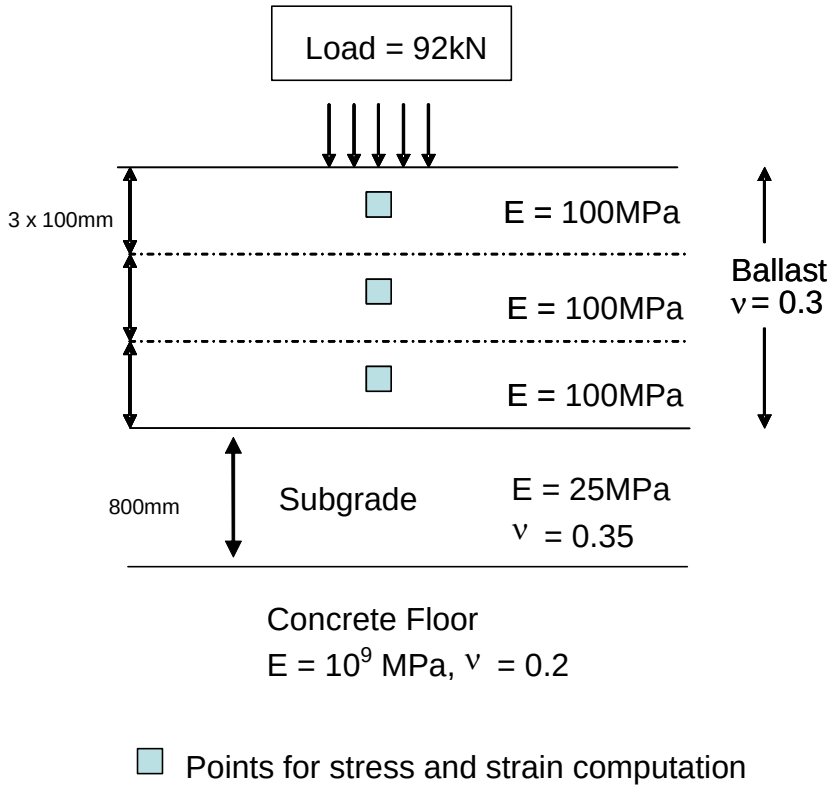

Figure 7.9 Structural details for RTF analysis

Figure 7.9 shows the structural details for the RTF analysis. The same iterative approach also applies to the RTF model. However, instead of using a adjustment factor of 0.7, the RTF data required a Adjustment Factor (AF) of 0.43 to match the measured RTF results at 1 million load applications. In order to simulate the measured deflection plots, a Settlement Plot Factor (SPF) was applied to each ballast layer at settlement intervals of 0.25, 0.5, 0.75 and 1 million cycles. The SPF is a factored value calibrated from the settlement plots of the measured data (data presented in Figure 5.19). The permanent strain for each of the three layers, for an unreinforced RTF, after e.g. 0.25 million cycles, $\varepsilon_{0.25m}$, can be shown by the expression

$$\varepsilon_{0.25m} = \text{Permanent Strain of layer x RTF AF x } SPF_{0.25m} \qquad (7.3)$$

Where the coefficients are illustrated in Table 7.4

Table 7.4 RTF coefficients

Settlement at (million cycles)	**RTF AF**	**SPF**
0.25	0.43	0.7
0.5	"	0.8
0.75	"	0.9
1	"	1

The GRF coefficients used for the CET model, as shown in Table 7.3, were applied in the RTF model as well. The computed and laboratory values of settlement, with the application of the coefficients, are given in Figure 7.10. The close correlation between the two reinforced plots demonstrated a satisfactory RTF settlement prediction model. The resilient deflection of the central RTF sleeper and the vertical transient stress at the top of the subgrade were also computed and compared to the measured values. The comparisons were again considered satisfactory as shown in Figures 7.11 and 7.12.

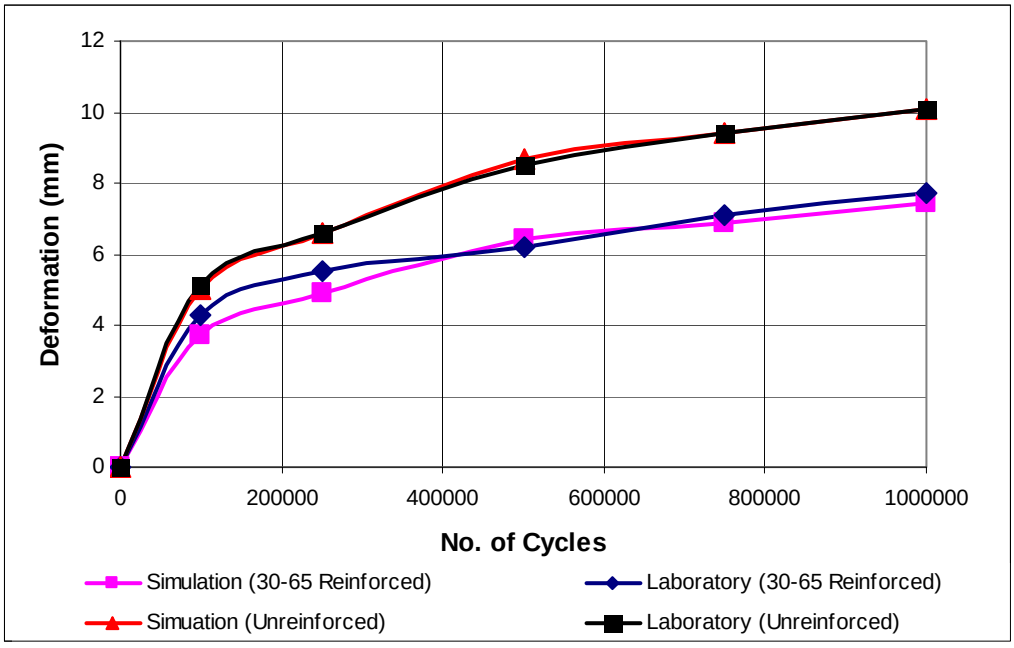

Figure 7.10 Comparison of computed and measured settlement for RTF

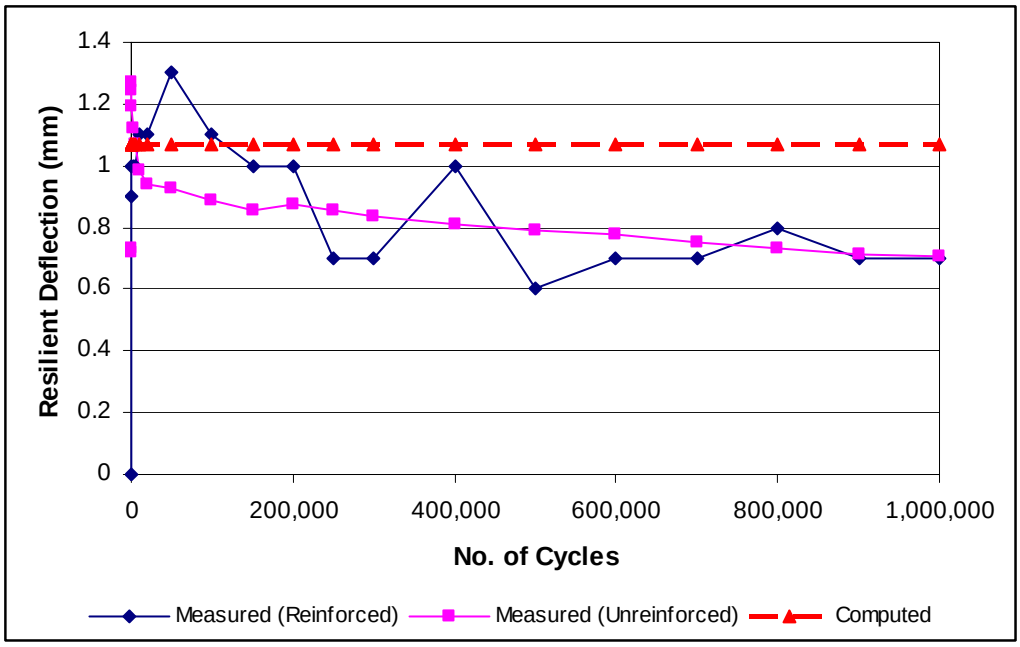

Figure 7.11 Comparison of measured and computed resilient deflections of the central sleeper in the RTF

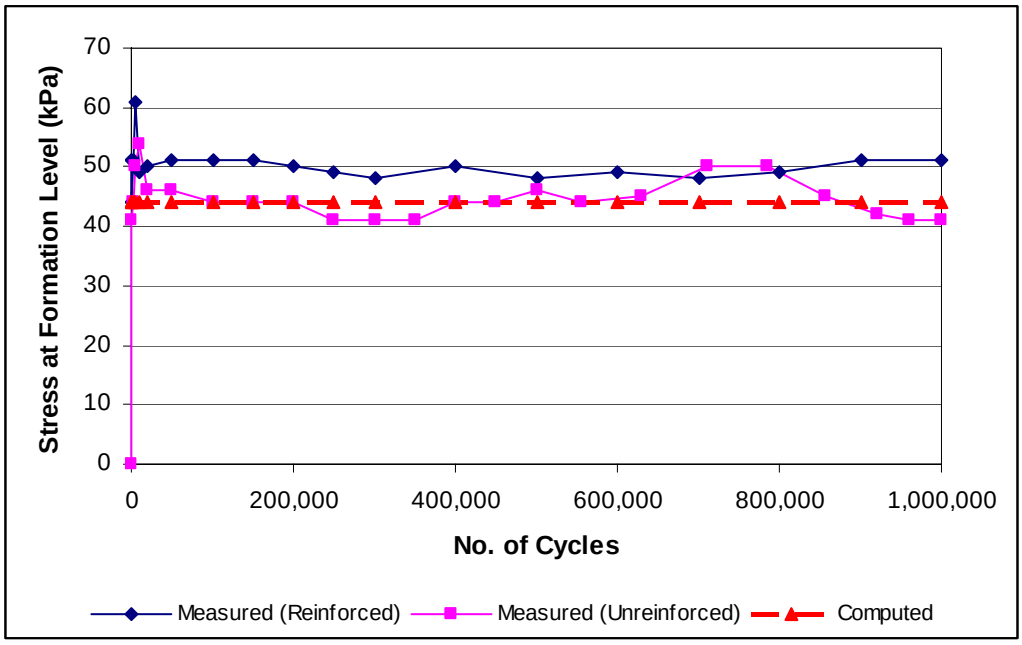

Figure 7.12 Comparison of measured and computed vertical stress at formation level beneath centre of sleeper

7.5 Model Used to Produce Design Chart

The purpose of the design charts is to provide a design guide for polymeric grid reinforced ballasted track design. Extension in track life is taken as the key parameter in this design guide. The Life Extension Factor (LEF) is taken as the number of cycles at a given settlement for the reinforced case divided by the number of cycles for the unreinforced case. If the number of cycles is set at the settlement which triggers track maintenance work, the LEF will be the extension in maintenance interval.

The RTF settlement model is taken to be a representation of real track and it allows variation of certain key parameters. The parameters that have been varied include the applied load, the subgrade resilient modulus, ballast thickness and the type of grid. The ballast in this investigation was kept consistent with the use of Glensanda ballast throughout the course of this project. The effect of contaminated ballast or different mineralogy or the effect of particle shapes will therefore not be included in the design consideration. These issues can be added in the future.

Figure 7.13 shows the predicted effect of subgrade stiffness on settlement. It can be seen from the figure that subgrade stiffness is predicted to have little influence on settlement. Traffic loading in practice is often quantified in Million Gross Tonnes (MGT) and the conversion from the number of load cycles in the RTF is 1MGT = 20,000 cycles at 92kN (Esveld, 2001). This indicated that the equivalent of 50MGT was applied in each of the 4 RTF tests.

Although the ballast strain model used is based on data in the published work of Selig and Waters (1994), it was found that is was not sensitive with regard to subgrade stiffness or to applied stress. Therefore, to establish a more realistic non-linear relationship between applied stress and ballast settlement, a modification of the ballast settlement law proposed in Ishida (2003) has been introduced in the model. Ishida (2003)'s settlement law assumption was used throughout for the RTF model The equation is expressed as:

$$Y_b = (P_t - b)^2 \qquad (7.4)$$

Where,

Y_b: Ballast settlement (mm/axle)

P_t: Pressure of sleeper base plate (kPa)

b: Coefficient (= 39.6kPa: ballast thickness of 250mm)

Design Charts

Figure 7.14 shows the effect of geogrid reinforcement with a 25MPa subgrade under a 100kN load using the settlement power law adjustment in Eqn 7.4. Only the 65mm aperture grids were considered as it has been shown in the CET and RTF tests to be the best performing grid. The 65mm aperture grid range was concluded to have the optimum size for effective reinforcement. Figure 7.15 presents the influence of applied load on computed Life Extension Factor (LEF) for a subgrade stiffness of 25MPa. Maintenance on a rail track is triggered by differential settlement and the relationship between absolute settlement and differential settlement is known to be complex but Thom and Oakley (2006) claimed an absolute settlement of 10mm or more will trigger maintenance. The LEF in this design chart is based on the accumulated number of cycles at the 6mm settlement mark which is conservative compared to the figure reported by Thom and Oakley.

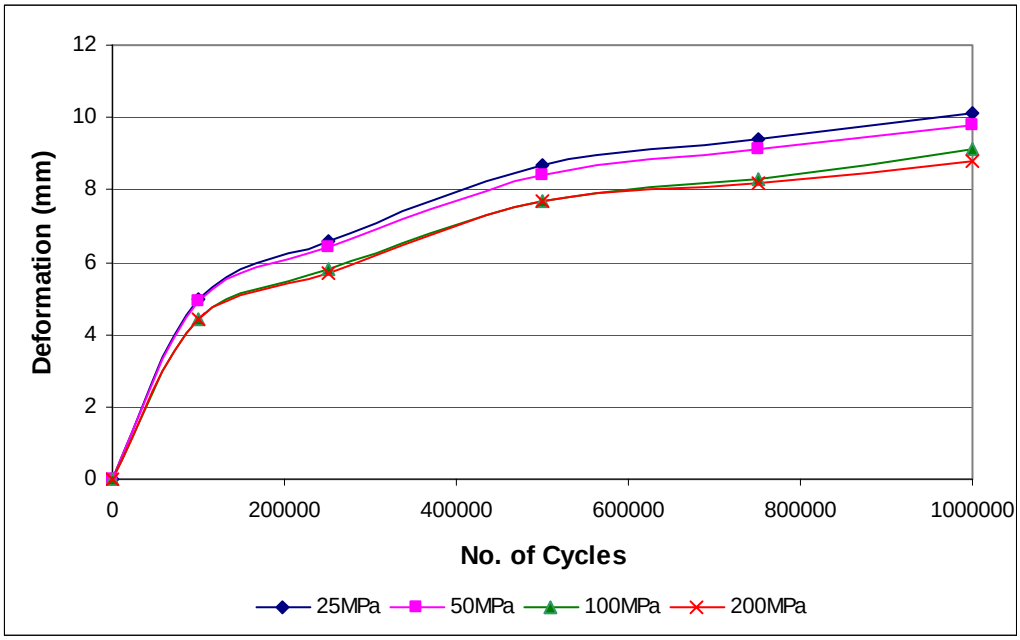

Figure 7.13 Influence of subgrade stiffness on computed settlement for unreinforced track

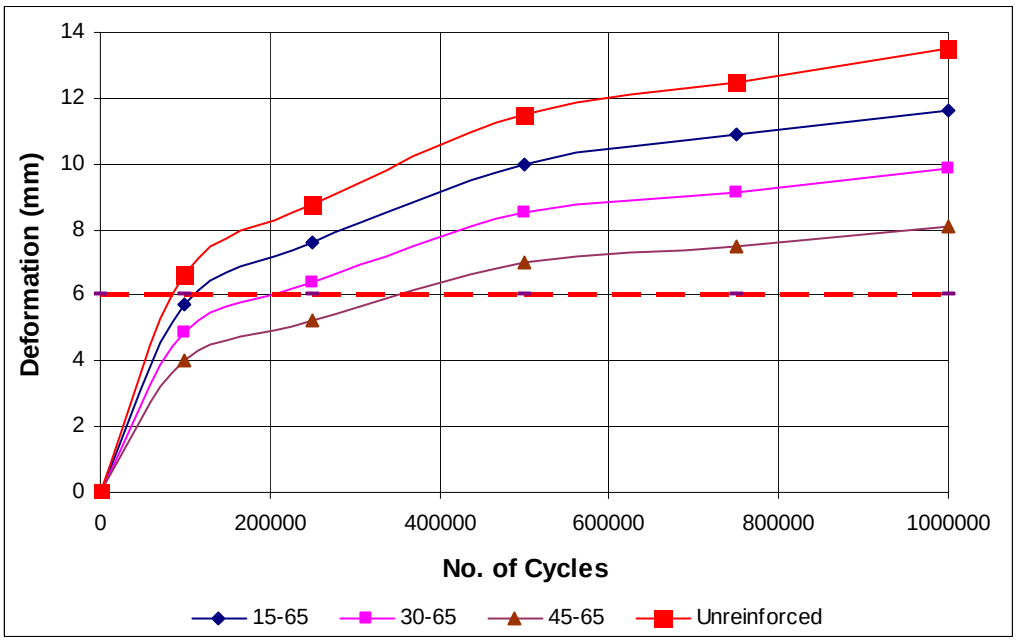

Figure 7.14 Effect of geogrid reinforcement with subgrade stiffness of 25MPa under a 100kN load

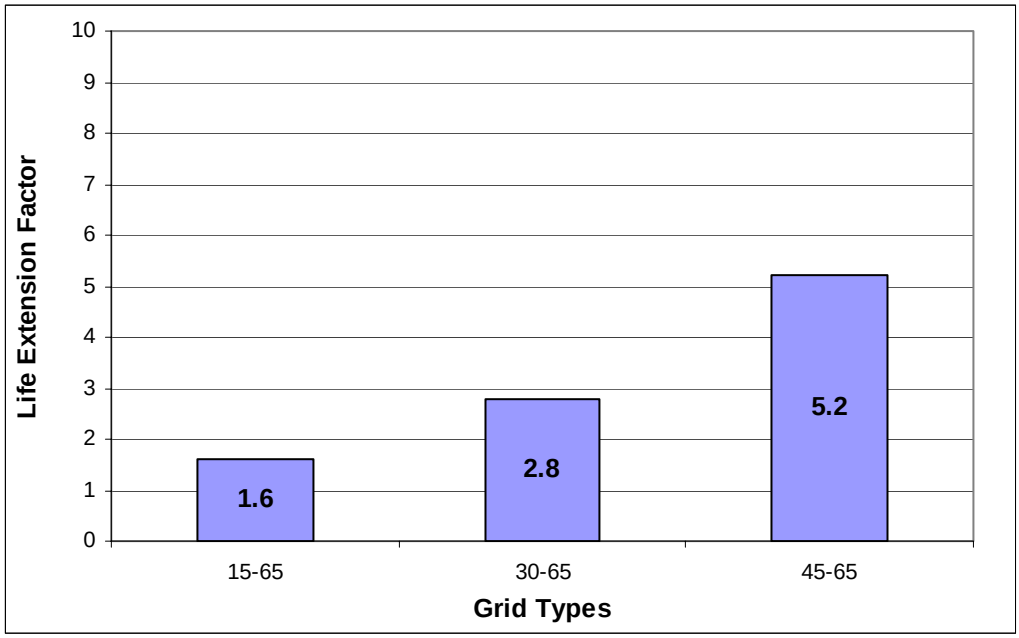

Figure 7.15 Effect of geogrid reinforcement with subgrade stiffness of 25MPa under a 100kN load on LEF

In Figure 7.15, the LEF is presented as the extension of track life with the installation of the various grids, at the 6mm settlement mark, in proportion to an unreinforced case. The influences of applied load, subgrade resilient modulus, and type of grid on the computed LEF are shown in Figures 7.16, 7.17, 7.18 and 7.19.

It can be seen that applied load has less influence on the LEF values compared to the stiffness of the subgrade. The LEF values, on the other hand, decrease with increasing subgrade stiffness. This is consistent with the CET findings where it was concluded that effect of geogrid reinforcement is observed to be particularly noticeable with soft subgrade.

For practical design purposes, a summary set of LEFs was produced and these are given in Table 7.6. The table shows the value of LEF for design of a geogrid reinforced track with a ballast thickness of 300mm. For the ease of use, two categories of subgrade are specified; 'soft' (E = 25 to 50MPa) and 'stiff' (E = 100 to 200MPa).

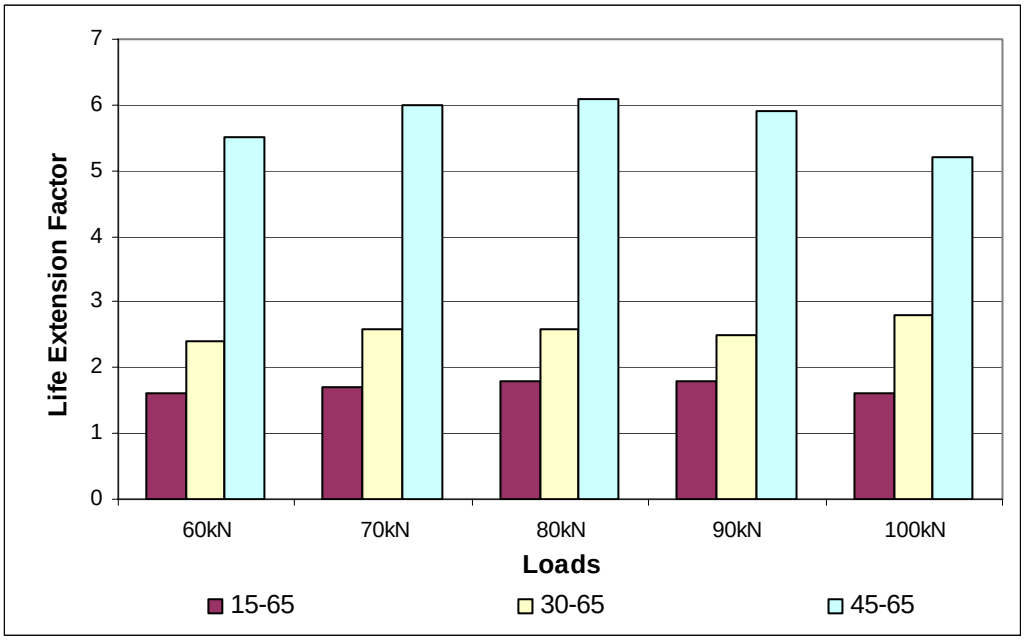

Figure 7.16 Influence of applied load on computed LEF values for a subgrade stiffness of 25MPa

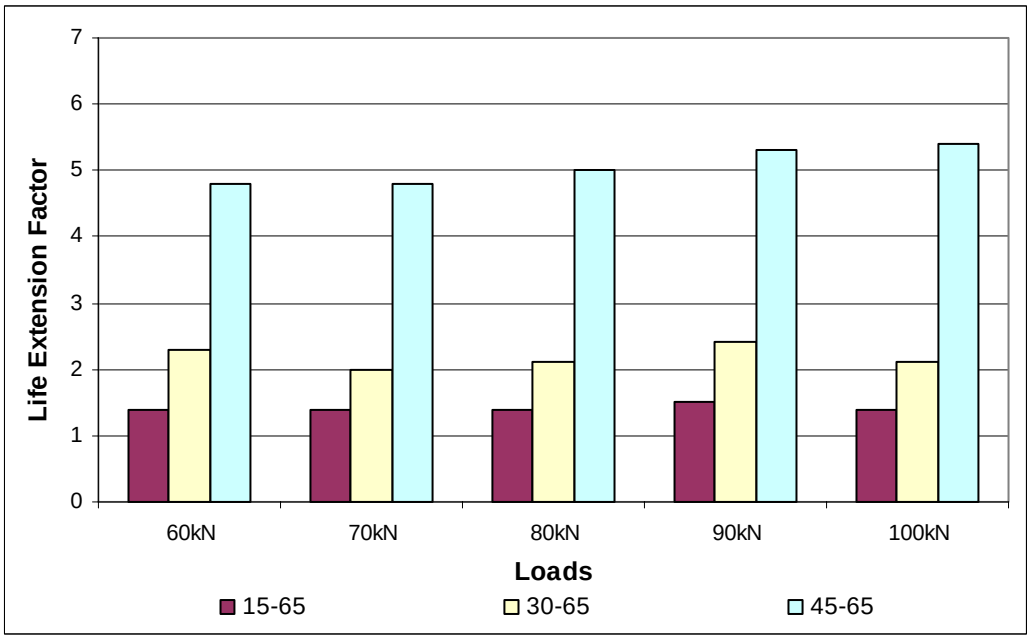

Figure 7.17 Influence of applied load on computed LEF values for a subgrade stiffness of 50MPa

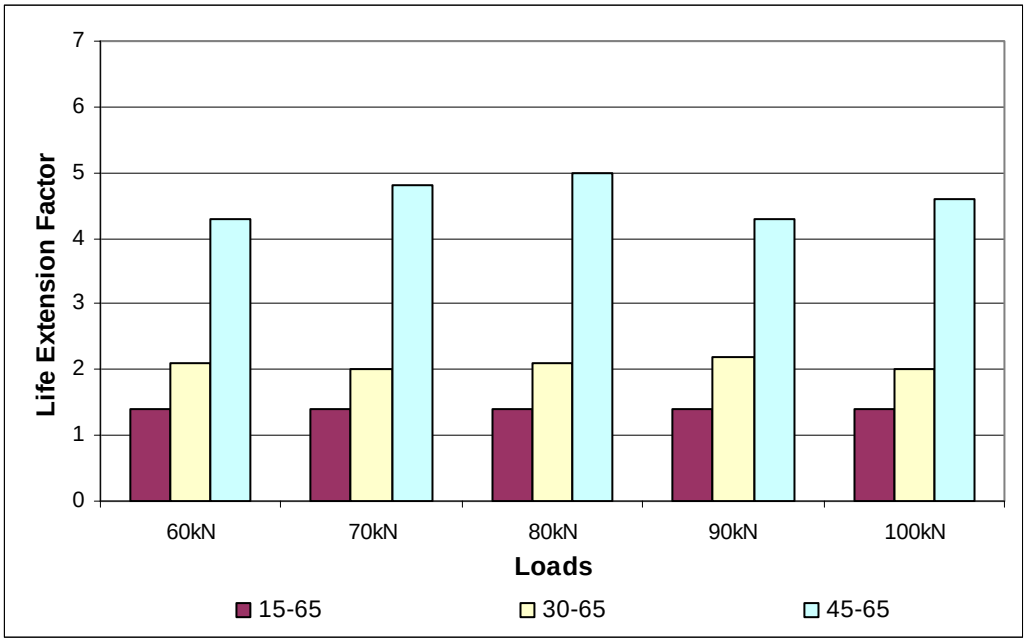

Figure 7.18 Influence of applied load on computed LEF values for a subgrade stiffness of 100MPa

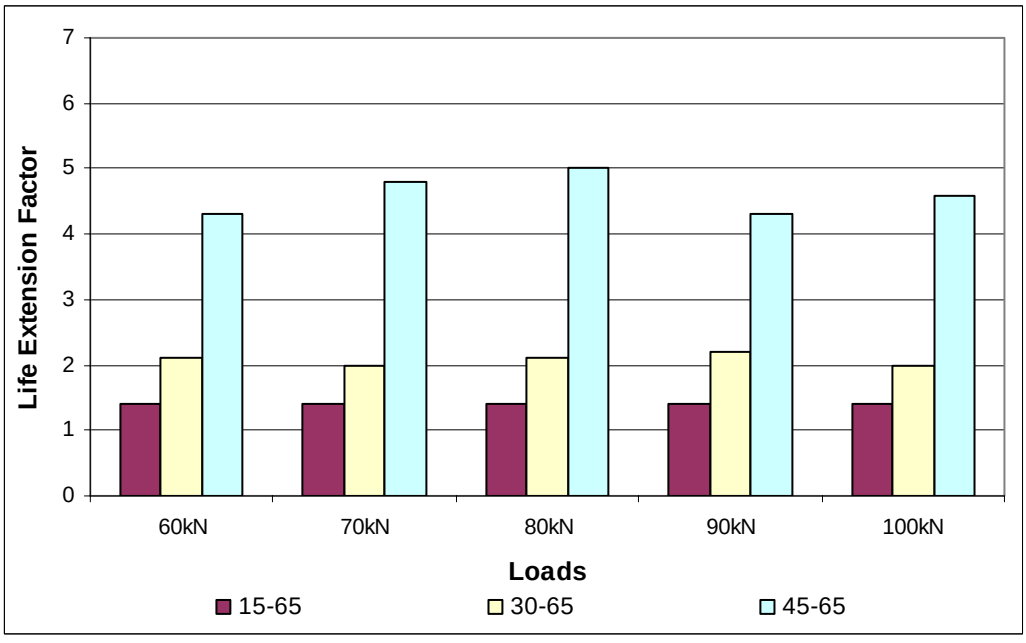

Figure 7.19 Influence of applied load on computed LEF values for a subgrade stiffness of 200MPa

Table 7.5 Proposed values of Life Extension Factor for design (Ballast thickness = 300mm)

Grid (A/B Ratio of 1.6)	**Load Extension Factor (LEF)**	
	Soft Subgrade (E = 25 to 50 MPa)	**Stiff Subgrade (E = 100 to 200 MPa)**
15-65	1.5	1.4
30-65	2.3	2.0
45-65	5.4	4.6

The effect of varying the thickness of ballast was also considered; considering ballast thicknesses of 210mm and 420mm. These figures were chosen for convenience as they are divisible by 3 hence allowing the easy definition of three equal sub-layers (70mm and 140mm for the two cases respectively). The new ballast thickness arrangements were put through the same prediction model.

Using the data from the Grid Reinforcing Factors (GRF) for the 30-65 grid as shown in Table 7.3 (based on 300mm ballast thickness), those values were extrapolated as shown in Figure 7.20. The extrapolated GRF plot allows the estimation of the effect of grid reinforcement at various distances away from grid.

Figures 7.21 and 7.22 show the computed relationships between settlement and number of load applications for the reinforced and unreinforced cases with ballast thicknesses of 210mm and 420mm respectively. The grid used is the 30-65 grid. The value of LEF was determined at a settlement equal to 60% of the total settlement at the 1 million cycles mark. This is consistent with the approach taken for the 300mm layer where the LEF was determined at the 6mm settlement mark, 60% of the total settlement, which was 10mm (see Figure 7.10).

Table 7.5 shows a summary of the LEF values for the various ballast thicknesses for the 30-65 grid under the soft subgrade condition, since the 30-65 grid is already a Tensar production type and the soft subgrade condition is deemed to be most relevant to reinforced track designers.

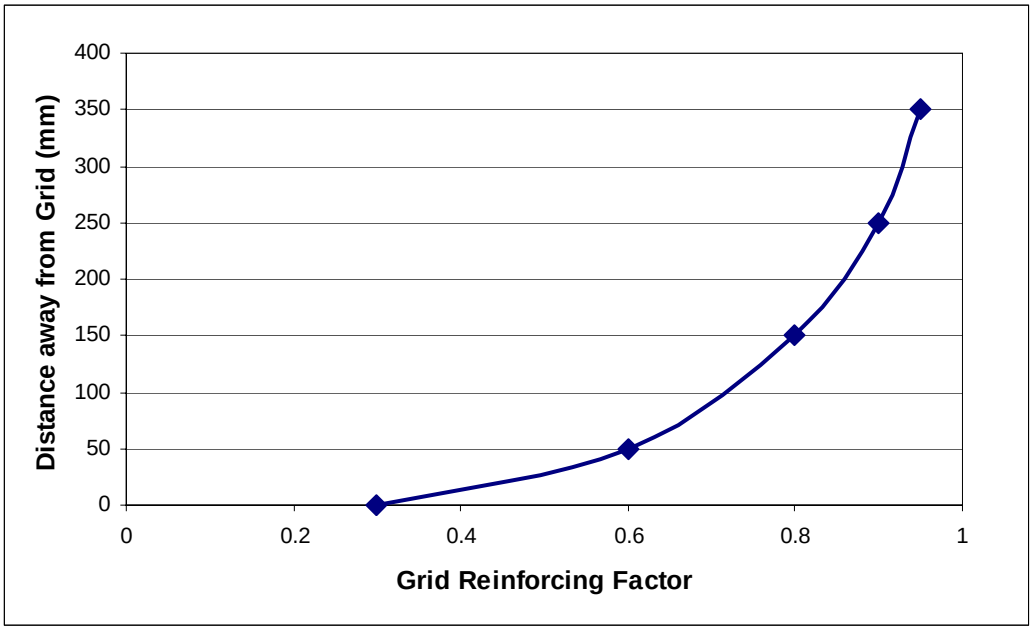

Figure 7.20 Grid Reinforcing Factors at various distances from a 30-65 grid

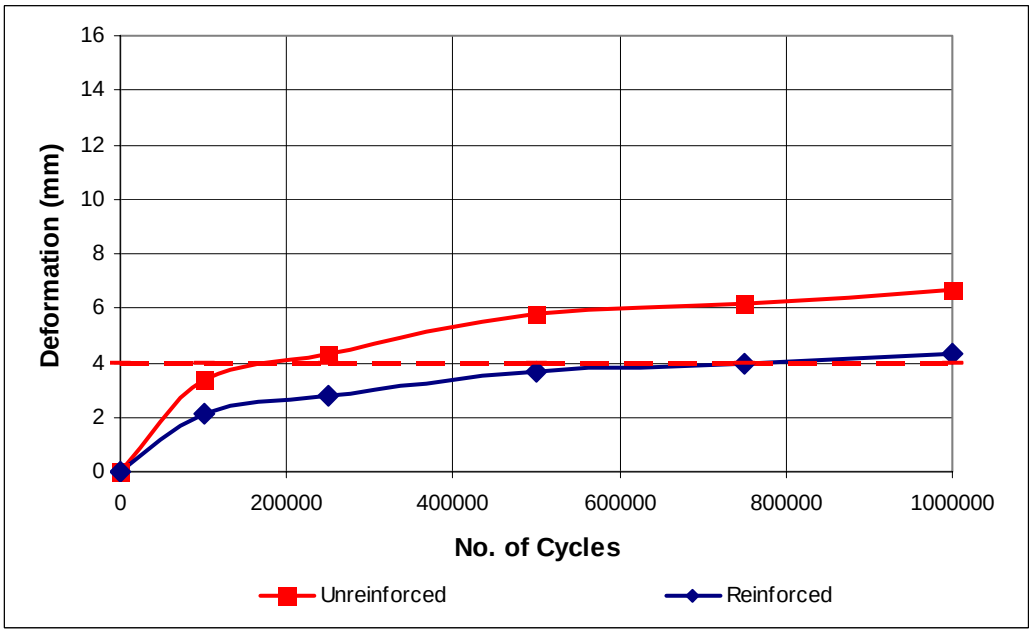

Figure 7.21 Computed settlement curves for a 210mm ballast layer

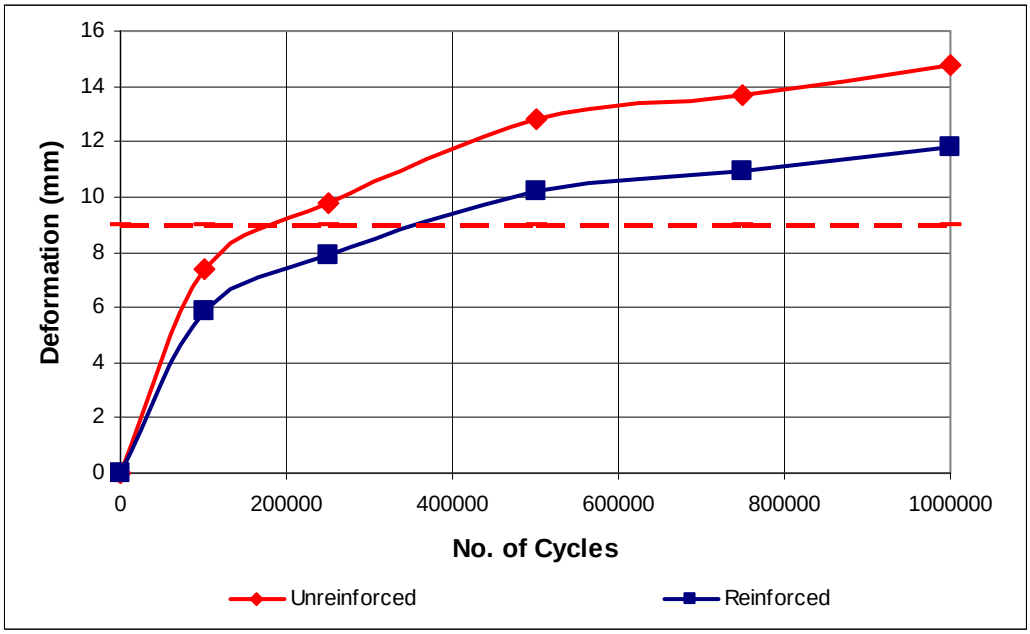

Figure 7.22 Computed settlement curves for a 420mm ballast layer

Table 7.6 Values of LEF as a function of ballast thickness for the 30-65 grid (A/B: 1.6)(Soft subgrade)

Ballast Thickness (mm)	**Life Extension Factor (LEF)**
210	3.9
300	2.3
420	2.1

From Table 7.6, the highest LEF value was achieved in the 30-65 reinforced 210mm thick ballast layer and the lowest in the 420mm thick ballast. This is consistent with the principle that the permanent strain would be reduced closest to the grid position. The ballast thickness of 210mm is approximately the minimum workable depth on a rail track without interfering with maintenance work such as tamping so grid must be placed beneath this depth.

7.6 Summary

The purpose of this design guide is to provide a basis for the design of a ballasted rail track incorporating high tensile polymeric geogrid reinforcement. Experimental data and simplified theoretical analysis were used in the development of the preliminary design guide for reinforced ballasted track.

The stress computation involves the use of the Shell BISAR multilayer linear elastic layered system program which computes the stresses, elastic strains and deflections in the structure. Non-linearity of ballast was introduced by means of a successive iteration approach used to compute the stress regime from surface loading.

A series of coefficients were used to calibrate measured results to computed results. The calibration was based on the CET and RTF unreinforced test results. The Grid Reinforcing Factor (GRF) as shown in Table 7.3 is based on the principle that the grid reinforcing effect decreases with increased distance from grid.

Design charts have been presented in terms of Life Extension Factor (LEF). The LEF can be linked to the extension in maintenance interval if the settlement is set to be the point which triggers site maintenance work, e.g. tamping or stone-blowing. From the charts, it can be taken that the effect of geogrid reinforcement was most noticeable under soft subgrade. This prediction is in good agreement with the findings of most reports (see Chapter 2.6).

The developed design method, based on a ‘mechanistic-empirical’ model has produced a workable design chart for grid reinforced track designers.

8 CONCLUSIONS AND RECOMMENDATIONS

8.1 Conclusions

The conclusions that can be drawn from this research are:

Grid/Ballast Interaction

- The series of element tests carried out, namely Pull-Out Test, Rib Test and Particle Friction Test have been successful in providing data and information to assist DEM modelling work performed by Harrireche.

- The results obtained from the Particle Friction Test were fairly consistent with the literature with a frictional coefficient of 0.6. Results from the pull-out test were satisfactory in terms of repeatability. Grid aperture and stiffness in terms of rib thickness were deemed to be two critical criteria as proven in both laboratory (pull-out) and simulation results.

- Harrireche's Discrete Element Modelling (DEM) simulation on size ratio agrees well with the experimental work in which it was concluded that the 65mm aperture grid induces a better interlock than the grid with a 32mm aperture for a 50mm nominal size ballast aggregate.

Composite Element Test (CET)

- Good repeatability of test was demonstrated by the consistency of test results achieved in the CET tests.

- Geogrid reinforced ballast layer showed a significant reduction in permanent settlement over the test duration. The improvement in permanent strain depended on the choice of grid used.

- The benefit of the grid reinforcement increases with softer subgrade condition.

- The aperture size of the geogrid was found to be very important as it influenced the grid/ballast interlock. The optimal aperture size was found to be at approximately 60-80mm. Results from the CET indicated the 65mm aperture size range grid to be most effective in reducing settlement for a 50mm nominal size aggregate.

- Grid stiffness was found to be an important factor in the reinforcement of ballast. The stiffest (45-65) grid was the best performer in the CET tests.

- Multiple layers of geogrid or the installation of a grid at mid-depth has little effect on performance in terms of reduced ballast settlement, compared to the standard case of reinforcement.

- A geo-composite does not match the performance of geogrid. The lack of ballast punch depth due to the presence of the geo-textile heat-bonded to the grid is likely to have prevented proper ballast/grid interlock.

- Grid junction strength was found to be important in promoting effective ballast/grid interlock hence reducing settlement.

- The rib profile of the geogrid was found to be a significant parameter and its influence is most prominently shown in the latter stages of loading, at higher strains.

- Findings from the CET provided a good platform for the design of experiments in the full-scale Railway Track Facility (RTF).

Railway Test Facility (RTF)

- The 30-65 grid was used based on the recommendation from the CET and the fact that it is a current production grid of Tensar International.

- The test was deemed to be repeatable with the results, especially those obtained without the inference of the tamping procedure, showing good correlation and consistency.

- Findings from the RTF were in good agreement with those from the CET where geogrid reinforcement was found to reduce permanent settlement.

- Geogrid reinforcement reduces the rate of track settlement. The required interval between maintenance interventions was found to have increased by a factor of about 2.5.

Field Trials

- A field trial on a geogrid-reinforced rail track section carried out at Coppul Moor served as a point of validation of the results presented in this thesis

- The trial concluded that the rate of deterioration is reduced where the 30-65 grid is installed even when compared to a section with a stiffer subgrade.

- The field trial, the CET and the RTF all produced similar findings; most notably that geogrid reinforcement can potentially reduce the rate of track deterioration and long term ride quality.

- Results from the trial also indicated that geogrid reinforcement has very little influence on the trackbed stiffness as the grid is utilised principally to limit the accumulation of plastic strain rather than resilient strains.

- The rate of track deterioration is reduced by approximately a factor of 1.9 with the use of the 30-65 geogrid.

Development of Design Method for Reinforced Rail Track

- Use of a simplified elastic analysis for the track structure formed the basis for successful modelling of the reduction in settlement observed in the CET and RTF tests.

- The model was calibrated with results from the CET and RTF.

- The benefit of grid reinforcement in the simulation is provided by the Grid Reinforcing Factor (GRF), a coefficient obtained through the results from the CET and RTF.

- The design charts are presented in terms of a Life Extension Factor (LEF), taken as the number of cycles at that settlement for the reinforced case divided by the number of cycles for the unreinforced case. It indicates the potential extension between track maintenance intervals.

- The design charts encompass variables such as applied load, stiffness modulus of subgrade (listed as ‘soft’ and ‘stiff’ in the charts), grid type as well as the thickness of ballast.

8.2 Overall Conclusions

The objective of this research project was to quantify the benefit of geogrid reinforcement on ballasted rail track and to investigate the mechanistic properties of geogrids that would deliver optimal performance. To achieve this aim, a design chart has been produced that is meant to conclude the findings from the research and to make them available, in simple format, to the grid reinforced track designers.

Results from fundamental element work, investigating grid/ballast interaction, were fed into the DEM work performed by Harrireche. The results from these element tests were deemed satisfactory and the conclusion from the DEM, supported by the data presented in this thesis, produced important findings, namely the importance of grid stiffness as well as the importance of grid aperture to particle size ratio. These early findings laid the foundation for the investigative work carried out in the CET.

The CET was not meant to be a direct representation of the field conditions but good comparable results were produced from this test. The series of tests performed in the CET was easily the most time consuming of the whole project but the conclusions and data collected from it formed the groundwork for the findings of this research. The author believes that the ease of use and the relatively quick turnover of tests of the CET will benefit many future works.

The results from the CET successfully isolated and clearly defined the importance of aperture to ballast size ratio, rib profile and the effect of grid stiffness.

Many, if not all of these attributes however, cannot be taken independently as they are often reliant upon the other. It is vitally important for any grid user or designer to acknowledge this.

The RTF is an important piece of equipment that attempts to bridge the gap between laboratory work and practical site work. Though no laboratory equipment can boast to be able to completely simulate the site conditions, the RTF as a test is sensitive enough to demonstrate the effect of grid reinforcement, shown in the tests performed in this research. The availability of a tamping bank further increased the scope of

work that could be done on the RTF, as well as having the increased realism since tamping is a common occurrence on many rail tracks. The effect of post tamping on the deformation characteristics of the grid reinforced composite has not be sufficiently explored due to time limitations. It is therefore, important to understand that any benefit of the reinforced grid does not include the unexplored initial settlement behaviour of the composite, post tamping. This also applies to the concluding LEF values presented in the Design Charts.

The Design Charts presented in Chapter 7 of this thesis defined the influence of geogrid reinforcement in a simple LEF format. The level of plastic strains simulated from the tests is within the realistic in-situ range. Generally, it can be conclude that the various LEF values presented in Chapter 7 gave a good appreciation and understanding of the effects of grid reinforcement on rail track performance. It must also be recognized that the design charts, at this moment, are still more of an interim piece of work rather than a direct representation of in-situ performance.

Having executed the whole series of experimental work in this thesis, it is concluded that the results, namely those from the CET and RTF, showed a general agreement that correct use of geogrid reinforcement is likely to help in the reduction of vertical plastic strain of the composite. However, it must also be emphasized the tests were all carried out under specific test conditions and that due diligence must be conducted in practical site application.

This thesis concludes in particular:

- Grid aperture needs to be at least 1.6 times the mean ballast particle size if good interlock, and hence good load transfer and reinforcement is to be achieved.

- Grid aperture should not be too large otherwise some of the reinforcing effect is diminished.

- The stiffness of the geogrid has little effect when good interlock is not achieved, but improves the reinforcing effect when interlock is good. This

improvement leads to less strain in the reinforced ballast system prior to reinforcement being effective and a greater reinforcing effect once it is.

- Reinforcement is much less effective in ballast that rests on stiff subgrades.

- Better reinforcing is achieved when a thicker rib is available to interact with the ballast.

- A Life Extension Factor has been introduced to model a trend of extended maintenance cycle interval. Values of LEF of up to 5 times have been obtained, although this is based on limited data. Application of this on site may be based on different sets of parameters and caution should be taken.

8.3 Recommendations for further research

The DEM work of this project could be extended to model the CET. Simplified clusters could be used to reduce the computation time. Important parameters, such as grid stiffness, rib profile, contribution of settlement at different ballast layers can then be investigated.

The walls of the CET could be made non-rigid for a more realistic simulation compared to site condition. Springs could be added to the walls to allow some movement, lowering confinement. Ballast particles will then have a greater degree of freedom to roll and displace laterally. The CET could also be modified to allow visual inspection of deformation or settlement of ballast particles at different stages of loading. A perspex wall could be installed for this purpose. This could allow possible measurement of ballast displacement in different layers at various points.

More work can be done on assessing the performance of geo-composite. One of the reasons given for the poor performance of the geo-composite is that the rubber sheet doesn't behave like soil. The lack of penetrability of the rubber sheet is likely to have influenced the results. Hence, it is recommended that the CET be modified to incorporate the use of real soil for the subgrade layer and that tests using geo-composites be carried out. It would also be useful to repeat tests on geogrids (not composite) over a soil subgrade.

A bending stiffness test could be carried out to investigate the importance of rib bending stiffness on ballast/grid interlock. It can be seen in the CET the formation of a shear failure plane formed when stiffer grids (higher bending stiffness) were tested. Such formation has a detrimental effect on the reinforcing ability of the geogrid. Hence, it will be useful and important to quantify the effect of grid bending stiffness on grid performance. A simple rib test can be introduced to fulfil such task.

More variables could be introduced into the RTF experiments. The subgrade used could be varied e.g. clay etc. There should also be a variety in the types of ballasts

used, with different shear strength. Different ballast thickness can also be investigated. A variation in ballast size will also serve to justify the experimental and theoretical findings of this project, that an aperture size to particle diameter ratio of 1.6 gives the optimal grid aperture size. In addition, the effect of reinforcement on wet or foul ballast will also provide interesting insights. Variation in loading set-up, including increasing load magnitude and frequency, will help to provide some validation for the predictions in the design guide. A more efficient method to move ballast material in and out of the test pit should also be devised so as to reduce experimental time.

This research would benefit from the availability of triaxial results on the ballast used in the RTF. This would give a more robust prediction in the design guide. The analysis utilised a programme based on linear elastic theory with the non-linearity addressed by a successive iteration approach. This method could be improved on with the introduction of the non-linear analysis of the aggregate for a better prediction of permanent strains, added to any future design method. This can be achieved with the Finite Element Simulation of plastic strain accumulation in ballast.

The empirical nature of the prediction of permanent deformation in this project, though effective, is far from satisfactory. Development of a proper scientific understanding of the deformation response under dynamic load with proper material modelling will better serve any modifications to the design guide. Finite Element Modelling and Discrete Element Modelling could be used to execute such work.

The issue of the relationship between absolute settlement and differential settlement should be investigated to improve on the accuracy of the prediction made in the design guide.

Having executed the whole series of experimental work in this thesis, I must conclude that the results, namely those from the CET and RTF, showed a general agreement that correct use of geogrid reinforcement is likely to help in the reduction of vertical plastic strain of the composite. However, it must also be emphasized the tests were all carried out under specific test conditions and that due diligence must be conducted in practical site application.

References

Allen, J.T. (1973) *"The Effects of Non-constant Lateral Pressure of the Resilient Response of Granular Materials"*, PhD Thesis, University of Illinois at Urbana-Champaign, Urbana, USA.

Allen, J.T. and Thompson, M.R. (1974) *"Resilient Response of Granular Materials Subjected to Time Dependent Lateral Stresses"*, Transportation Research Record 510, pp: 1-13.

Alva-Hurtado, J.E.D. and Selig, E.T. (1981) *"Permanent Strain Behaviour of Railroad Ballast"*, Proc. of 10th International Conference on Soil Mechanics and Foundation Engineering, Jun 15-19, Stockholm Sweden, Vol. 1, pp: 543-546, A.A. Balkema, Rotterdam, the Netherlands.

Barksdale, R.D and Itani, S.Y. (1989) *"Influence of Aggregate Shape on Base Behaviour"*, Transportation Research Records, 1227, pp: 173-182.

British Standard: BS 812 (1983) *"Methods for Sampling and Testing of Mineral Aggregates, Sands and Filters"*.

British Standard: BS 812-103.1 (1985) *"Methods for Determination of Particle Size Distribution- Sieve Tests"*.

British Standard: BS 812-105.1 (1989*) "Methods for Determination of Particle Shape Flakiness index"*.

British Standard: BS 812-110 (1990*) "Methods for Determination of Aggregate Crushing Value (ACV)"*.

British Standard: BS EN 13450 (2002*) "Aggregates for Railway Ballast"*.

Bowles, J.E. (1979) "*Physical and Geotechnical Properties of Soils"*, McGraw Hill Book Company.

Boyce, J.R. (1976) *"The Behaviour of Granular Material under Repeated Loading"*, PhD Thesis, University of Nottingham, United Kingdom.

Boyce, J.R., Brown, S.F., and Pell, P.S. (1976) *"The Resilient Behaviour of a Granular Material under Repeated Loading"*, 8th ARRB Conf. on Material Construction and Maintenance, Part 3, pp: 1-12.

Boyce, J.R. (1980) *"A Non-Linear Model for the Elastic Behaviour of Granular Materials under Repeated Loading"*, Int. Conf. on Soil under Cyclic and Transient Loading, Swansea, pp: 285-294.

Brown, S.F. (1974) *"Repeated Loading Testing of a Granual Medium"* Journel of Geotechnical Engineering Div., ASCE, 100, pp: 852-841.

Brown, S.F. and Hyde, A.F.L. (1975) *"Significant of Cyclic Confining Stress in Repeated Load Triaxial Testing of Granular Material"* Transportation Research Records, TRB, 537, pp: 47-58.

Brown, S.F. (1996) *"The Use of Geosynthetics in Pavement Engineering"* Proc. of 1st European Geosynthetics Conference, Sept 30-Oct 19, Maastricht, Netherlands, pp: 47-55, A.A. Balkema, Rotterdam, the Netherlands.

Brown, S.F. (1996) *"Soil Mechanics in Pavement Engineering"*, *Geotechnique* 46(3) pp: 383-426.

Brown, S.F., Brunton, J.M, Hughes, D.A.B. and Brodrick, B.V. (1985) *"Polymer Grid Reinforcement of Asphalt"*, Proc. of Conf. on Association of Asphalt Paving Technology, 54, pp: 18-41.

Brown, S.F., Brunton J.M., Hughes, D.A.B. and Brodrick, B.V. (1985*) "The Use of Polymer Grids for Improved Asphalt Performance"*, Proc of 3rd Eurobitume Symp., (1), pp: 223-228.

Brown, S.F., Brunton J.M. and Armitage, R.J. (1989) "*Grid Reinforced Overlays*", Proc. Conf. on Reflective Cracking in Pavements, Leige, Belgium.

Brown, S.F. and O'Reilly, M.P. (Editors) (1991) *"Cyclic Loading of Soils: from Theory to Design"*, Blackie, Glasgow, Van Nostrand, New York.

Brown, S.F., Thom, N.H. and Kwan, J. (2006) "Optimising the Geogrid Reinforcement of Rail Track Ballast", Paper offered for Railfound Conference, 2006.

Caltabiano, M.A.C. (1990) *"Relective Cracking in Asphalt Pavements"*, PhD Thesis, University of Nottingham, United Kingdom.

Chaddock, B.C.J. (1988) *"Deformation of Road Foundations with Geogrid Reinforcement"*, TRL Research Record 140.

Chan, W.K. (1990) *"Permanent Deformation Resistance of Granular Layers in Pavement"*, PhD Thesis, University of Nottingham, United Kingdom.

Chan, W.K., Barksdale, R.D. and Brown, S.F. (1989) *"Aggregate Base Reinforcment of Surfaced Pavements"*, Geotextiles and Geomembranes 8(3), pp: 165-189.

Cundall, P. A. & Strack, O. D. L. (1979) "*A discrete numerical model for granular assemblies*", *Géotechnique* 29, No. 1, pp: 47-65.

Dahlberg, T. (2001) *"Some Railway Settlement Models- A Critical Review"*, Proc. Institute of Mechancial Engineers, Vol 215, Part F.

Esveld, C. (2001*) "Model Railway Track"*, MRT-Productions, the Netherlands.

Haas, R., Walls, J. and Carroll, R.G. (1988) *"Geogrid Reinforcement of Granular Bases in Flexible Pavements"*, Transport Research Record 1188.

Hamed, A.A.H (1987) "Geogrid Reinforcement of Ballast Track" Msc Dissertation, University of Birmingham, United Kingdom.

Haynes, J.G. and Yoder, E.J. (1963) *"Effect of Repeated Loading on Gravel and crushed Stone Base Course Materials Used in the AASSHO Road Test"*, Hwy. Res. Rec. 39.

Heydinger, A.G., Xie, Q.L., Randolph, B.W. and Gupta, J.D. (1996) *"Analysis of Resilient Modulus of Dense and Open-Graded Aggregates"*, Transportation Research Record 1547, pp: 1-6.

Hicks, R.G. (1970) *"Factors Influencing the Resilient Properties of Granular Materials"*, PhD Thesis, University of California at Berkeley, USA.

Hicks, R.G. and Monismith, C.L. (1971) "*Factors Influencing the Resilient Properties of Granular Materials*", Highway Research Records 345, pp: 15-31.

Hughes, D.A.B. (1986) "*Polymer Grid Reinforcement of Asphalt Pavements"*, PhD Thesis, University of Nottingham, United Kingdom.

Indraratna, B. and Salim, W. (2003) *"Deformation and Degradation Mechanics of Recycled Ballast Stablised with Geosynthetics"*, Japanese Geotechnical Society 43(4), pp: 35-46.

Ionescu, D. (2004) *"Ballast Degradation and Measurement of Ballast Fouling"*, Conf. on Railway Engineering 2004, London.

Jewell, R.A., Milligan, G.W.E, Sarsby, R.W. and Dubois, D. (1984) *"Interaction Between Soil and Geogrid"*, Proc. of Conf. Sponsored by Science and Engineering Research Council and Netlon, London, pp: 18-30, Thomas Telford, London, United Kingdom.

Karasahin, M. (1997) *"Resilient Behaviour of Granular Materials for Analysis of Highway Pavements"*, PhD Thesis, University of Nottingham, United Kingdom.

Knutson, R.M. (1976) *"Factors influencing the Repeated Load Behaviour of Railway Ballast"*, PhD Thesis, University of Illinois at Urban-Champaign, USA.

Kolisoja, P. (1997) *"Resilient Deformation Characteristics of Granular Materials"*, Publication Number: 223, Tampere University of Technology, Finland.

Lekarp, G., Isacsson, U. and Dawson, A. (2000a) *"State of the Art. I: Resilient Response of Unbound Aggregates"*, Journal of Transportation Engineering, ASCE 126(1), pp: 66-75.

Lekarp, G., Isacsson, U. and Dawson, A. (2000b) *"State of the Art. I: Permanent Strain Response of Unbound Aggregates"*, Journal of Transportation Engineering, ASCE 126(1), pp: 76-83.

Lim, W.L. (2004) "*Mechanics of Railway Ballast Behaviour"*, PhD Thesis, University of Nottingham, United Kingdom.

Little, P.H. (1993) *"The Design of Unsurfaced Roads using Geosynthetics"*, PhD Thesis, University of Nottingham, United Kingdom.

McDowell, G.R. and Stickley, P. (2006) "Performance of Geogrid Reinforced Ballast", Ground Engineering (January), pp: 26-30.

McDowell, G.R. and Bolton, M.D. (1998) *"On the Micromechanics of Crushable Aggregates"*, *Geotechnique* 48(5), pp: 667-679.

McDowell, G.R. and Harireche, O. (2002a) *"Discrete Element Modelling of Soil Particle Fracture"*, *Geotechnique* 52(2), pp: 131-135.

McDowell, G.R. and Harireche, O. (2002b) *"Discrete Element Modelling of Yielding and Normal Compression of Sand", Geotechnique* 52(4), pp: 299-304.

McDowell, G.R., Harireche, O., Konietzky, H., Brown, S.F. and Thom, N.H. (2006) *"Discrete Element Modelling of Geogrid-Reinforced Aggregates"*, Geotechnical Engineering 159, pp: 35-48.

Matharu, M.S. (1994) *"Geogrid Cut Ballast Settlement Rate on Soft Substructures"*, Railway Gazette International, March.

Meeker, L.E. (1990) *"Engineering and Econmic Factors Affecting the Cost of Railroad Ballast"*, Msc Dissertation, University of Neveda, USA.

Milligan, G.W.E and Love, J.P. (1985) *"Model testing of geogrids under an aggregate layer on soft ground"*, Proc Symp. Polymer Grid Reinforcement, Thomas Telford, London.

Miltry, F.G. (1964*) "Determination of the Modulus of Resilient Deformation of Untreated Base Course Material"*, PhD Thesis, University of California at Berkeley, USA.

Monismith, C.L., Seed, H.B., Mitry, F.G. and Chan, C.K. (1967) *"Prediction of Pavement Deflections from Laboratory Tests"*, Proc., 2nd Int. Conf. Struct. Des. of Asphalt Pavements, pp: 104-140.

Morgan, J.R. (1966) "*The Response of Granular Materials to Repeated Loading"*, Proc., 3rd Conf., ARRB, pp: 1178-1192.

Pappin, J.W. and Brown, S.F. (1980) *"Resilient Stress-strain Behaviour of a Crushed Rock"*, Proc, Int. Symp. Soils under Cyclic and Transient Loading, Swansea, pp: 169-177.

Potyondy, J.G (1980) *"Skin Friction between Cohensive Granular Soils and Construction Materials"*, *Geotechnique* 11(4), pp: 339-353.

Railtrack (2000). Railtrack Line Specification RT/CE/S/006 Issue 3: Track Ballast.

Raymond, G.P. and Bathurst, R.J. (1987) *"Performance of Large-Scale Model Single Tie-ballast systems"* Transportation Research Record 1131, pp: 7-14.

Raymond, G.P. (2001) "Reinforced Ballast Behaviour Subjected to Repeated Loading", Geotextiles and Geomembranes 20, pp: 39-61.

Sato, Y. (1995) "Japanese Studies on Deterioration of Ballasted Track" Veh. System Dynamics, 24(Suppl.), pp: 197-208.

Sato, Y. (1997) *"Optimisation of Track Maintenance Work on Ballast Track"*, Proc. of the World Congress on Railway Research (WCRR '97), Florence, Italy, Vol B, pp: 405-411.

Schlosser, F. and Juran, I. (1979) *"Soil Reinforcement"*, Gen. Report. Proc. of the 8th European Conf. of Soil Mechanics and Foundation Engineering, Helsinki.

Seed, H.B., Chan, C.K., Lee, C.E., (1962) *"Resilient Characteristics of Subgrade Soils and their Relationship to Fatigue Failures"*, Proc. Int. Conf. Structural Design of Asphalt Pavements, pp: 611-636.

Selig, E.T. (1985) *"Ballast for Heavy Haul Track"*, Track Technology Conf., Nottingham, United Kingdom.

Selig, E.T. and Waters. J.W. (1994) *"Track Geotechnology and Substructure Management"*, Thomas Telford, London.

Selig, E.T., Parsons, B.K. and Cole, B.E. (1993) *"Drainage of Railway Ballast"*, Proc. of the 5th International Heavy Haul Conference, Beijing, China, pp: 200-206.

Sharpe, P., Brough, M. and Dixon, J. (2006) *"Geogrid Trials at Copull Moor on the West Coast Mainline"*, Paper offered for Railfound Conference, 2006.

Shenton, M.J. (1974) *"Deformation of Railway Ballast under Repeated Loading Conditions"*, British Railway Research and Development Division.

Shenton, M.J. (1985) *"Ballast Deformation and Track Deterioration"*, Proc. of a Conf. on Track Technology, University of Nottingham, 11-13 Jul 1984, Thomas Telford Limited, London.

Sparrow, R.W. (1981) *"The Effect of Traffic Loading in Ballast Vertical Deformation"* Lecture to China Academy of Railway Science Scientific Research Insitute, Beijing, China.

Sweere, G.T.H (1990) *"Unbounf Granular Basis for Roads"*, PhD Thesis, University of Deflt, the Netherlands.

Tensar International (2001a) *"The Properties and Performance of Tensar Biaxial Geogrid"*, Technical Publications.

Tensar International (2001b) *"Railways- Reinforcing Ballast Under Railway Track"*, Technical Publications.

Thom, N.H. and Brown, S.F. (1987) *"Effect of Moisture on the Structural Performance of a Crushed-limestone RoadBase"*, Transp. Res. Rec. 1121, pp: 50-56.

Thom, N.H. and Okaley, J. (2006) "Predicting Differential Settlement in a Railway Trackbed", Paper offered for Railfound Conference, 2006.

Uzan, J. (1985) *"Characterization of Granular Material"*, Transp. Res. Rec. 1022, pp: 52-59.

Vuong, B. (1992) *"Influence of Density and Moisture Content on Dynamic Stress-strain Behaviour of Low Plasticity Crushed Rock"*, Transp. Res. Rec. 1(20), pp: 88-100.

Wright, S.E. (1983) *"Damage Caused to Ballast by Mechanical Maintenance Technique"*, British Rail Research Technical Memorandum TM TD 15, May 1983.